Extracting gradient boundaries using hyper-temporal image analysis: progress towards a tool for gradient analysts

Rory G. Scarrott
March, 2009

Course Title:	Geo-Information Science and Earth Observation for Environmental Modelling and Management
Level:	Master of Science (Msc)
Course Duration:	September 2007 - March 2009
Consortium partners:	University of Southampton (UK) Lund University (Sweden) University of Warsaw (Poland) International Institute for Geo-Information Science and Earth Observation (ITC) (The Netherlands)
GEM thesis number:	27

Extracting gradient boundaries using hyper-temporal image analysis:
progress towards a tool for gradient analysts

by

Rory G. Scarrott

Thesis submitted to the International Institute for Geo-information Science and Earth Observation in partial fulfilment of the requirements for the degree of Master of Science in Geo-information Science and Earth Observation for Environmental Modelling and Management

Thesis Assessment Board

Chair	Prof. Dr. Ir. E.M.A. Smaling
External Examiner	Prof. K. Dąbrowska-Zielińska
Internal Examiner	Dr. Y.A. Hussin
1st Supervisor	Dr. Ir. C.A.J.M. de Bie
2nd Supervisor	M.Sc. A. Kooiman

ITC International Institute for Geo-Information Science and Earth Observation
Enschede, The Netherlands

Disclaimer

This document describes work undertaken as part of a programme of study at the International Institute for Geo-information Science and Earth Observation. All views and opinions expressed therein remain the sole responsibility of the author, and do not necessarily represent those of the institute.

Abstract

Environmental gradients overlay each other across the earth's surface. These environmental heterogeneities are expressed by the plant communities living within them. Some gradients change temporally as well as spatially, reflected in the phenological responses of the local vegetation. Gradient analysts, attempting to understand these gradients, currently have little to aid them to stratify their sampling, along the logic of what they are studying (gradients). Furthermore, current landuse classifications compound the issue, providing little indication of landscape gradients, and giving little aid to the gradient analyst.

This exploratory research hoped to produce a piece of logic, capable of guiding research into providing a tool for gradient analysts to stratify their sampling regimes. It investigated whether it was possible to devise a method, to extract gradient boundaries solely from temporal remotely sensed imagery, exploiting hyper-temporal NDVI datasets available from the SPOT-VEGETATION instrument.

The research consisted of firstly, an appraisal of environmental heterogeneity in the study area, using ISODATA classification, and subsequent NDVI class characterisation with rice crop calendars. Secondly, the research explored two methodologies to extract gradient boundaries from hyper-temporal NDVI datasets. These gradient boundaries were thought to bound regions that were heterogeneous in nature, representing regions over which fluctuations in environmental conditions were eliciting a phenological response in the vegetation. The first methodology was based upon Principal Components Analysis and its ability to summarise the hyper-temporal variability. The second, involved a temporal use of Edge Detection, exploiting the asymmetry of time to help define and extract gradient boundaries.

Both methods successfully extracted logical gradient boundaries. These did bound regions which were logically heterogeneous in nature, and therefore representative of areas of gradient flux. However, these boundaries, despite coinciding in many areas, did not universally match. Whilst it was evident that both methods are in need of further refinement, it was also evident that the different methodologies extracted boundaries based on different, though entirely gradient-relevant criteria. It was recommended that further research into a hybrid method, should follow research into refining the two attempted methodologies. This does not exclude research into other, alternative methodologies, provided they are founded in gradient logic.

Acknowledgements

This thesis is dedicated to my parents, Robert and Constance Scarrott, and my family, for their unfailing support and encouragement over the years.

To my supervisors Dr. Kees de Bie, Prof. Mark Friedl, and Andre Kooiman, thank you for granting me the opportunity to learn with you, your constructive criticism, and your patience, no matter how many times I had to be pulled out of a giant sticky puddle of incomprehension!

To Dr. Simon Harrison, thank you for all your advice and helpful comments, since I first looked at this course and walked into your office looking for some guidance.

A massive thank you must go to the coordinators and developers of the GEM Msc. It cannot be easy getting our crew successfully around Europe in one piece! I also wish to thank the E.U. Action 3 programme, for allowing me the opportunity to study in Boston University. It was a truly rewarding experience and opportunity, and one for which I am deeply grateful.

To Mark, Alex, Carol, Janet, Phil, Claire, Eavan, Pete, Niall, O' Mahony, Aoife-Mac, Miss Ha, Amjad, and Stella. Some of you I knew before, and some I've met along the way. You have all helped keep me going throughout this time mo chairde, and words cannot express how grateful I am.

And finally, to my GEM buddies. You have enriched my life beyond belief, and I will cherish our time working together, laughing together, and learning together. In particular I'd like to thank Daphne, Fernanda, Kath, José, Aidin, Tawanda and Betty for their companionship, tea, adventures, help, and general randomness over the 18 months (with a sprinkling of festivities!). I sincerely hope to see you all again sometime in the not too distant future but until then,

Go n-éirí an bóthar leat.
Go raibh cóir ghaoithe i gcónaí leat.
Go dtaitní an ghrian go bog bláth ar do chlár éadain,
go dtite an bháisteach go bog mín ar do ghoirt.
Agus go gcasfar le chéile sinn arís, go gcoinní Dia i mbois a láimhe thú.

(May the road rise to meet you.
May the wind be always at your back.
May the sun shine warm upon your face,
the rain fall soft upon your fields.
And until we meet again, may God hold you in the palm of his hand.)

Table of contents

List of figures

List of tables

1. Introduction

1.1. Gradients, vegetation communities, and gradient analysis

"We have abandoned any hope of ecological meaning in some idealised, uniform and constant environment" (Sparrow, 1999), rather, embracing the view that the world is heterogeneous and non-equilibrial (Chesson & Case, 1986). For every environmental condition (e.g. soil moisture, precipitation, cloud frequency, among others), a gradient exists, from low to high (or vice versa). These gradients overlay, cross, and enhance each other across the earth's surface. It can be seen that in reality, each area/point on the earths' surface represents the confluence of *n* number of environmental (both abiotic and biotic) gradients (Begon et al., 1990), which are consequently, a useful abstraction for explaining the distribution of species in space and time (Austin, 1985).

All species live in a characteristic, minimum range of habitats (Ter Braak & Prentice, 1988). A species, living in a locality, has to be tolerant of the sum of all those constraints under which it must live (Hutchinson, 1958). According to Whittaker (1953), any community at a point is composed of species tolerant to the conditions at that point (see figure 1). Since communities are essentially groups of species occurring together (Giller, 1984), they are subject to the same environmental influences as their components (Hugget, 1995). The composition of biotic communities thus changes along environmental gradients. For example, vegetation communities appear to have distinctive vegetation types that change over the landscape. These appear to be separate. However, when concentrating on the distributions of individual species, the individual species abundances overlap considerably (figure 1), exhibiting a distinct lack of sharp boundaries, even where intra-dependent communities build up (Begon et al., 1990).

Gradient representation has become a standard technique for the examination of vegetation patterning (Gosz, 1992). However, a form of gradient representation cartographically, appears illusive in the literature on remote sensing. Gradients remain as abstract interpretations of different zones in images, which exist only in the mind of the reader. Gradient models are a human construct, allowing empirical relations between environmental conditions, distributions and species abundances to

be explored. Essentially, they serve to organise environmental and biotic heterogeneity in a logical way (Keddy, 1991).

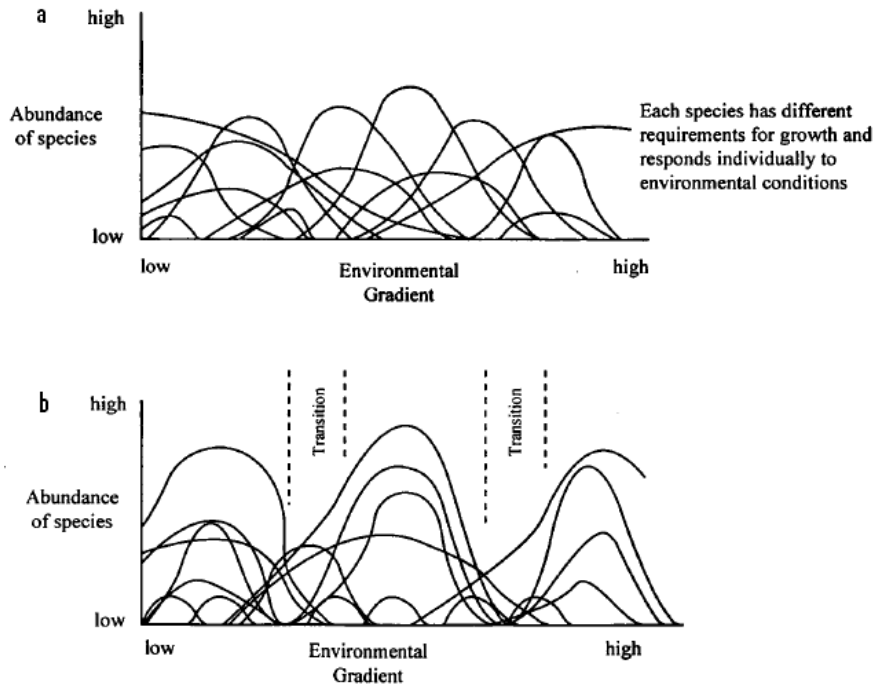

Figure 1: Views of plant communities expressed as species response curves along an environmental gradient - (a) the Gleasonian (Gleason, 1917; 1926; 1939) view of plant communities expressed as species response curves along an environmental gradient; (b) Whittaker's (1953) climax pattern hypothesis expressed as species response curves along an environmental gradient (adapted from Kent *et al., 1997).*

It was this use which was kept as a guide, whilst defining gradients for the purpose of this study. In this research, a gradient was seen as a fluctuation in a subjectively chosen environmental condition (or complex of conditions) which illicits a phenological response in the locality's' vegetation. Confusion often arises with conceptualising gradients. Position on a gradient, and position spatially are often mixed up (Austin, 1985). Sites with similar values on a specified gradient, need not be related spatially (figure 2). Aside from their ability to suggest hypotheses by emphasizing patterns in the data, gradients also provide a tool for conducting experiments (Keddy, 1991), specifying predictable and quantifiable changes in environmental states. This is the use to which gradients are put in gradient analysis.

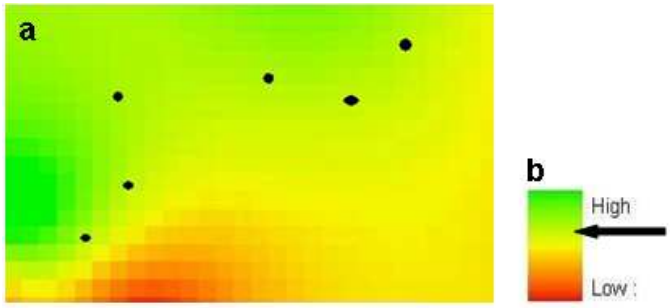

Figure 2: Difference between spatial position, and position on a gradient. (a) Multiple species occurrence sites, spatially spread out, experiencing a similar environmental condition denoted by black dots. (b) The environmental gradient, showing the single position about which the species located in (a) survives.

This "gradient analysis" has become a major input into studies of species communities by environmental scientists, and in particular ecologists (Whittaker, 1967). It is a research approach for studying these shifting species distributions, based predominantly on the spatial patterning of vegetation. It seeks to understand the structure and variation of a landscape's vegetation in terms of gradients in space, at three levels- environmental factors, species and populations, and characteristics of communities (Whittaker, 1967). It has been described as a "powerful technique" (Gosz, 1992), to analyse and detect changes in the dynamics, structure and functioning of ecosystems, and is a major alternative approach to studying communities through classification (Whittaker, 1973).

The approach is not without criticisms. Begon et al. (1990) highlight one of the major criticisms of gradient analysis, as a way of detecting patterns in communities. They note that "the choice of the gradient is almost always subjective". An investigator organises the data they have about a species, along a gradient or a factor they deem to be important to the organisms. Unfortunately, this may not necessarily be the most appropriate factor (Begon et al., 1990).

In order, to make their work more viable, gradient analysts turn to randomising their sampling methods, combined with sampling as many environmental variables as possible. They rely on comparing the results of ordination to the sampled variables (Begon et al. 1990). For example, White and Hood (2004) in studying vegetation response to soil variables in the Mexican Yucatan, utilised a natural escarpment to delineate a transect, along which they could sample (figure 3). Such a method could have missed the strongest gradient acting across the local area in different directions to the transect alignment. Such a gradient could have been captured better, had their sampling been orientated differently, or even not aligned along a transect at all.

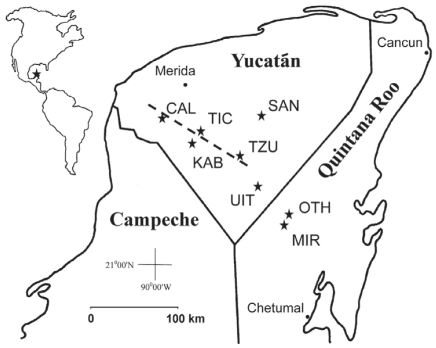

Figure 3: White & Hoods' sampling transect. Sample sites are represented by stars, and associated code, whilst the escarpment from which they were orientated is represented as a dotted line (white & Hood, 2004)

This sampling problem is also evident in current mapping techniques, which appear to ignore the logic of gradients and landscape heterogeneity. Classifications essentially homogenise portions of the landscape, creating hard boundaries between zones. Current classification techniques assign a pixel to a class on the basis that they are within a threshold of similarity to that class, then divides the image accordingly into what the algorithm deems are distinct class areas. A landuse class is either one thing or another, there is no identifiable "in between. This sampling problem is most effectively illustrated in figure 4. Here, it is easy to draw a boundary line between two zones along line A. However, in contrast, for line B, where does one class end, and the next begin? Meanwhile figure 5 shows one such landuse classification as an example of the lack of "in between" representation.

Figure 4: Problems in defining class boundaries in the Mekong Delta. Transect "A" has an easily discernable cut off point along its axis, where the vegetation obviously changes. However, the change along transect "B" is much more gradual, making it difficult to discern where the class located at one end, turns into the class located at the other end of the transect. (image from www.envisat.int, 2009)

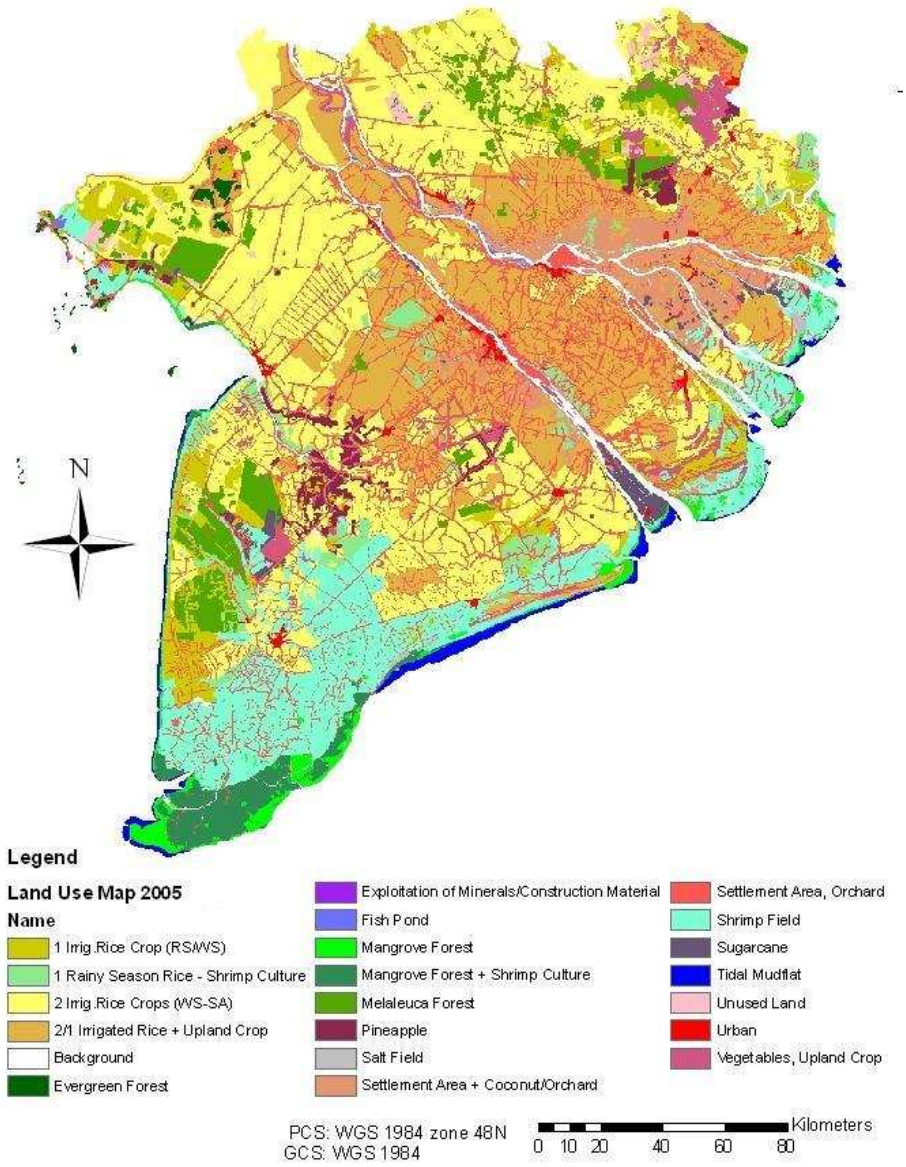

Figure 5: Mekong Delta Landuse map 2005. This clearly shows the distinct class areas, with no transition zones or gradient representation incorporated into the map (obtained from the National Institute of Agricultural Planning and Projection, Vietnam Ministry of Agriculture and Rural Development).

Figure 6 shows some theoretical classes to emphasize this mapping issue. Arbitrarily numbered classes 1, 2, 3, and 4 are considered distinct entities, to be characterised by abrupt boundaries as their end points. Unfortunately, this does not take into

account the reality of the situation. Class 1 gradually becomes class 2, which gradually becomes class 3. Class 4 on the other hand, gradually develops into class 1, yet has no common properties with classes 2 or 3.

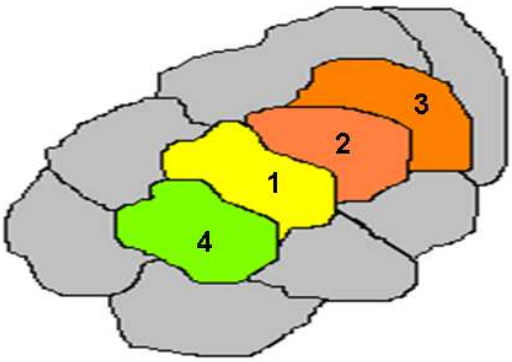

Figure 6: Inter-class relations along gradients. Theoretical representation of classes, identified as distinct by image analysis, though are in reality grouped together along a common factor.

Some map classifications designate so called “transition zones”, though this raises the question “where does the transition zone begin and end?” This of course, is not to say that map classification is wrong. It merely emphasizes the point that currently, map classification is insufficient to the task of truly telling the entire story of the landscape. Critical to this research was the understanding that classification does pick out areas that are fundamentally different. despite placing a boundary line somewhat arbitrarily. This arbitrary drawn line is not depicted as a “soft” line, which could denote a transition.

For example, when the classes in figure 6 grouped together logically, a different aspect is revealed, that of gradients. If such a logic is applied to classes 1, 2, 3, and 4 above, not only could we see a natural grouping (1, 2, 3 and 4), but also the direction of change (4 to 1 to 2 to 3). This logic is seen to be that of “Gradients”, i.e one of infinitely fluctuating environmental conditions across the Earths’ surface. A gradient analyst could apply this logic to his/her sampling scheme. They could identify areas that are fundamentally different, and then see how they are grouped, or not grouped. Their sampling regime would therefore be stratified entirely from satellite data, and specifically to capture the primary agent of change between the classes. This could allow the correct agent to be subsequently identified, and studied in depth.

1.2. Normalised Difference Vegetation Index, hyper-temporal imagery, and gradients.

Communities, including crops, on the Earths' surface are structurally represented by plant species, detectable to a degree using the Normalised Difference Vegetation Index (NDVI). As each plant member or cluster grows, sickens, heals, and dies, the concentrations of chlorophyll in its tissues and its biomass fluctuate over time, a change which is detectable by NDVI (Tucker, 1979).

Not only has the relationship between NDVI and productivity been well established (Pettorelli *et al.*, 2005), but the effects of some environmental conditions on NDVI have also been documented (e.g. Jingyong *et al.*, 2003; Roerick *et al.*, 2003; Wang *et al.*, 2003). These studies have shown that NDVI does indeed fluctuate along environmental gradients.

There are reservations expressed about using NDVI, well summarised by Pettorelli *et al.* (2005). However, despite these, supporting the use of NDVI for this research were the arguments that:
1: the index is relatively simple, easy to calculate, and also readily available online as a pre-prepared product.
2: hyper-temporal datasets of NDVI existed, or were obtainable, for multiple sensors (e.g. SPOT-VEGETATION, MODIS, AVHRR) if required, some dating back over 10 years or more.
3: The core focus of this research is simply to use fluctuations in vegetation phenology, not to determine which the best measure of those fluctuations is.

The NDVI effectively provides us with information on the vigour and abundance of the vegetation community (Campbell, 1996). However, NDVI can also provide us with information on vegetations' spatial and temporal distribution, and it is this temporal aspect which was also exploited during this research through using hyper-temporal imagery. The chosen vegetation was not only to be spatially analysed, but also analysed in how it changes in time.

Stutheit (1991) pointed out that multi-temporal functionality should become a fundamental enhancement to all spatial analysis systems. "Time is the fourth dimension; it is unlike the first three dimensions in that it is asymmetrical, and difficult to envision, much less comprehend" (Saab & Haythornthwaite, 1990). However, it can greatly enhance the information gain from remote sensing imagery. For example, Zhang *et al.* (2004) used what is considered multi-temporal imagery

(composed of 16 day composites over a 1 year period) to track vegetation "green-up" over the northern hemisphere. In their study of arctic sea-ice changes, Piowar and Le Drew (1995) noted that time sets of nearly 30 years, with near-daily revisit times, had been collected so far. They termed these extensive daily repeated datasets as "hyper-temporal" datasets, and called for research into "hyper-temporal image analysis" techniques, to take swift advantage of the oncoming "temporal data explosion".

"Hyper-temporal" data" is essentially "multi-temporal" data, collected with a very fine temporal resolution (with sensor repeat times of approximately 1 day). Despite Piowar and Le Drews' (1995) tentative efforts, and the increasingly frequent use of the term in scientific literature, the term is still somewhat ill-defined and subjective. Here, it is taken to be imagery, or composite imagery, derived from near-daily repeated datasets. For the purpose of this research, there had to be at least two composite images produced within a calendar month, for a period longer than 3 years (i.e. that used by Thenkabail *et al.*, 2007, in their study using AVHRR data).

Piowar and Le Drew (1995) called not only for new techniques to be developed, but also existing image processing tools to be adapted. They noted that hyper-temporal images could be considered analogous to hyper-spectral images, with each timeframe analogous to a different spectral band (Figure 7). Arguing this point, they promoted adapting methods such as unsupervised multispectral classification (Staenz & Goodenough, 1990), and Principal Components Analysis (Chavez & Kwarteng, 1989).

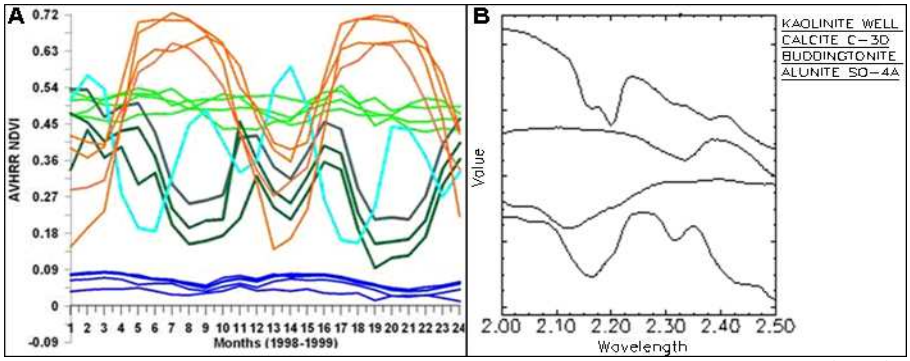

Figure 7: The analogy between hyper-temporal and hyper-spectral. A shows hyper-temporal profiles of landuse NDVI signatures. (from Thenkabail *et al.*, 1999). These can be considered to the hyper-spectral profile of different minerals shown in B (from www.ltid.inpe.br).

De Bie *et al.* (2008) used hyper-temporal imagery to identify land-use classes, previously indiscernible from NDVI images taken at single time frames. As a case study they used this "hyper-temporal image analysis" and concurrent hyper-temporal profiling of classes, to delineate some possible gradients in the Limpopo Valley. This was suggested using visual comparison to an ASTER image. They showed that, using hyper-temporal NDVI imagery, land classes based along fluctuating gradients were visibly interpretable. However a scientifically rigorous and automated method to delineate the zones where a dominant gradient is affecting multiple classes (so-called gradient effect zones), was not investigated further.

Furthermore, it must be noted there was a lack of documented attempts of different methodologies to analyse hyper-temporal data. The field of hyper-temporal image analysis is relatively new. Consequently, the research here was in essence, exploratory, investigating different possible avenues. Hyper-temporal image analysis was chosen, as it appeared to be of fine enough temporal resolution to capture the fluctuations of vegetation in response to changing environmental conditions (such as flooding and salinity intrusion for example) on a local scale. It progressed from the logic that temporal changes in gradients, would be expressed by the vegetation communities through their NDVI signature (see figure 8). These fluctuations were hoped to be discernable, due to the high temporal resolution of the hyper-temporal datasets used.

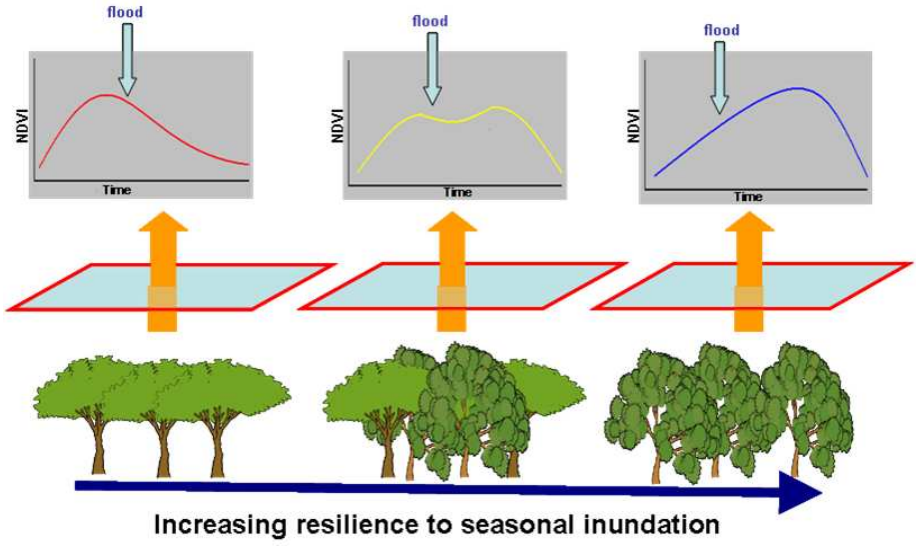

Figure 8: Theoretical representation of how community and temporal NDVI changes along gradients.

1.3. Rice crop calendars as "windows" into gradient activity

Rice (Oryza sativa) was chosen as the "window" into the landscape, through which hyper-temporal NDVI image analysis would explore along the logic of gradients. It has a strongly fluctuating NDVI signature (figure 9) due to its' unique feature of being grown on flooded soil (Xiao et al., 2002), and its growth cycle that effectively saturates NDVI. Wetland rice crops (such as those in the Mekong Delta studied here) have three distinctive, main periods in their temporal development (Le Toan et al., 1997). These are the sowing-transplanting period, the growing period, and the fallow period (figure 10).

1: The sowing-transplanting period

Fields are flooded to remove pests and weeds. They are subsequently drained and plants are either transplanted, or seeds sown directly into the wet soil. The NDVI signature is therefore low until the young plants grow.

2: The growing period

The sub-stages here can be recognised as a) vegetative, b) reproductive, and c) maturation.

a) The vegetative stage, is characterised plants increasing in both height, and the number of leaves. NDVI increases with the higher biomass. After 50 to 60 days, rice biomass covers almost any space between plants, saturating NDVI.
b) The reproductive stage lasts about 25 to 30 days. The number of side shoots decreases slightly during this time. As New leaves are no longer produced, and no longer erectophile, ground-coverage is not severely impacted, maintaining the high NDVI value.
c) The maturation stage is characterised by firstly, the development of seed heads, and secondly by a decrease in stem moisture content and in the number of leaves. This results in a gradual decrease in the NDVI level, which proceeds to fall abruptly when the crop is harvested.

3: The fallow period.

The fields can be either left bare and dry, or weed covered (with a relatively low NDVI). The field may be flooded early to prevent weed growth, or naturally to add fertile alluvium. Pre-sowing, the farmers purposely flood the fields, bringing them back to the rice sowing-transplanting period.

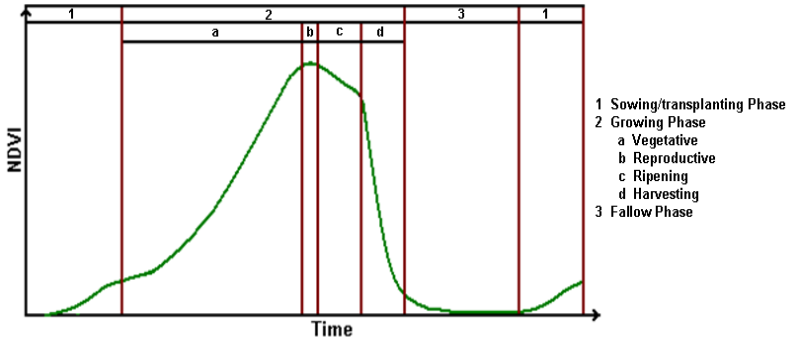

Figure 9: NDVI signature of the rice crop calendar, logically adapted from Le Toan *et al.*, 1997.

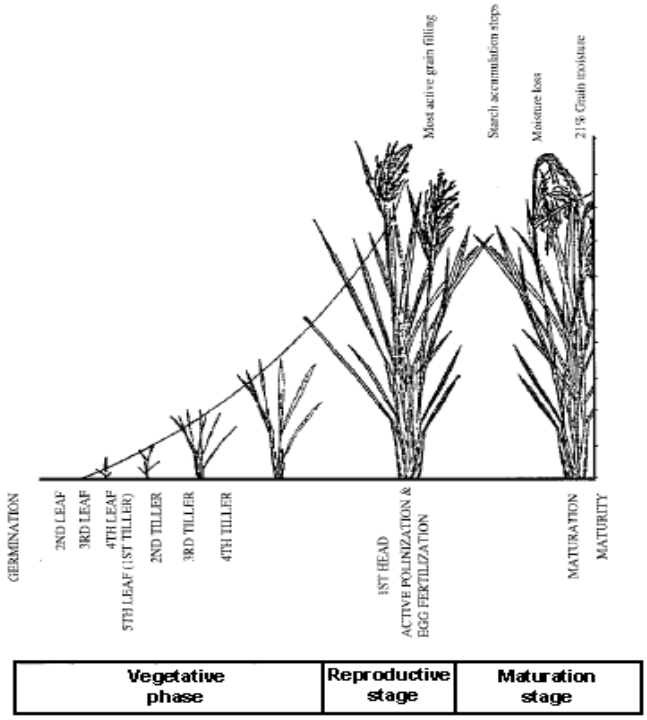

Figure 10: The Growth phase stages of rice , *Oryza sativa* (adapted from Le Toan *et al.*, 1997).

As Sklenár *et al.* (2008) noted, gradients can influence changes over time. They showed this by noting that temporal changes in cloud frequency were being reflected by changes in species composition. Zhang *et al.* (2004) charted the progression of vegetation "green-up" during the growing season of the Northern Hemisphere. Using MODIS multi-temporal imagery, they showed the temporal variability in

vegetation phenology were related to the predominant environmental conditions of temperature and precipitation.

These changes can also be exhibited in crop calendars, defined by De Bie (2000) as a "sequential summary of the dates/periods of essential operations including land preparation, planting, and harvesting, for a specific land use; it may apply to a specific plot, but is frequently generalised to characterise a specific area". Irrigated rice crops (predominant in the study area) require farmers to flood their fields. It is in fact a vital part of the cropping cycle. These farmers depend on sufficient water being present and available to irrigate their crops, but not flood them out. A floods' arrival, or the precipitation that leads to a floods' arrival, can vary in time by a few weeks. Consequently, so too do the crop planting times, and hence the crop calendars, fundamentally due to temporal fluctuations in environmental conditions (gradients).

Furthermore, It is well established that different varieties of rice are grown to suit different environmental conditions (evident in the current work of the Cuu Long Delta Rice Research Institute developing cultivars of rice to suit the conditional variety across the Mekong Delta). It was seen that rice, through its' extent and specific NDVI signature, could act as a "window" into the Mekong Delta's landscape, exhibiting the dominant changes in environmental conditions, and thus aid the gradient boundaries to be extracted.

1.4. What is a "boundary"?

In order to fully understand the logic of this research, the term "boundary" must be clarified. Kent *et al.* (1997) noted there are two extreme boundary situations - ecotone and ecocline (Van der Maarel, 1990). Kent further summarised that:

- "An ***ecotone*** is a zone of relatively rapid change between two plant communities and a dynamic zone of interaction which as a consequence, is often unstable"
- .An ***ecocline,*** in contrast, is defined as "a more gradual gradient of vegetation change between two plant communities, corresponding to a progressive spatial change in one or more underlying environmental or biotic factors"

To illustrate this point, figures 11 and 12 show graphically and with ecological examples, the meaning of the two terms.

For this research, boundaries in gradients were assumed to occur at ecotones (such as that shown in figure 11). Features such as escarpments, large rivers, and man-made barriers, all serve to disrupt the continuum of a gradient across a landscape. By identifying these features via vegetation, we can see where the gradients continuums are effectively broken. The 1km resolution of the SPOT-VEGETATION data was deemed to be of low enough resolution, not to necessarily identify these breaks, but to spatially map their effects. The NDVI values between pixels change, but it was not deemed important, at this stage, to identify the exact reason why.

The boundaries or "natural breaks" sought for by the research logic, represent ecotones in the landscape. These form the boundaries which disrupt a gradients continuum across the landscape. Essentially the entire Mekong delta is viewed as one large transition zone, changing from any point in the image, to any other. This follows from "there are no homogenous environments in nature" (Begon *et al.*, 1990). The landscape is instead a continuum of ecoclines and ecotones (figure 13), of which ecotones are used here to conceptualise the essence of a gradient "boundary". If an area bounded displays multiple unique classes, despite being within one bounded region, it can be viewed that conditions are changing within the region. Therefore logically, gradients are operating across the region, or "gradient effects zone".

With the asymmetry of time inherent in hyper-temporal datasets, a distinction could also be drawn between a relatively "permanent" boundary, and a relatively "impermanent" boundary. For the purposes of this research, a permanent boundary was defined as one which stays for a period longer than a month in a given area. Shown in figure 14, is an example of how gradients could have relatively permanent and impermanent boundaries, using the example of a flood gradient.

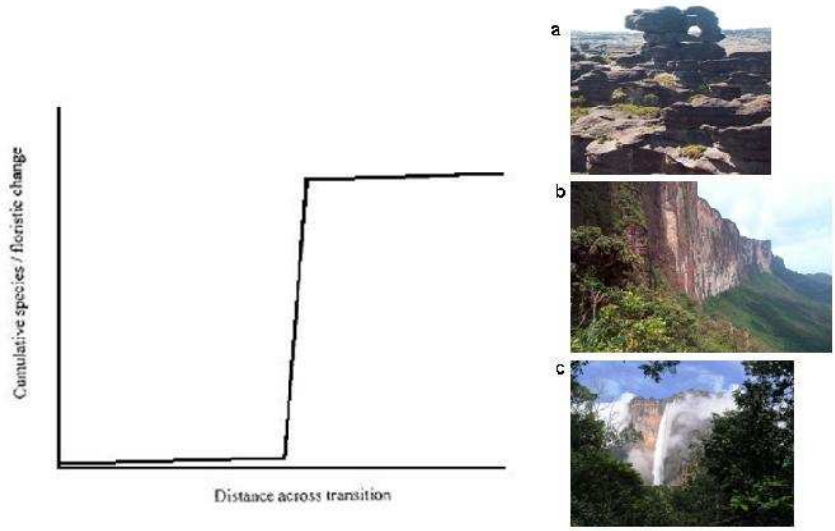

Figure 11: Graphical representation of species change across an ecotone (adapted from Kent *et al.*, 1997). Also included are images of "tepui" (or table top mountains) of Canaima National Park, in the Gran Sabana region of Bolivar State, Venezuela. The escarpments (b) represent an ecotone, dividing the higher ecosystem (a) from the lower ecosystem (c) and disrupting the gradient continuum between them. (Image sources: a- www.wikipedia.org, 2009a; b-www.wikipedia.org, 2009b; c- www.wikipedia.org, 2009c)

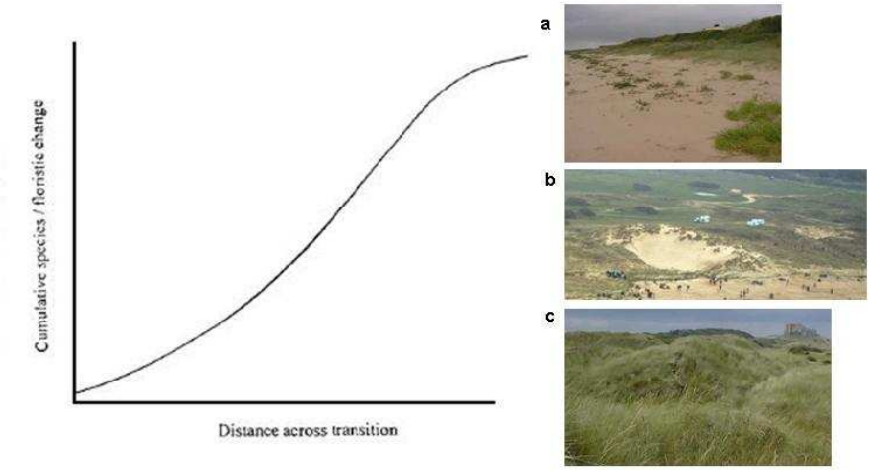

Figure 12: Graphical representation of species change across an ecocline (adapted from Kent *et al.*, 1997). Also included are images of sand dune systems in North-western Europe. The transition from a - sandy beach with colonising species to c – a progression of grassland to shrubland shown in the background, cannot be delineated clearly. Where does the transition occur looking at image b? (Image sources: a- www.kscience.co.uk, 2009a; b- cache.daylife.com, 2009; c-www.kscience.co.uk , 2009b)

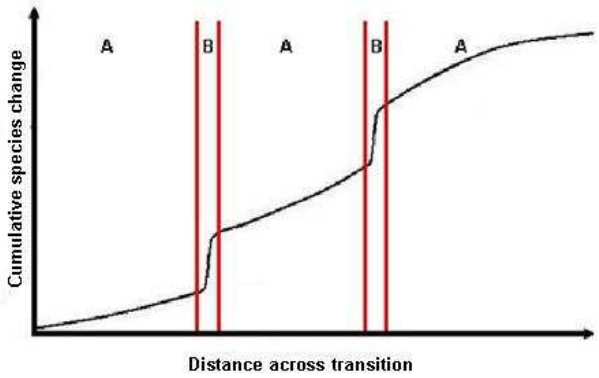

Figure 13: Ecoclines and ecotones across a landscape. A represents areas considered as ecoclines where species change slowly, whilst B represents zones of rapid species transition, or ecotones. (adapted from Kent *et al*., 1997).

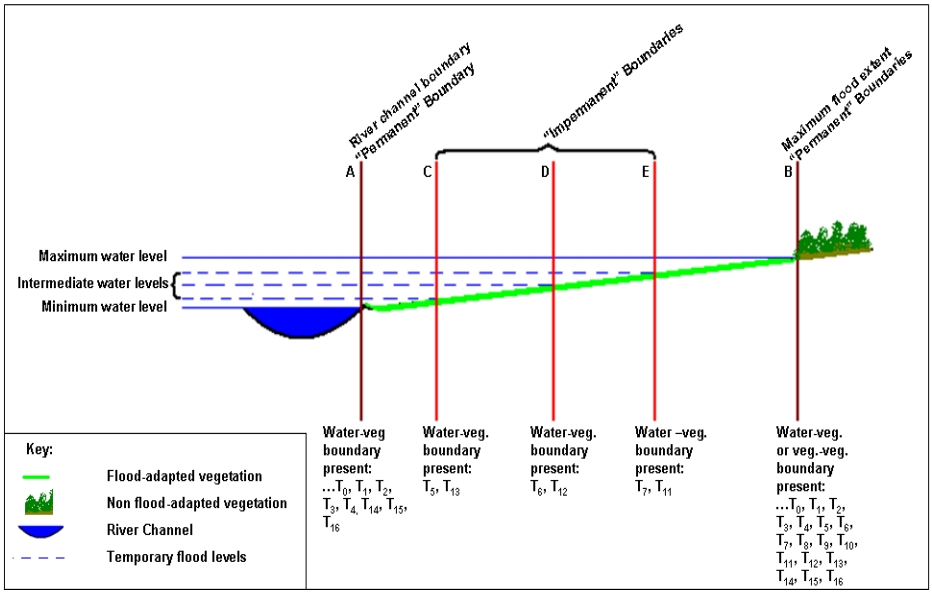

Figure 14: The different between "permanent and "impermanent" gradient boundaries, based on the logic that "permanent" boundaries repeat successively over periods of time**.**

During a non-flood season, the river has a constant boundary (boundary A in figure 14) repeatedly and successively imaged at times T0 to T4. However, upon the progression of flooding, the water-vegetation boundary shifts across the boundary,

over vegetation adapted to floods to varying degrees. The boundary is captured in non-successive images, as a temporally shifting boundary, or impermanent boundary (boundaries C, D, and E in figure 14). The vegetation at point B, is totally unadapted to flooding, and thus exhibits a different phenology to that vegetation which is adapted. The contrast between the two thus forms another permanent boundary, repeatable successively during the flood event around the time for flood maximum, and during the recover phase after the flood. This is then considered as another permanent edge.

2. Research approach

2.1. Problem statement to hypotheses

2.1.1. Problem statement

Until recently, classification methods in remote sensing have been based on images taken at a single time, or at most a few available with multi-temporal images. As a result, these classifications' ability to capture, and summarise the temporal variability across the Earths' surface (and especially concerning the subject of gradients) is severely limited.

We are now in the "explosion" of hyper-temporal datasets becoming available that Piowar and Le Drew (1995) envisaged. Within the last ten years in particular, Earth observation systems such as SPOT-Vegetation, MODIS, MERIS, and AWIFS have been added to the list of sensors with datasets of high enough temporal resolution, and long enough datasets, to be considered hyper-temporal.

The same concern expressed by Piowar and Le Drew (1995) is also present. Namely, that there is a distinct lack of methods currently available, to interpret and exploit this new data resource to its' full potential. Concerning this research for example, there is a lack of methods available to group hyper-temporal profile classes together, accepting that classes, though fundamentally different, are connected along gradients acting over the landscape within, and between them.

The aim of this research was to explore methods to extract boundaries, or natural breaks, where the effects of a strongly acting gradient logically cease to influence the vegetation, and a new gradient takes over. In grouping the classes associated with that gradient (whatever it may be) together, the research aimed to produce a tool which exploits the newly available resource of hyper-temporal imagery.

By identifying the boundaries of gradients, the research hoped to demarcate zones, over which one can assume that a strongly impacting gradient changes markedly. The approach was to produce a method that extracts required information from the satellite data alone, without identifying which specific gradients are causing the spatial variation. Thus it could allow gradient analysts to exploit the resource of cheaply available remote sensing products, to logically stratify their study areas as input for their fieldwork, saving them time, effort, and resources.

2.1.2. Research objective

- to explore possible methods which could be capable of grouping together map units which have equal status to NDVI classes. These NDVI classes would be obtained from ISODATA classification of data derived from the same hyper-temporal stack of NDVI images. Meanwhile the grouping methods would follow the logic that classes grouped together are affected by the same, strongly acting landscape-level gradient(s).

2.1.3. Specific objectives

To ascertain whether there is logical variability in rice crop calendars across the Mekong Delta, ascertaining whether the fundamental assumption of this thesis is valid, i.e. that there are, in fact, gradient attributable variations in rice crop calendars.

To explore various methods, which may be capable of recognizing boundaries, or "natural breaks", indicative of an abrupt change in gradient effect.

.

To compare and contrast the various promising methods. This is tasked to investigate which one is the "best" at grouping detailed mapped NDVI classes together as they appear to be the result of the same landscape-level gradient(s).

2.1.4. Research questions

1 - Assuming the ISODATA classification results are NDVI classes that are fundamentally different, can these differences be seen, expressed in rice crop calendar data collected in the field?

2 - Could shifts in rice crop calendars be attributable to landscape heterogeneity in environmental conditions across the Mekong Delta?

3 - Are there methods capable of recognizing and delineating boundaries, or "natural breaks" in a gradients' effects upon the landscape, using hyper-temporal satellite data alone?

4 - Of any promising method(s), how do they compare at recognising boundaries or natural breaks, thus delineating the borders of regions within which crop calendar heterogeneity occur, as caused by the same landscape level gradient.

2.2. Study Approach

The study consisted of three primary steps (figure 15). The first step was the production of a landuse map and legend showing crop calendars for different NDVI classes, across the Mekong Delta. This was produced using a combination of collected field data on rice crop calendars, and hyper-temporal image classification.

The second steps was more exploratory, involving trying out different methods of extracting natural breaks or gradient boundaries from the hyper-temporal NDVI image data. It aimed to produce maps showing NDVI classes, identified in step 1, grouped by the natural breaks or gradient boundaries identified by the boundary extraction methods. Both steps 1 and 2 utilised the same hyper-temporal NDVI data of the Mekong Delta.

Lastly, step three involved comparing the landuse map and legend, and the natural breaks and groupings maps from the various promising methodologies. This was done to see whether or not boundaries coincided, and whether areas enclosed by the "natural breaks" were logical entities having a gradient that impacted on the respective series of rice crop calendars.

The final product of the research was to have been a discussion on the various methodologies which were seen to hold promise. The various methodologies strengths and weaknesses were to be clarified, and a recommendation given on whether or not (and if so, how) to proceed in this line of research.

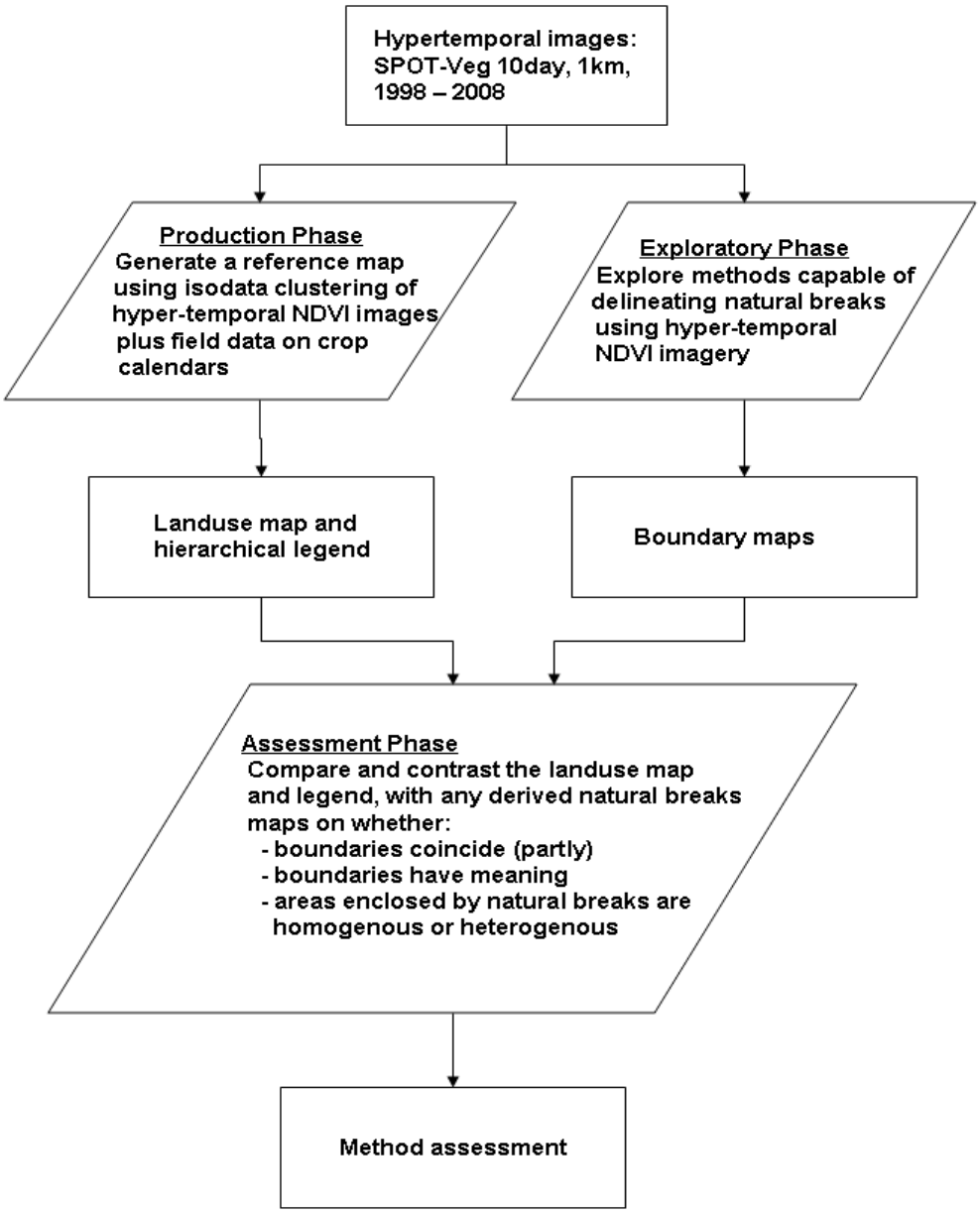

Figure 15: Summary of the study approach, showing the three primary steps taken, the inputs, and the outputs of the research.

3. Methodology

3.1. Method overview

As outlined in the study approach, the research's progress can be summarised into 3 main steps (see figures 15 and 16):
Step 1 - the production phase, assessing rice crop variability
Step 2 - the exploratory phase, exploring methods to extract boundaries
Step 3 - the assessment phase, appraising the products

The production phase involved the construction of a landuse map and legend. This was done using NDVI classes derived by ISODATA classification of a 10 year (1998-2008) stack of hyper-temporal NDVI imagery. These classes were then characterised with field data on crop calendars and rice varieties collected in the Mekong Delta, and flooding information derived from the hyper-temporal 10 year stack.

The exploratory phase consisted of using a 3 year (2004-2007) subset of the original 10 year stack of images, to explore methods capable of extracting logical gradient boundaries, or "natural breaks" in the gradient continuum. Principal Components Analysis (Chavez & Kwarteng, 1989) was followed by extraction of transition features, and subsequent boundary delineation. A new, innovative, and logical use of edge detection was also attempted. Methods were constantly reappraised, with the final products (maps of boundaries, and the NDVI classes they grouped) coming from the more promising methods.

The final phase of the research (the assessment phase) involved comparing the product of the exploratory phase products (satellite-down products) both to each other, and with the production phase product (a field level-up product). Feature recognition and extraction was ascertained, whilst common boundary similarities were qualitatively assessed. Furthermore, qualitative logical analyses of class heterogeneity within bounded regions were carried out.

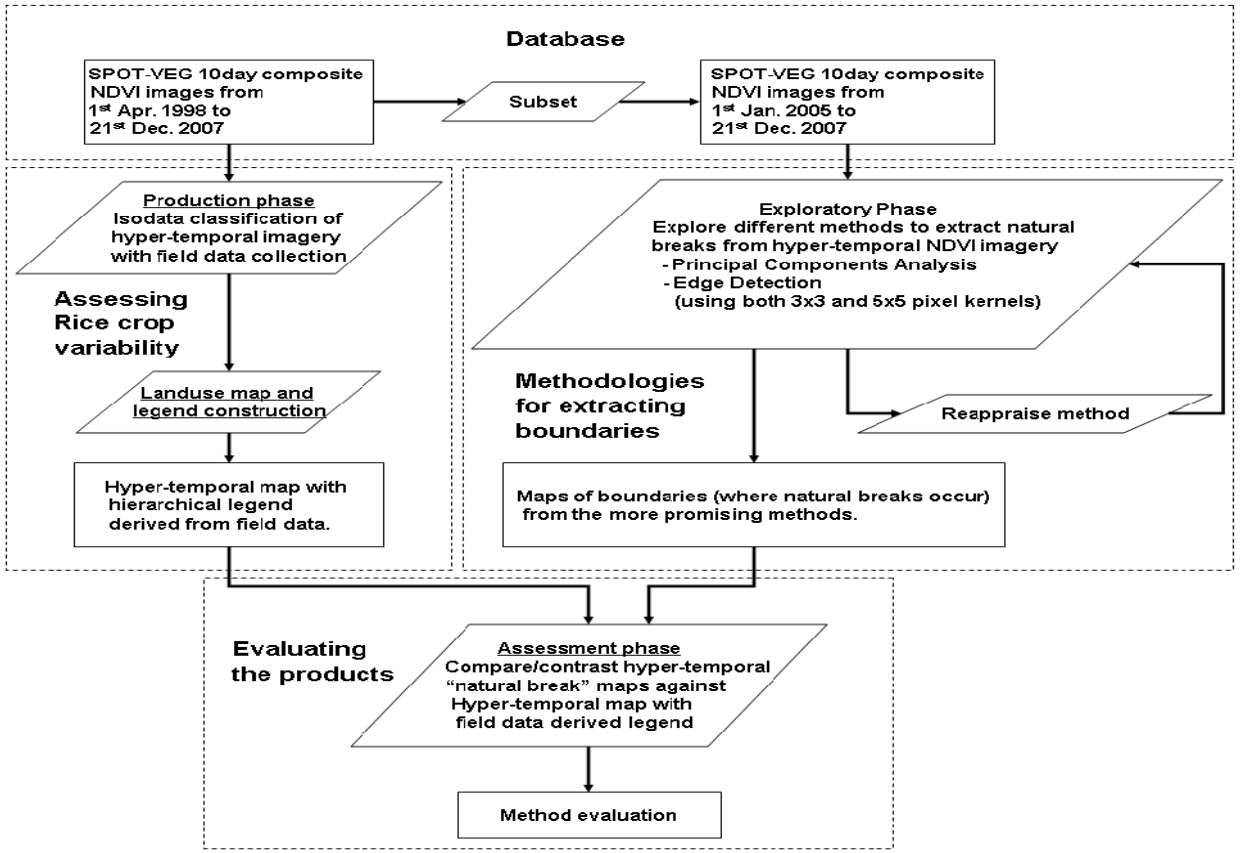

Figure 16: Methodology flowchart, depicting the progression of research, and the principal components in each step.

3.2. Study area

The study area was the Mekong Delta, situated in the southern part of Vietnam (Long: 8°60'N to 10°N, Lat: 104°50'E to 106o80'E), shown in figure 17. It is a low-lying plain with an area of approximately 40,000km2, crisscrossed by a complex system of canals and rivers (Nguyen, 2007). The region experiences a savannah climate, with well-defined wet and dry seasons, associated with the annual monsoon rains (Sakamoto *et al.,* 2006). Average air temperatures range between 18°C to 30°C (Sakamoto *et al.,* 2006). With heavy wet season precipitation, and a low-lying topography, the region experiences extensive flooding (Sakamoto *et al*., 2006).

Distributary channels of the Mekong overflow their banks in the northern delta every year (figure 20), inundating more than a third of the delta (Hori, 1996). Approximately 1 billion cubic metres of sediment is deposited onto the delta annually, extending it up to 80 metres into the sea per year (Nguyen, 2007), and fertilising its' soils. However, due to its' low-lying nature, and newly created soils, saline intrusion, is a notable environmental feature of the landscape, especially near the periphery (see figure 18). Furthermore soils, despite being alluvial in origin, vary in composition and chemistry across the delta (figure 19).

The delta is one of Vietnams' two most important rice granaries, alongside the Red River Delta in the north (Nguyen, 2007). The main crop in the delta is rice, grown in the irrigated lowlands (IRRI, 1993), occupying approximately 10,000 km^2 of the delta (Nguyen, 2007), and making up about 70% of the regions' agriculture (Nguyen *et al.,* 2004). A general idea of the landuse evident in the region can be gained from figure 5, (obtained from the Can Tho University).

The study area was chosen for a number of reasons. Firstly, as it is low-lying, it was hoped that the elevational gradients most commonly studied will not be as influential on the vegetation phenology as in other studies (e.g. Peet, 1978). Spatially the region is small enough to be considered relatively homogenous climatically for the purposes of this research. With these two frequently dominant gradients reduced, it was hoped that lower level gradients might be expressed in the data. Thirdly the area is technically tropical in nature contrasting sharply with the temperate climates studied by Zhang *et al.* (2003, 2004). Secondly, the tropical nature of the area, with its' high potential for cloud cover, allowed the research to see whether the any methodologies could be affected by cloud cover.

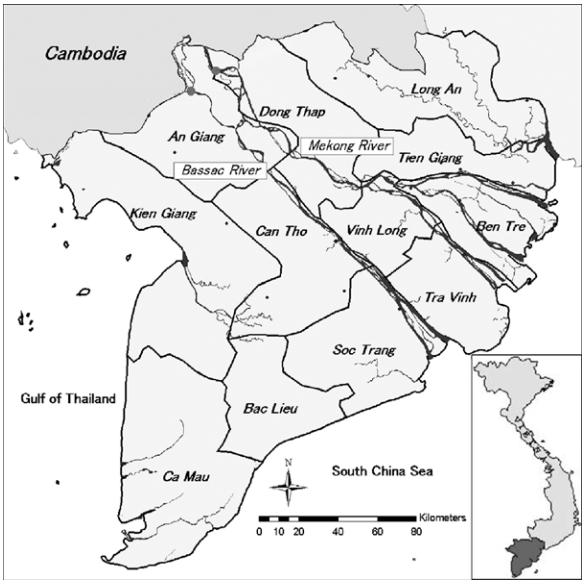

Figure 17: The Mekong River Delta, showing the administrative areas. Also included are the major river channels the Mekong, and the Bassac rivers. Inset is the Delta's position in Vietnam. (adapted from Berg, 2001, and Sakamoto *et al.*, 2006).

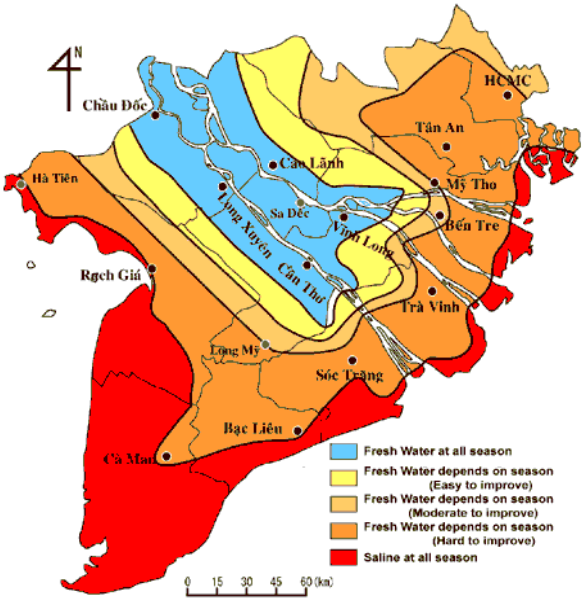

Figure 18: Saline intrusion conditions in the Mekong Delta. (from www.cantho.cool.ne.jp , 2009a).

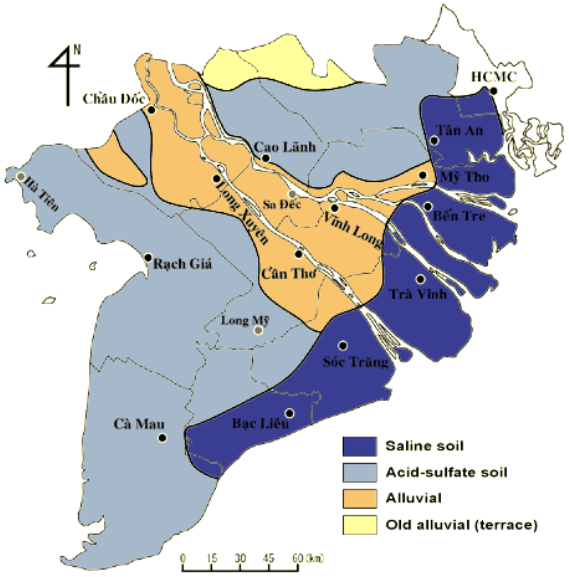

Figure 19: Soil map of the Mekong Delta (from www.cantho.cool.ne.jp, 2009b)

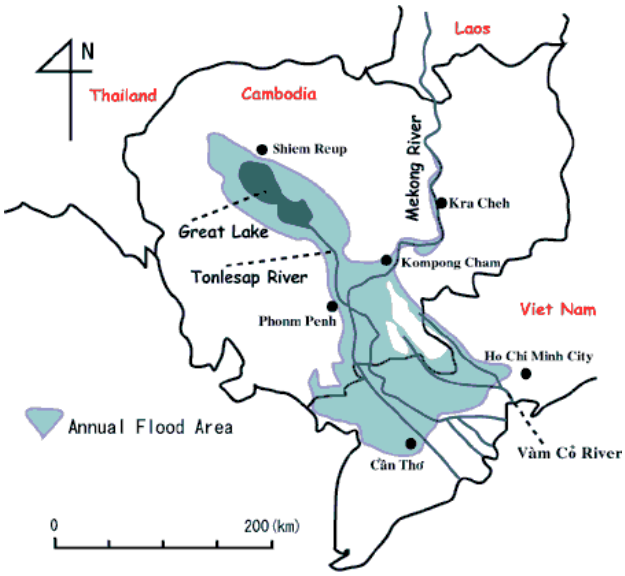

Figure 20: Extent of annual flooding in the Mekong Rivers' lower reaches.
(from www.cantho.cool.ne.jp, 2009c)

3.3. Data used

The hyper-temporal data used were SPOT-VEGETATION 10-day composite NDVI images at $1km^2$ resolution. Images were dated from the 1st April, 1998 to the 21st January, 2008. These were obtained from www.VGT.vito.be, as part of the SPOT S10 product.

The S10 product is derived from the Système pour l'Observation de la Terre (SPOT) program, started by the French Space Agency (Centre National d'Etudes Spatiales, CNES) in which Sweden and Belgium now participate. (Cracknell & Hayes, 2007).
The S10 product is derived from data gathered by the VEGETATION instrument aboard SPOT-4 (launched in 1998) and SPOT-5 (launched in 2002) from 1998 onwards. This is a wide-swath (2200km), low resolution (about 1km) scanner with 4 spectral bands, designed for large scale monitoring of the Earths' vegetation (Cracknell & Hayes, 2007)

This product (described in detail in Maisongrande *et al.*, 2004) is published as de-clouded and geo-referenced images. Quality flags were obtained with the S10 product images which indicated the viability of each pixel. Only pixels rated "good" or higher radiometric quality from bands 2 (Red: 0.61-0.68µm) and 3 (NIR: 0.78-0.89µm), whilst also not having "shadow", "cloud", "uncertain", but "velar" as general quality were retained. All other rejected pixels were re-labelled as "missing".

The red and NIR bands had been used to calculate the NDVI index for each pixel, using the formula in section 1.2. Though the NDVI ration can range from -1 to 1, these NDVI values were converted to unsigned-8-bit integer (with -1 equal to a Digital Number (DN) value of 0, and 1 equal to 255) using the formula:

$$DN = \frac{NDVI + 0.1}{0.004}$$

The 354 images were then stacked. A subset of the images from the 1st January, 2004 to the 21st January, 2008 was extracted to be used in the exploratory phase.

The NDVI product was chosen because it represents a repeated and constant, single measure. This incorporates all the fluctuations in a single aspect of vegetation phenology, consistently over 10 years. Furthermore, with 10 day composites from near daily repeat times, the data can be considered hyper-temporal. Whilst there are alternative products from the MODIS system (of both NDVI and EVI, the Enhanced

Vegetation Index) that could be considered hyper-temporal, and freely available, the SPOT 1km product was assumed to be of an adequate spatial resolution to capture landscape-level gradients. Furthermore with the extensive hyper-temporal dataset, it was seen as an adequate starting point of investigation.

Other data used included the landuse map 2002 of the Mekong delta (see appendix A) and the land use map 2005 of the Mekong Delta (Figure 5) obtained during fieldwork from staff at Can Tho University. These were used in both the determination of rice classes, and in the construction of the land-use map and legend.

3.4. Assessing rice crop calendar variability

3.4.1. ISODATA classification

The 10 year stack of 10-day composite SPOT-VEGETATION NDVI images was classified by unsupervised classification, using the ISODATA clustering algorithm of Erdas-Imagine software (for more information see Leica Geosystems, 2005). The unsupervised classification is simply a process, where a predefined number of classes is obtained with no additional data, or expert guidance (De Bie *et al.*, 2008), from multi-temporal imagery. The classification was run to obtain from 10 to 100 classes with 50 iterations each, and the convergence threshold set to 1.0.

Each iteration performs an entire classification, with the ISODATA algorithm minimising the Euclidian distances to form clusters (Leica Geosystems, 2005; Swain, 1973). The separability of each number of classes was assessed using the Erdas signature evaluator (Leica Geosystems, 2005), measuring the divergence of classes from each other, within a given classification. Average (of all classes) and minimum (between the most similar classes) separability values of divergence were plotted (figure 21), and the optimal number of classes was chosen by visual inspection.

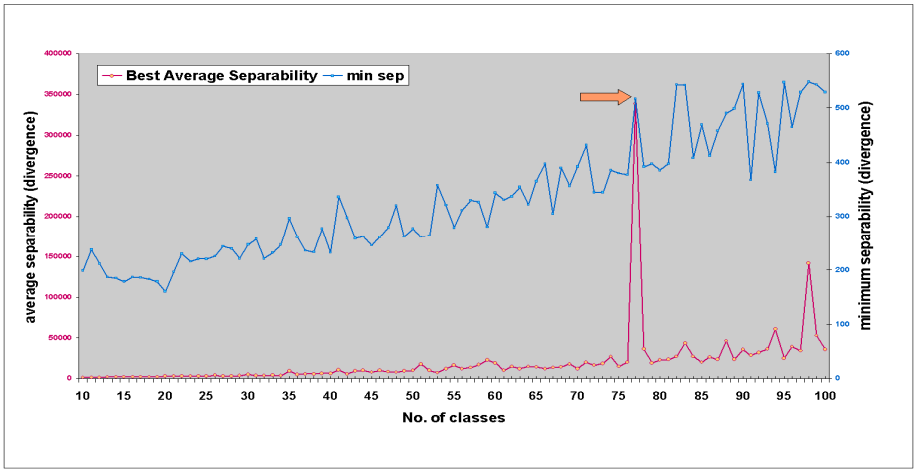

Figure 21: Selection of the optimal number of classes to represent landscape classification in the 10 year SPOT NDVI stack. Average separability (measured by divergence) is graphed in red, whilst, minimum separability is graphed in blue. An orange arrow indicates the peak in average, and the coinciding peak in minimum that indicates that 76 classes is the optimal choice.

Where a peak in the average separability, and/or a peak in the minimum separability occurs, indicates an optimal number of classes. The clear presence of a peak in separability classes at 76 classes indicated the optimal choice. The landuse map 2002 (in appendix A), was subsequently used, to identify NDVI classes where rice was known to be the dominant landuse. Out of the mapped 76 classes, 26 classes were selected to design the sampling scheme for the field work, and for crop calendar characterisation.

3.4.2. Field data collection

Field collection took place between the 21st September, 2008, and the 19th October, 2008. During this time, each of the 26 classes were visited. They were firstly confirmed as being rice producing areas, and secondly sampled.

A clustered randomised representative sampling scheme was applied, with the sampling unit comprising a single rice field. Certain selection criteria applied before a farmer was interviewed. These were:

1 – the field had to be mapped using a hand held GPS.
2 – the farmer had to know the dates of sowing, and harvesting his/her rice crops for the period in question.
3 – the farmer had to know the varieties of rice he/she grew in the field for each crop.

Each farmer was interviewed, with crop calendar (sowing and harvesting) dates and crop rice variety details being collected for all crops grown over the period of August, 2007, to October 2008. Dates were collected in the local lunar calendar, and then subsequently converted to the Western Julian calendar. Whilst the interviews were been conducted, the field boundary was mapped using ArcPad running on an Ipaq. Farmers whose fields were located close to each other tended to sow and harvest within a week of each other. This was due to their reliance on contractors and machine hire for ploughing machinery. These machine operators operate around the region, so farmers in a locality tended to coordinate when they hired the machinists' services.

Overall, all 26 classes were confirmed as rice, and had their crop calendars characterised. Up to seven samples (farmer + field) were taken for each class, with their overall distribution throughout the delta seen in figure 22. In total, 110 samples were collected, though the number of samples did vary between classes, depending on local conditions, and difficulties encountered.

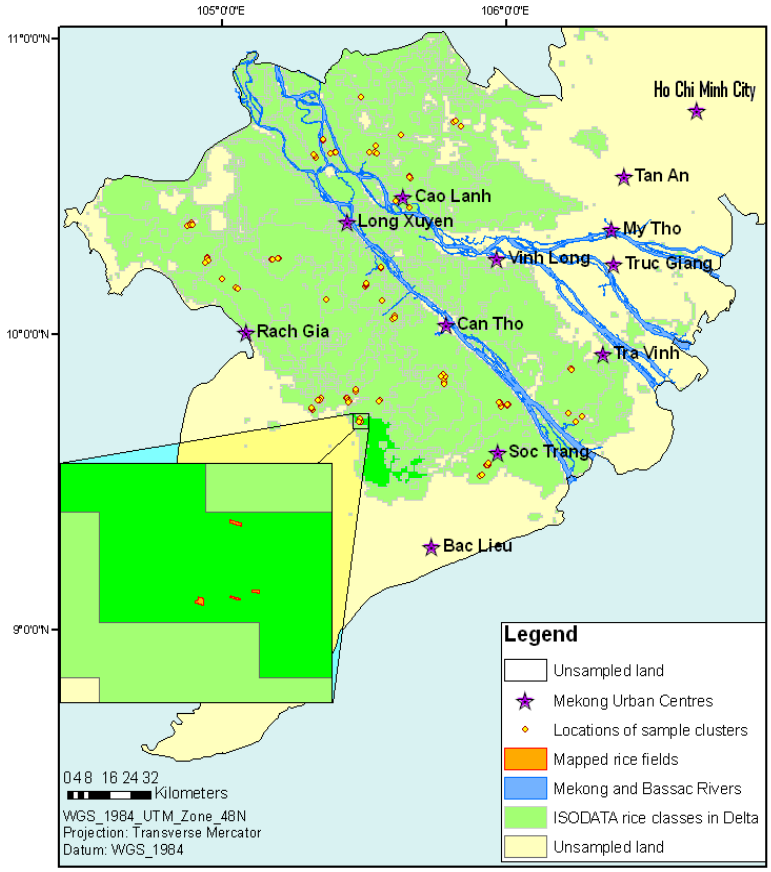

Figure 22: Distribution of the sample clusters over sampled rice area in the Mekong delta. Clusters can contain up to 3 samples, all taken between the 21st September, 2008, and the 19th October, 2008. Inset is an example of one cluster, showing the field distributions within that cluster.

3.4.3. Constructing the landuse map and legend

The final landuse map and legend (Ali, 2009) was intended to contain four primary points of information:

1 - the distribution of rice classes

2 - summaries of the rice crop calendars per class, and the corresponding flooding regime.

3 - details of the predominant rice crop varieties used for each crop in each class

4 - a hyper-temporal NDVI profile representing the NDVI flux over a number of years within the class.

The distribution map was compiled from three main sources of data (figure 23). The 26 rice class distribution map (henceforth referred to as “rice map 2009”) produced by the ISODATA classification formed the core component of the map. From the Landuse map 2005, areas officially known to be rice, were extracted to indicate unsurveyed rice areas. Roadside housing and garden crops, noted during fieldwork to be a major landuse, along the Mekong Deltas road networks, were also extracted from the Landuse map 2005. This served to screen out the detailed small regions that the relatively coarse (1km pixel) NDVI classification could not pick up.

Shapefiles on the Bassac and Mekong river channels, urban centres, Vietnamese, Mekong and Cambodian administrative areas, were then incorporated to provide logical spatial frames of reference to the map. All the data was projected to UTM zone 48N, using the WGS 1984 datum.

This landuse map required a meaningful legend, vital for qualitatively interpreting the results of any promising, exploratory phase method. The legend was compiled from different sources of data (figure 24). Shown in figure 25 is how the legend represented the ranges of sowing and harvesting dates reported by farmers by class. The reported variety of rice grown for each crop, in each class, was the dominant variety grown for that crop period. Meanwhile, supplementary data on problems encountered by farmers concerning environmental conditions were also incorporated as comments.

As flooding is considered a vital part of the rice crop cycle, a flooding component was included. The timing of flooding in each class was determined using the 10 year, SPOT 10-day composite NDVI stack. This was then averaged to create a mean stack of 36 NDVI images spanning a single year, representing the NDVI values of 10 years. The idea was founded on the assumption that low NDVI values indicate flooding (because surface water absorbs light in the NIR spectrum). The assumption has been used in past studies. For example, De Bie *et al*. (2008) used low NDVI values to look at flooding in the Limpopo valley, Mozambique. Xiao *et al*. (2002) noted that fluctuations in NDVI could be used in flood monitoring.

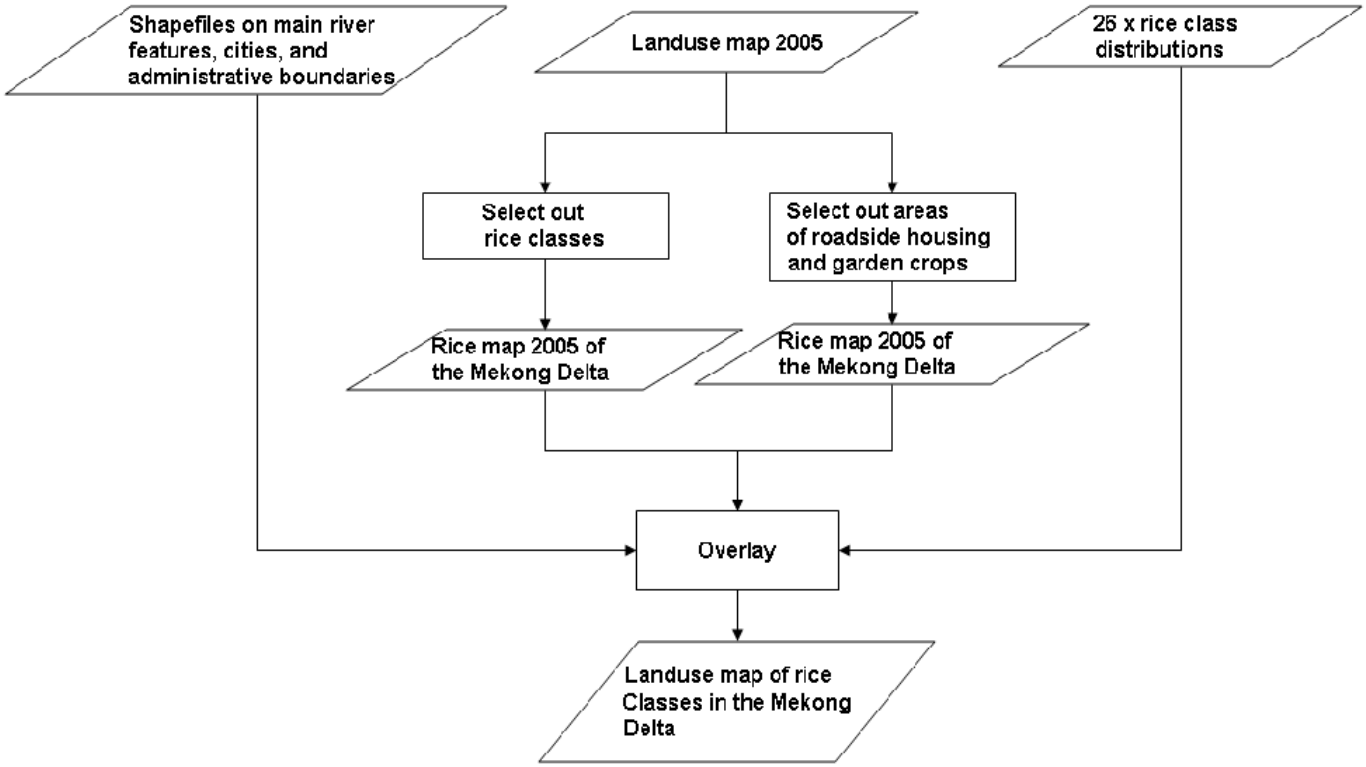

Figure 23: How the Landuse map was compiled using different sources of data.

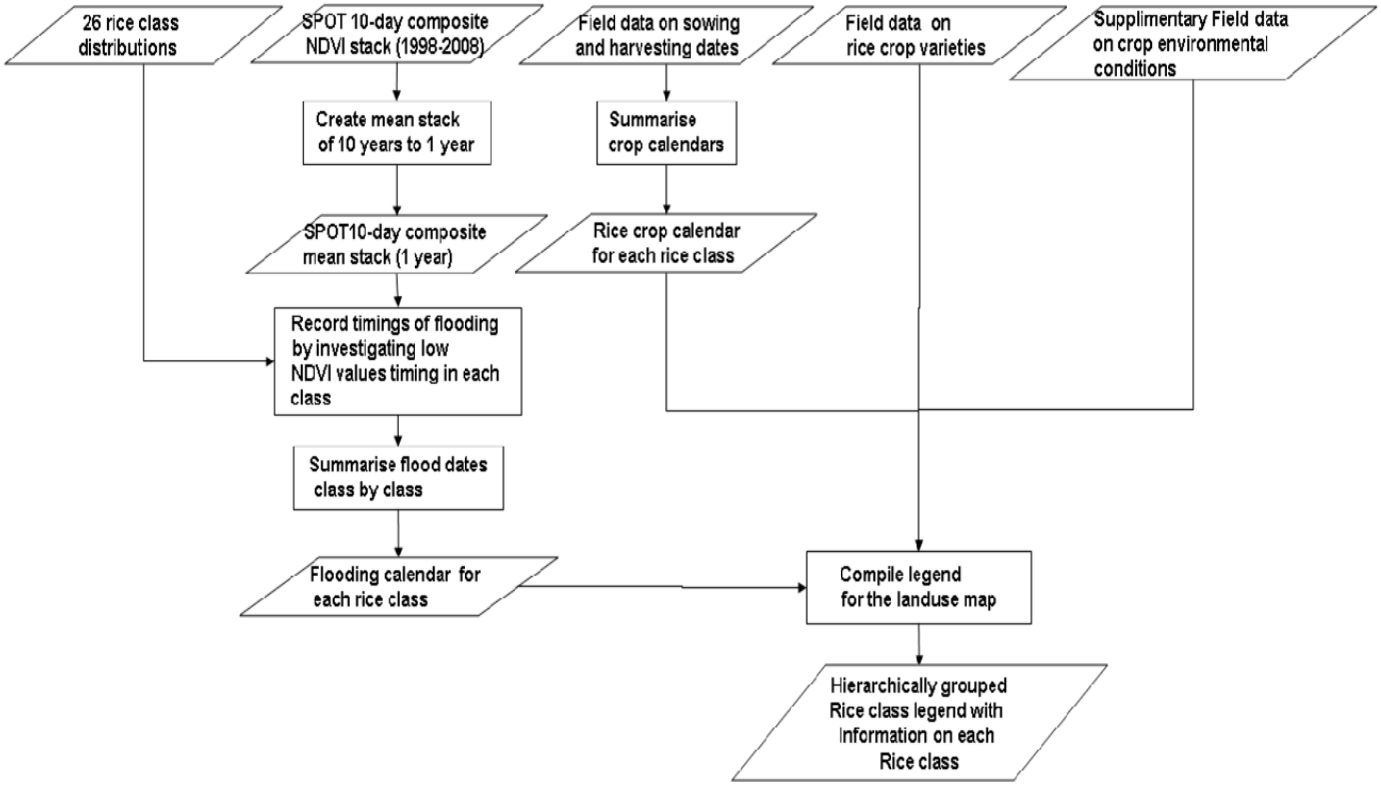

Figure 24: How the hierarchical legend , complementing the landuse map product, was compiled using various sources of data.

Building upon this work, four dates were collected to characterise the flood regime (figure 26). These were:

1 - the date of flood onset (when NDVI values indicative of flooding began to appear in temporal analysis of the rice class in question)
2 - the date of flood peak (when NDVI values indicative of flooding had the maximum extent within the class)
3 - the onset of flood recession (when NDVI values indicative of vegetation began to reappear)
4 - the date of total flood dissipation (when NDVI values representing surface water ceased to recede from the class).

From these four dates, a flood regime was derived (figure 26). Flooding was also classified as partial (where flooding did not entirely cover the class in question) or extensive (where flooding completely covered the class in question).

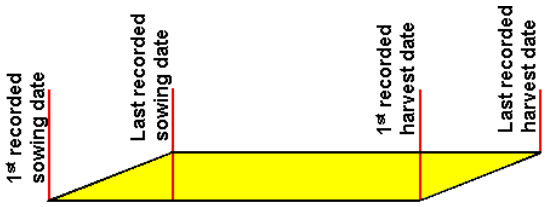

Figure 25: Summarising rice class crop calendars, and representing the variability in the sampled data in the legend product.

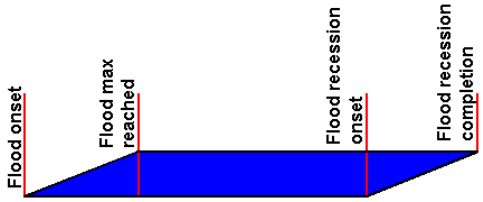

Figure 26: Summarising rice class flood regimes, and representing the variability in the sampled data in the legend product.

Lastly, the hyper-temporal profiles for 3 years (2004 to 2007), for each class were derived from the signature files produced during the ISODATA classification. The flood calendars, crop calendars, predominant rice crop varieties, supplementary information on environmental conditions, and hyper-temporal profiles, were finally collated, to form a meaningful, hierarchical, and informative legend, designed to relate to NDVI.

3.5. Methodologies for extracting boundaries

3.5.1. Principal Components Analysis and region growing

The 3 year stack (2004-2007), unmasked, of hyper-temporal NDVI images contained 111 images, with each pixels having 111 varying values. Piowar and Le Drew (1995) had noted this variability inherent in hyper-temporal datasets, and had envisioned Principal Components Analysis (Chavez &Kwarteng, 1989) as being a possible approach to analyse hyper-temporal imagery. This approach was seen as an adequate starting point for the exploratory phase.

Principal Components Analysis (PCA) essentially compresses bulk of the variability in 111 images into three to four images. It creates a new image band (a principal component) through undertaking an linear transformation of a set of image bands. The components are uncorrelated and are ordered in the amount of variance explained in the data (Eastman & Fulk, 1993). It can be used to compress the information content of n number of bands (images) into fewer than n number of principal component images (Richards & Jia, 1999). Though there are two main types (Standardised and Unstandardised), previous studies have shown that Standardised PCA (Singh & Harrison, 1985) appears to be more effective when used to analyse multi-temporal datasets (Eastman, 1992; Fung & Le Drew, 1987). Standardised PCA was also chosen as it gives each time image equal weighting. The product of the PCA would then be 3 to 4 images summarising the bulk of the variability in the image stack.

The 3 year unmasked stack was entered into a PCA in Erdas (see Leica Geosystems, 2005, for details on how to do so). Only the first four components were extracted, with their accompanying eigenvalues. However, here it must be noted that Eastman and Fulk (1993) made the point that there are no clear guidelines on when to stop the analysis, despite the availability of eigenvalues.

Following PCA, the individual components were overlaid by the 76 class polygon identified by ISODATA classification. (figure 27). For each polygon, zonal statistics in ArcGIS were used to calculate the mean value of that particular component within a polygon (Ai and Aii). The resulting homogenised image (B) was then reclassed into 2 classes, with the assumption that the midpoint of the component (shown in Table 1 represented the transition point within the image (C in figure 27). Whilst for the 1st component, the mid-value was chosen from the image, the subsequent three

components were chosen as 0, the value representing the cross-over between positive variability from the component, and negative. Converting these raster classes into polygons then yielded the boundaries as determined by PCA.

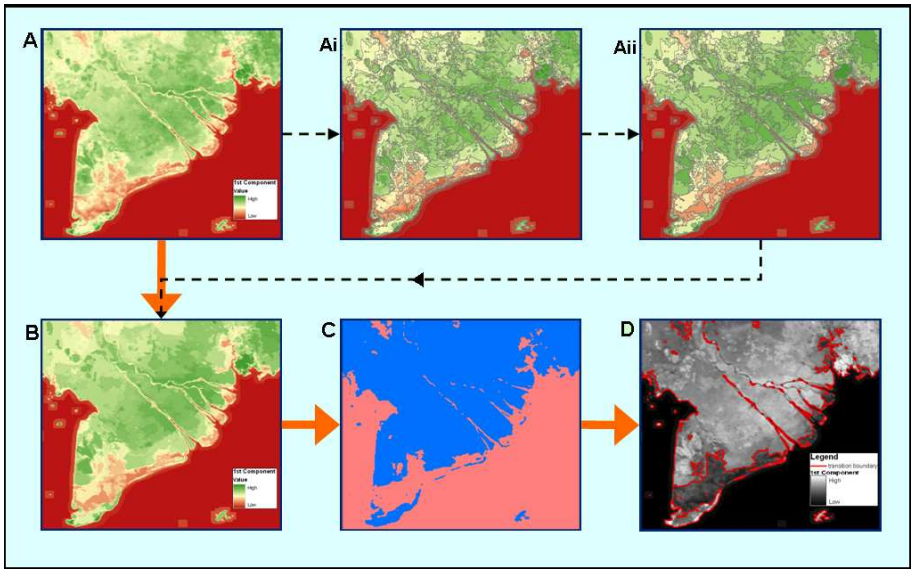

Figure 27: Deriving boundaries from principal components. Shown is the process by which boundaries, representing transition zones in principal components. The original 1st component (A), was overlaid by 76 classes with each polygon being homogenised (Ai, Aii and B). Reclassification produced C, and finally boundaries over the original principal component can be seen in D.

Table 1: Midpoint values of the principal components used to determine reclassification

Component	Midpoint value
1st	1022.54
2nd	0
3rd	0
4th	0

As Saab and Haythornthwaite (1990) noted, time is asymmetrical. PCA takes into account the simple fact that the pixel values vary. However it does not take into account when pixel values vary. This was related to the concept of boundaries, in particular the permanency of a boundary. To encompass this, a new use of edge detection was devised, which could take into account both the asymmetry of time, and the relative permanence or impermanence of gradient boundaries.

3.5.2. Edge Detection

This method developed from the assumption that gradient boundaries, or "natural breaks" in gradient continuums, would logically cause such a change in vegetation phenology, that there would be a rapid shift spatially in NDVI. Leica Geosystems (2005) emphasizes that "there are no perfect edges in raster data, hence the need for edge detection algorithms". These Edge Detection (ED) algorithms can emphasize these rapid changes. For each NDVI image, there was theoretically a multitude of NDVI edges present, ranging from low to high. Further more, some of these edges were repetitive, others successively repetitive, and others still only temporary.

These edges (of varying characteristics), were thus broken down into two groups by this methodology- those edges that the research considered to be representative of gradient boundaries due to their permanence and relative strength, and those that were not considered to be representative, due to their weakness and impermanence. To factor in this logic, a series of edge cleaning steps were incorporated into the methodology (see figure 28 for method outline, or appendix B for method process details). Edges remaining at the end of the process were deemed representative of gradient boundaries, and thus representing the borders of gradient effects regions.

To take into account the permanence or impermanence of boundaries, the methodology incorporated a temporal cleaning process, whilst weak edges were removed following histogram analyses. Edges which were weak overall, and occurred infrequently were also removed.

The 3x3 pixel edge detection method began with the running of all 111 images in the 3 year (2004-2007) SPOT-VEGETATION hyper-temporal stack through the Erdas Imagine edge detection algorithm. Two 3x3 pixel ED models were used (see appendix C for model details in Erdas) – the unweighted prewitt ED model, and the weighted sobel ED model. Sobel was abandoned during the testing process as software issues became evident (see appendix D for details), and began excessively disrupting the process. All edge detected images were shrunk, removing a 2 pixel periphery from every image, account for by image boundary effects. Ocean pixels were also masked out.

A histogram analysis was then done on each edge detected and masked image. All edges below the median value for each image were reclassified (in ArcGIS software), as non-edges (boundaries), and given the value of zero. The principle here was that a value indicating non-edges must be sought from the data itself, hence the

need for histogram analysis. All reclassified images were then converted into binary format (1/0) with a value of 1 representing a potential edge (boundary) and 0 representing a non-edge (boundary). This was done using the binary operation in Erdas Imagine (Leica Geosystems, 2005).

The binary images were then entered into the temporal cleaning phase. Here, each image was multiplied by the image immediately preceding it in time, and the image immediately following it in time (figure 29). For an edge to be kept, it had to be present in both the time image immediately preceding it, and the time image immediately following it (see figure 30). All the multiplication operations were done using the Erdas Imagine operations function (Leica Geosystems, 2005).

The 109 remaining, temporally cleaned, edge images were then run through the "clump" and "sieve" functions of Erdas Imagine (Leica Geosystems, 2005), to reduce the amount of noise in the images. Here, "noise" meant clusters of pixels no larger than 6 pixels in size. Effectively, this meant that the research assumed that a boundary would not occur only at a single spot, but along a series of spots, much like a barrier. Small clusters of spots therefore were not deemed to represent gradient boundaries, but more inconveniences at that time, around which the gradient continuum existed. Following from this logic, all pixel clumps of less than 6 pixels in size were removed (figure 31).

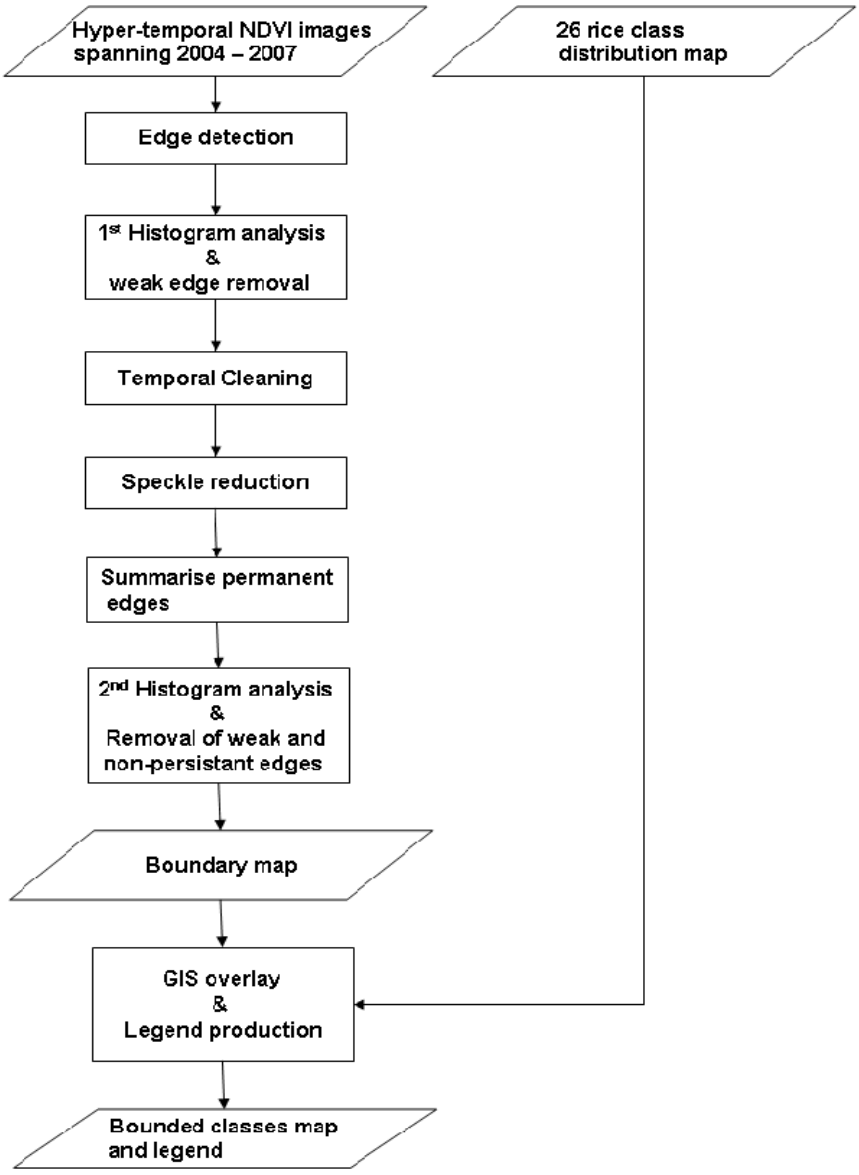

Figure 28: Overall method of extracting gradient boundaries using the edge-detection method.

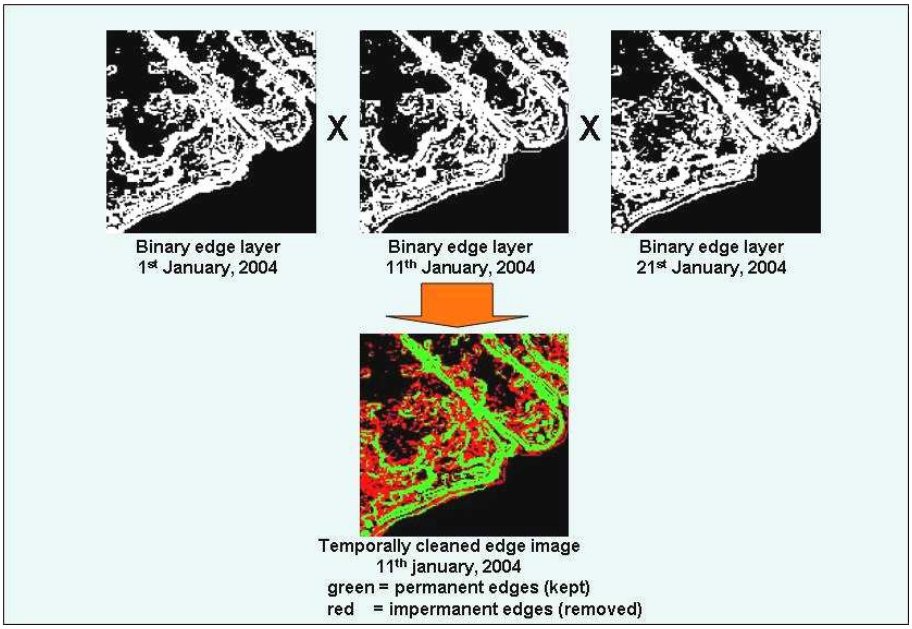

Figure 29: Temporal cleaning of edge detected NDVI image from the 11th Jan., 2004. The temporally cleaned product shown here, also incorporated those edges which had been removed.

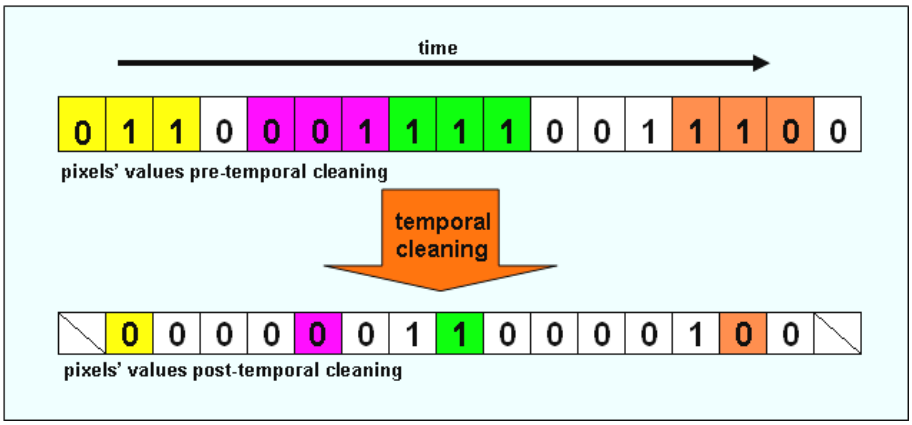

Figure 30: Temporal cleaning of a single pixel. 1 indicates edge present, 0 indicates no edge present. Edge values pre cleaning, are modified according to whether they are present three successive times in the hyper-temporal stack.

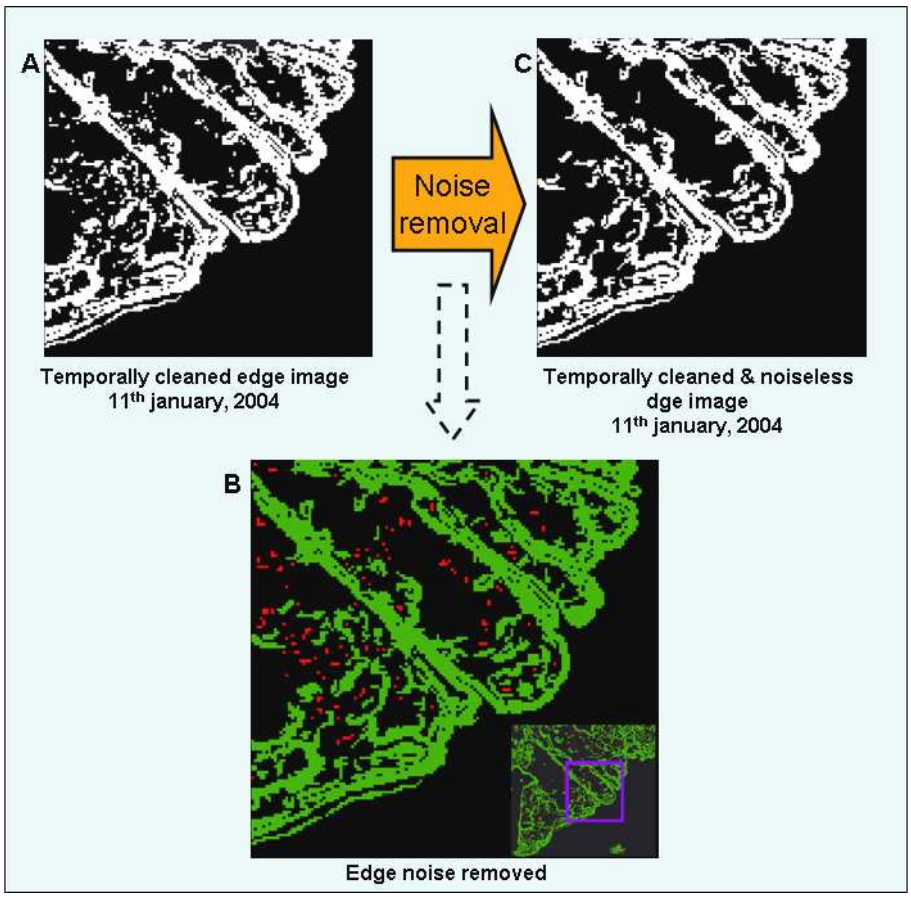

Figure 31: Noise reduction of the temporally cleaned images. Image A is the temporally cleaned image of the 11th January, 2004. Following noise removal, small clusters of pixels (seen as red in image B) were removed, produced the temporally cleaned and considered noiseless image C. Inset in B is the shown area's location in the delta.

The 109 (11th January, 2004 – 11th January, 2007) noise reduced, and temporally cleaned edge images (in binary format) were each multiplied by its' corresponding edge detected image, using the multiply operation in Erdas Imagine. This produced 109 images of edges of varying strengths which has been temporally cleaned and noise reduced. The 109 images were then summed, and the result divided by 109, to get a summary of the average strength of permanent edges in time, over the 3 year period (see figure 32). The summary contained information not only on the average strength of an edge, but resulting from the division by 109, it also introduced a measure of the edges' permanence.

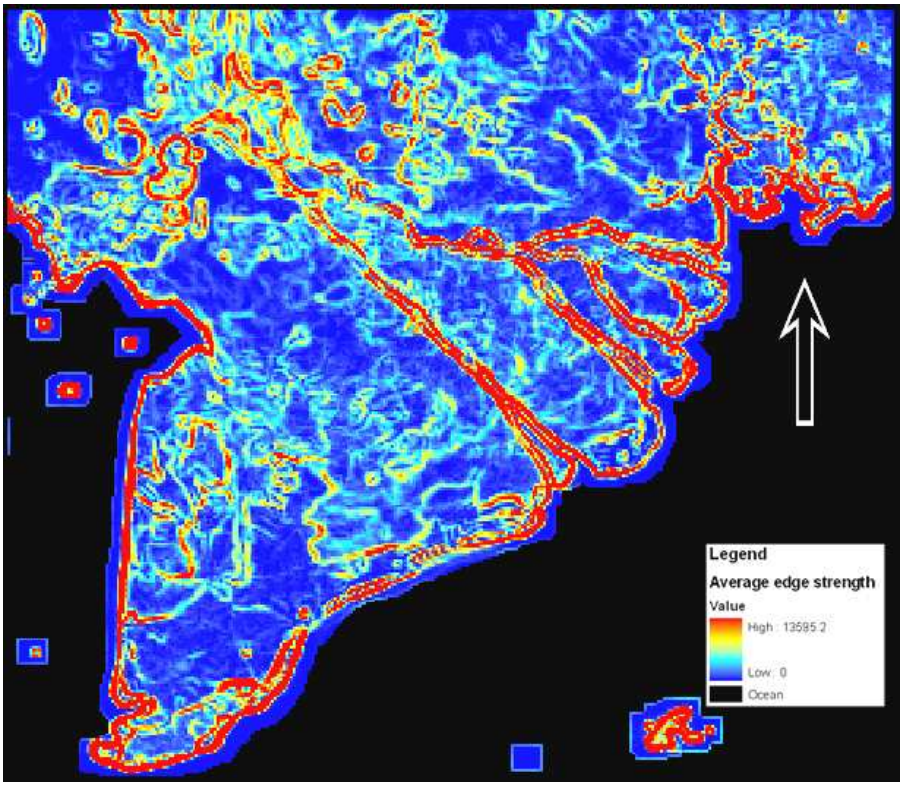

Figure 32: Average strength of permanent edges in the NDVI hyper-temporal stack.

Further edge cleaning was needed, though of a different nature. Edges that were both strong, and persistent, were recognised as representing "true" boundaries. Likewise, edges that were infrequent, though strong when they existed, were also recognised as "true" boundaries. If an edge was of a middle strength nature, though did persist throughout the time period, it too was recognised as a "true" edge. However, edges that were consistently weak, and infrequent, were considered as non-boundaries, and had to be removed (table 2).

Table 2: Is an edge a "true" boundary or not? Logical criteria for evaluating the temporally cleaned and noiseless edges.

Edge strength	Edge persistence	Overall average value	"true" edge?
High	Persistent	High	Yes
High	Infrequent	Medium	Yes
Low	Persistent	Medium	Yes
low	Infrequent	Low	No

To achieve this selection, a second histogram analysis of the edge images was performed in Erdas Imagine. However, as the histogram was extensively skewed (figure 33a), a log derivative of the average image was made which had a more useful histogram (figure 33b). Here, weak edges were deemed to be those with values below that of the mode in the log image. Any pixels with such values were reclassed as non-edges. Any edges remaining were subsequently converted to binary (with 1 indicating a "true" edge, and 0 indicating no edge). These "true" edges were then assumed to represent natural breaks in gradient continuum, thereby delineating the boundaries of gradient effects zones. The end product was a map of gradient boundaries extracted using a 3x3 pixel edge detection kernel.

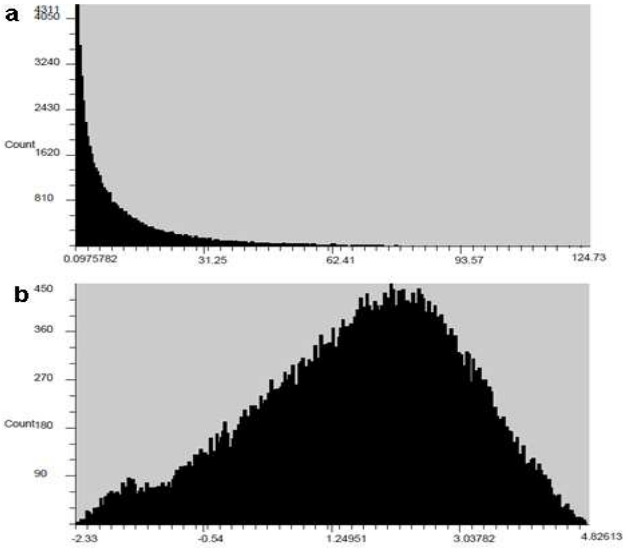

Figure 33: 2nd histogram analysis, finding the "true edge". Histograms of the summarised average edges image shown in figure 33 (a), and the log of summarised averaged edges image (b).

Following the production of boundary maps by using a 3x3 pixel edge detection method, it was noted that larger template arrays provide greater noise immunity, despite being computationally more demanding (Leica Geosystems, 2005). With this in mind, it was to edge detect using a 5x5 pixel window, to see if it would produce more gradient representative boundary images.

Two problems were encountered here. Firstly, the kernel had to be defined. To achieve this, an adaptation of the unweighted 3x3 prewitt window was used (figure 34). Secondly, with a 5x5 pixel window, edge detection had to occur in four directions, and not two as is all that is possible using a 3x3 window. To achieve this, a 3x3 prewitt model in Erdas (shown in appendix C) was adapted to incorporate

four 5x5 windows moving in the directions North, East, Southeast, and Southwest (figure 34). These directions were chosen as they do not cancel each other out.

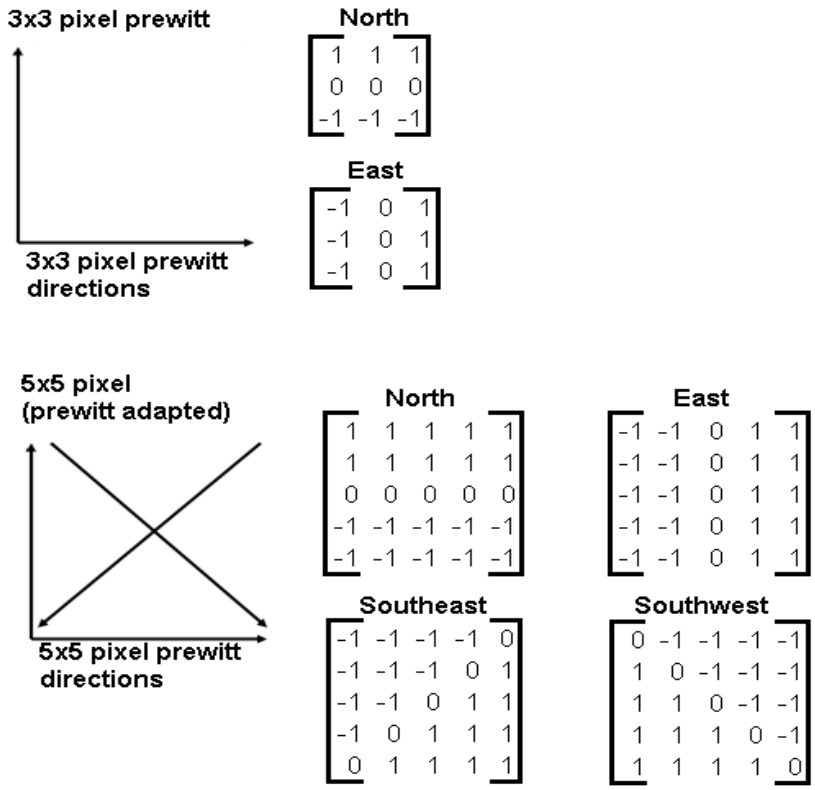

Figure 34: Directional and kernel differences between the 3x3 edge detection prewitt model, and the 5x5 model adapted from the prewitt model in Erdas Imagine. Kernels show the weightings of surrounding values in determining the ultimate centre value.

Meanwhile, the distance function employed by the 3x3 prewitt model in Erdas, taking the form of :

$$edge = \sqrt{(edgeNorth)^2 + (edgeEast)^2}$$

was adapted to take into account of four variables, and not just two. This gave it the form of:

$$edge = \sqrt{(edgeNorth)^2 + (edgeEast)^2 + (edgeSouthwest)^2 + (edgeSoutheast)^2}$$

Following the production of 5x5 kernel edge detected images by the improvised model, the same process was employed as for the 3x3 model. There was an alteration to the method concerning noise reduction. The 5x5 window tended to produce wider edges. Hence, with noise reduction, a decision was made to remove larger groups of pixels. Pixels groups of less than 10 pixels were therefore removed as noise. The end product was a map of gradient boundaries extracted using a 5x5 pixel ED kernel.

3.6. Product Comparison

Following the production of a landuse map and legend, boundaries for each of the four principal components, and edge detected boundaries from both the 3x3 kernel ED, and the 5x5 kernel ED, the products were overlaid and visually inspected. Comparisons and contrasts were made between the different boundaries produced, and how they might be interpreted in looking at the landuse map and legend.

The resulting permanent boundary maps from the edge detection methodologies were combined with the 26 rice 2009, and the 76 classes, produced by the ISODATA classification. This was done to evaluate whether or not the region successfully grouped ISODATA classes. The 76 classes were also combined with the collated principal components boundaries.

The various boundaries were finally compared to two basic RGB composites of the principal components. An RGB:1st, 2nd, and 3rd component, and an RGB 2nd, 3rd, and 4th component were made for this purpose. These were combined with the 76 ISODATA classes, the 3x3 and 5x5 edge detected boundaries, and the boundaries produced by principal components.

In all combinations, coincident boundaries were noted, as were those aspects of boundaries which did not coincide. Features of interest, such as the spatial characteristics of classes in areas where boundaries from either edge detection or principal components were present, were also noted.

4. Results

4.1. Assessing rice crop calendar variability

4.1.1. ISODATA classification

Figure 35 shows the distribution of the 76 land classes (the 76th was the class representing open-ocean and has been removed) identified using the ISODATA clustering algorithm. From the separability analysis (figure 21 in chapter 3), it was determined that 76 classes best classified the landscape into distinct classes. From the 76 classes, 26 classes, officially known in 2002 to contain rice, were selected to sample during field data collection. This yielded the rice distribution map shown in figure 36.

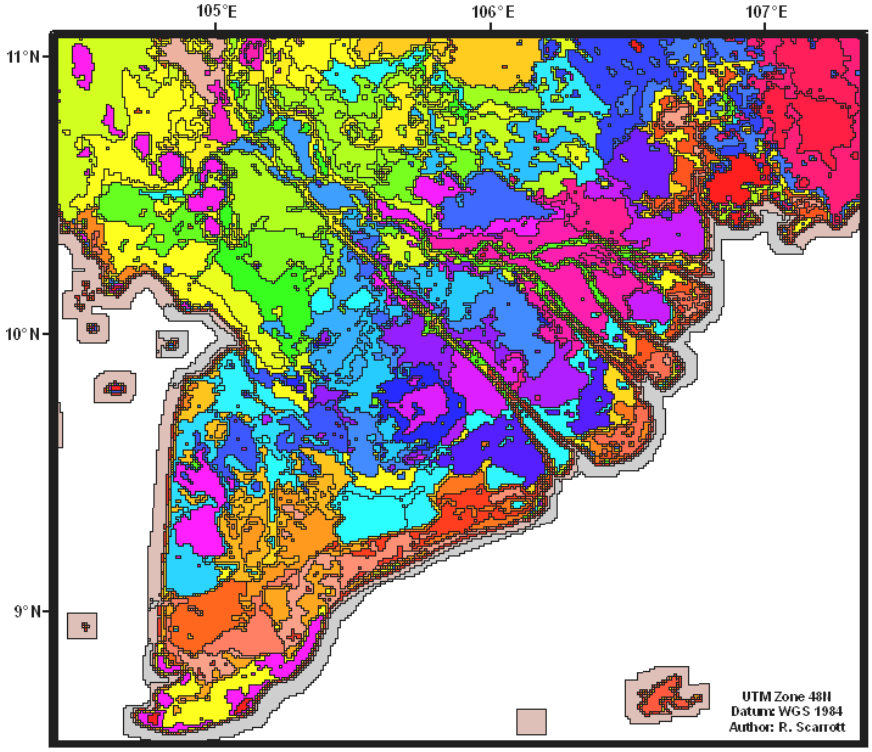

Figure 35: Distribution of 76 classes identified by ISODATA classification of the 10 year SPOT NDVI hyper-temporal image stack.

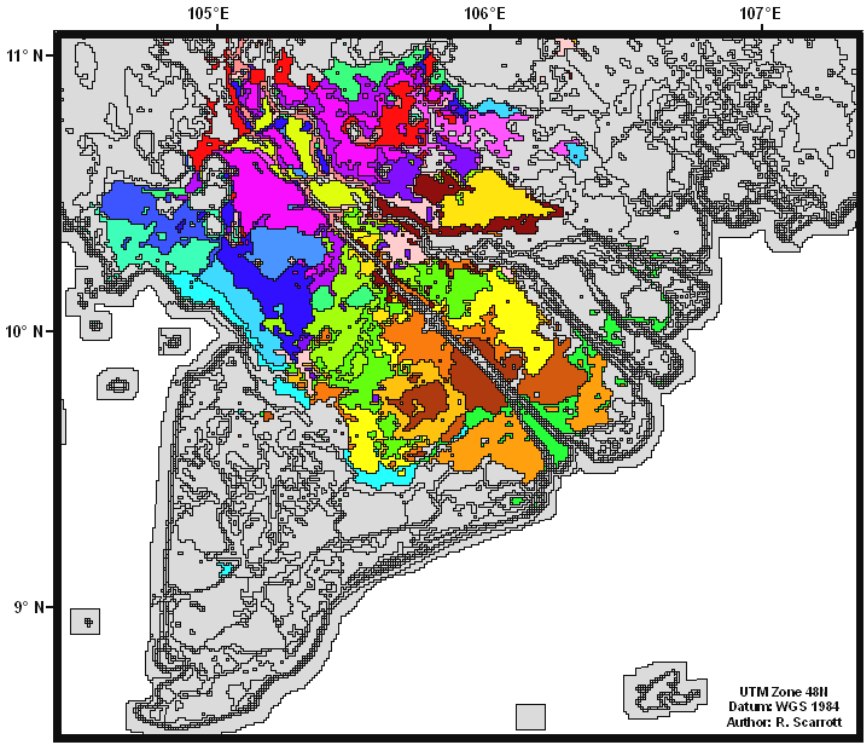

Figure 36: Classes identified and sampled as rice, and extracted from the 76 class distributions. Classes were identified as containing rice by comparison with the 2002 landuse map, and sampled during field data collection.

4.1.2. Landuse map and legend

Shown in figure 37 and figure 38, are the landuse map and legend derived from a combination of ISODATA classification products, and data collected in the field (courtesy of Ali, 2009). The map (figure 37) shows the distribution of sampled rice classes (identified during the ISODATA classification process) across the Mekong Delta. The map also shows areas of rice that were left unsurveyed during fieldwork. Roadside housing and homestead gardens have been removed from the classes to highlight purer rice areas. Meanwhile, the Mekong and Bassac river channels are included to provide a means of reference.

Included in the map is a summary mini-legend, highlighting the variety of flooding conditions experienced by each class grouping, and the cropping systems in evidence across the delta ("2x Rice", and "3x Rice"). Classes were grouped hierarchically on the basis of the flooding they experience. These hierarchical

groupings are represented by a letter in the mini-legend, which links to the more extensive, and detailed legend shown in figure 38.

The primary legend (figure 38) displays information relating to the variability in environmental conditions across the delta. Individual classes are coloured to match with the map (figure 37). Furthermore, the number of samples used to characterise each class during fieldwork is also shown.

Information on environmental conditions deemed noticeable to farmers is available in the form of comments on salinity and alkalinity with the associated classes. Note that some classes (e.g. classes 42, 29, and 33) experience problems with acidity when trying to grow rice. Meanwhile, overcoming salinity conditions is required in classes 61, 46, and 66.

The legend also shows information concerning the temporal characteristics of the landscape. For example, crop calendars appear to demonstrate a high variability. For example, variation in harvesting dates can be seen between classes 28 and 41. Here, the farmers only started harvesting the 2nd crop in class 41, following the total harvesting of the crop in class 28. Meanwhile, class 42 is in the middle of its' 2nd crop cycle. Likewise, the 3rd crop of class 51 is already sown, whilst the 2nd crop in class 28 is not yet harvested. This indicates a degree of temporal variability in crop calendars.

This temporal variability can also be seen in the flood regimes. For example, flooding onset dates vary by up to 5 weeks between classes 32 and 29. Furthermore, the period of inundation experienced by various classes differs considerably. Class 32 experiences flooding for approximately 16 weeks. In contrast, class 42 is inundated for only 7 weeks. Stark contrasts can be seen between those areas where flooding is controlled (e.g. class 54) and those which experience uncontrolled flooding (e.g. class 53).

Concerning flooding, the hierarchical grouping reveals a variety of flooding conditions experienced by rice crops across the delta. Classes can be flooded, or remain outside any flood influence. Within flooded classes, the flooding can be controlled or uncontrolled, and further still, the flooding can be partial, or extensive.

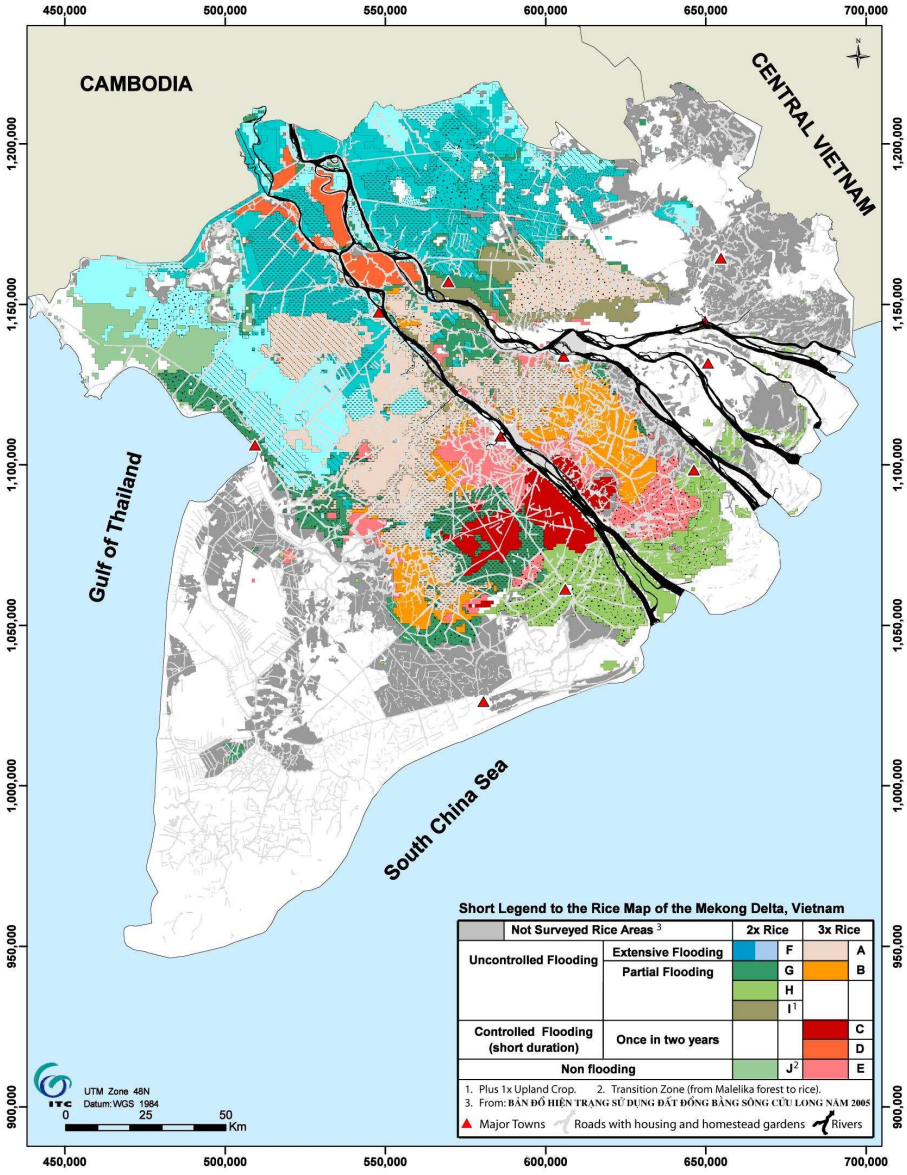

Figure 37: The landuse map, and mini-legend, derived to appraise variability in rice and environmental conditions across the Mekong Delta area.

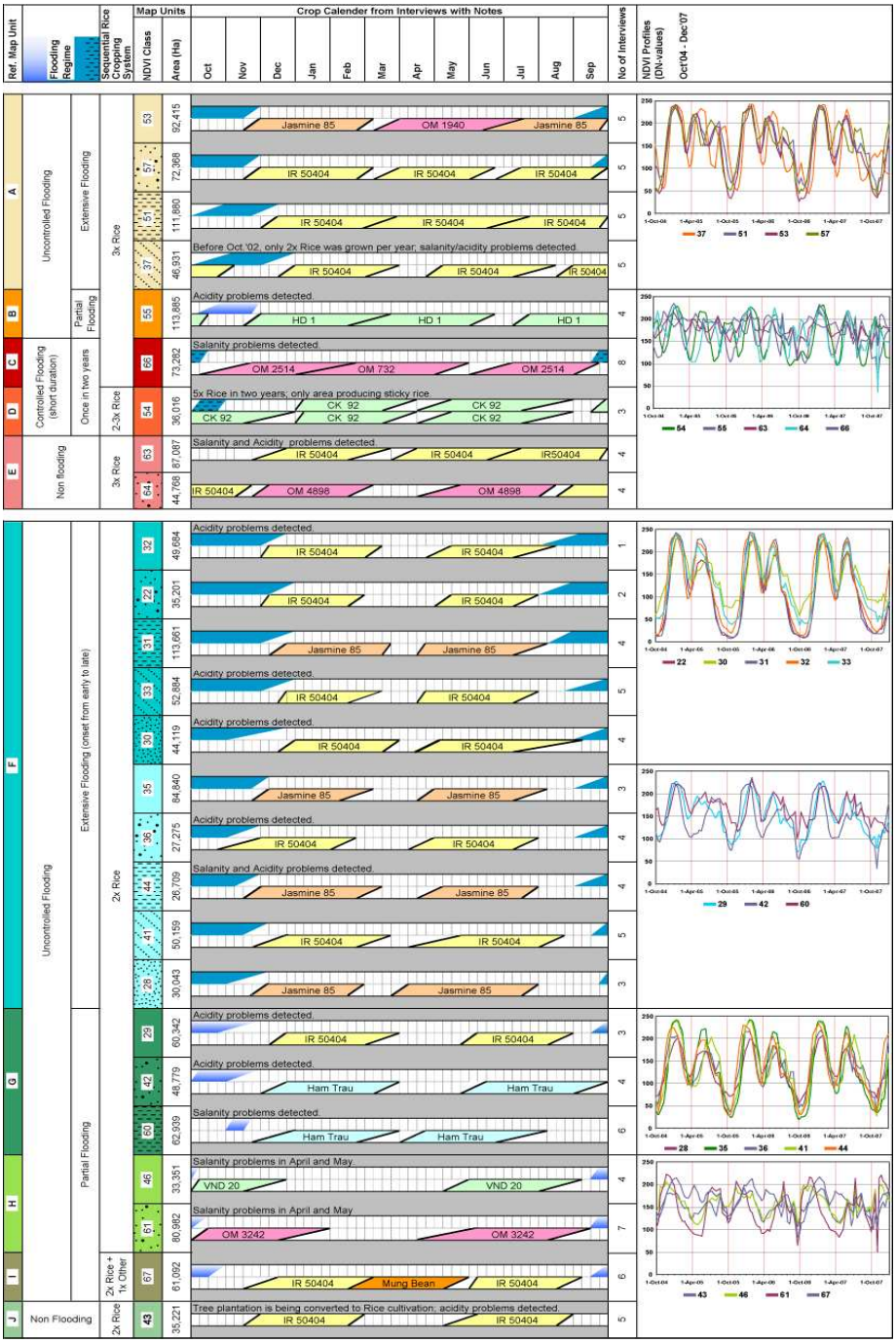

Figure 38: Detailed legend complementing the landuse map. Rice class groupings are linked to the landuse maps' mini-legend by way of alphabetic letters on the left-most margin.

Also depicted in the legend, is the multitude of rice varieties (with their specific adaptations to variations in environmental conditions) grown across the delta. For example, in class 54, variety CK-92 is grown, whilst other classes grow IR-50404 (class 63, 22 and 41). Still others grow Jasmine-85 (classes 31 and 28), or Ham Trau (classes 60, 42).

Varieties also change within classes. For example, in class 53, Jasmine-85 is grown as the 1st crop, is replaced by OM-1940 for the second crop, and reverts back to Jasmine-85 for the 3rd crop. Likewise, in class 66, OM-2514 is grown as the first crop, shifting to OM-732 for the second, and back to OM-2514 for the third.

Overall, there is evidently variability in the conditions experienced by farmers such as alkalinity, salinity, rice varieties, and flood extent across the delta. Furthermore there appears to be extensive temporal variability in not only flood regimes, but also in rice crop calendars.

4.2. Methodologies for exctracting boundaries

4.2.1. Principal Components Analysis

Shown in Figure 39 are the 1st four components of the PCA performed on the 3 year hyper-temporal NDVI images stack. Each component displays a progressively smaller proportion of the variability attributable to that component's axis (shown in table 3). Consulting the supplementary eigenvalues, produced with the components, it could be seen that together, the 1st four components summarised 89.41% of the variability within the hyper-temporal dataset. The eigenvalues for all components can be found in appendix E.

Boundaries for each component were successfully extracted (see figures 40 and 41). Each component displayed visually sharp transition areas (e.g. at points A, and B in figures 40 and 41), which were used to define the boundaries. A summary of all four component boundaries can be found in figure 42. All boundaries extracted, and the principal component from which they were extracted, can be found in appendix F. Furthermore, in looking at solely the principal components and their boundaries, some interesting points can be noted. For example in looking at figure 43, it can be seen that the boundaries extracted did not successfully delineate some features (e.g. feature A in figure 43).

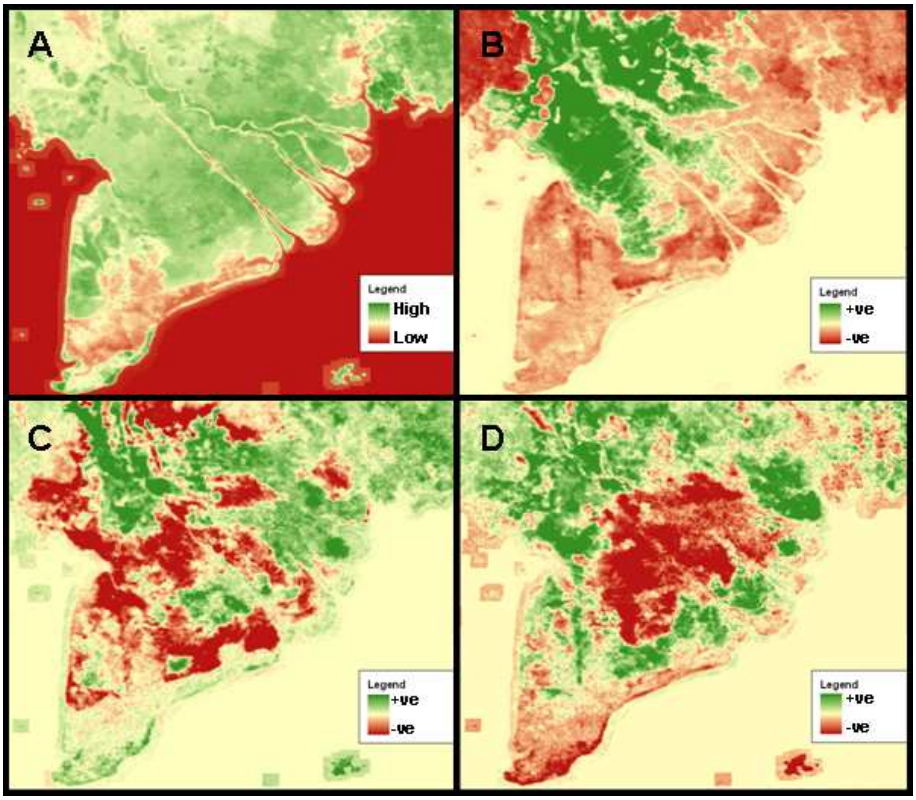

Figure 39: Principal components from a Principal Components Analysis of a 3 year hyper-temporal dataset. 1st (A), 2nd (B), 3rd (C), and 4th (D) component images are shown. (All images are in UTM Zone 48N, using the datum WGS 1984).

Table 3: Proportions of hyper-temporal stack variability, attributable to each principal component.

Principal Component	**Proportion of attributable variability**
1st Component	79.41%
2nd Component	7.57%
3rd Component	1.50%
4th Component	0.93%
Subsequent Components	10.59%

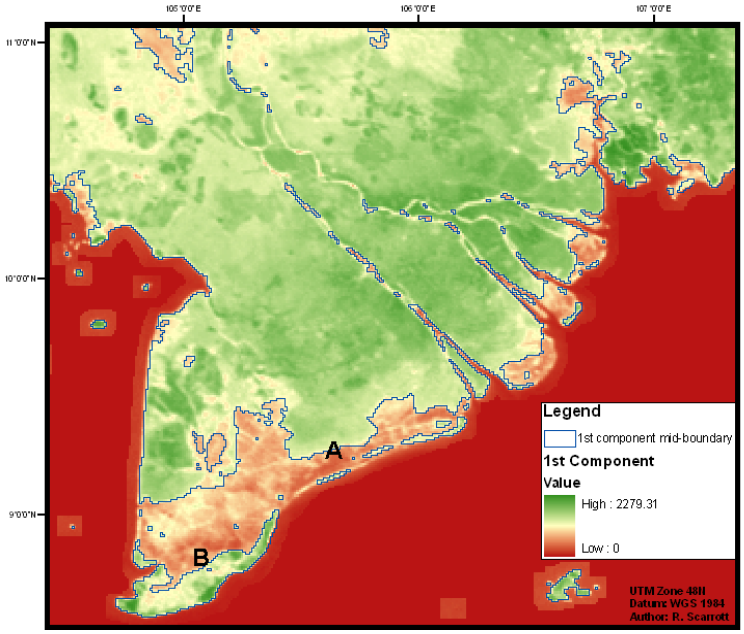

Figure 40: 1st Principal component, and mid-value boundary. The mid value of 1022.54 was used to divide the image into two classes, and define the boundary

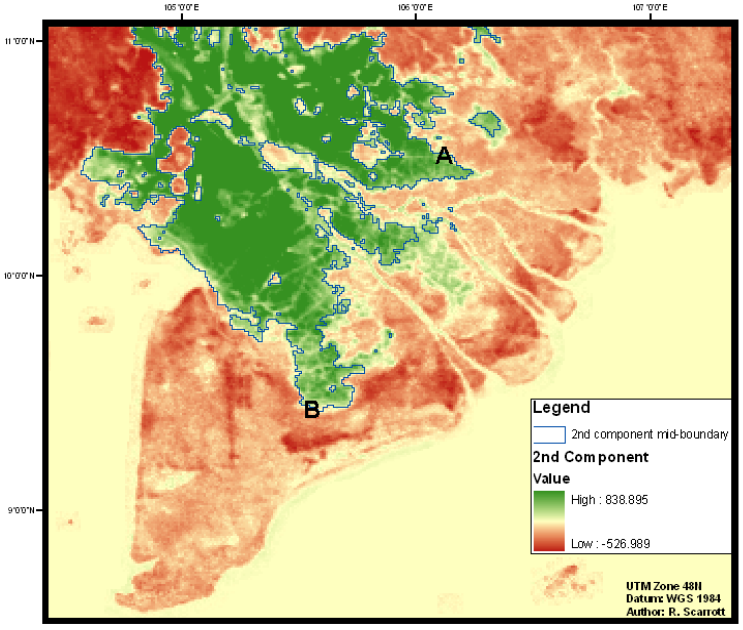

Figure 41: 2nd Principal component, and zero-value boundary. The mid value of 0 was used to divide the image into two classes, and define the boundary

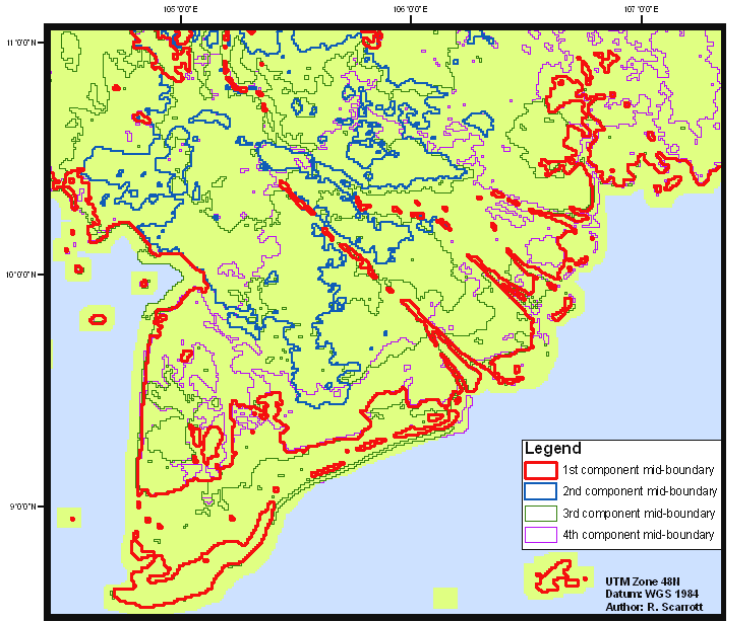

Figure 42: Four boundaries extracted from the 1st four principal component images.

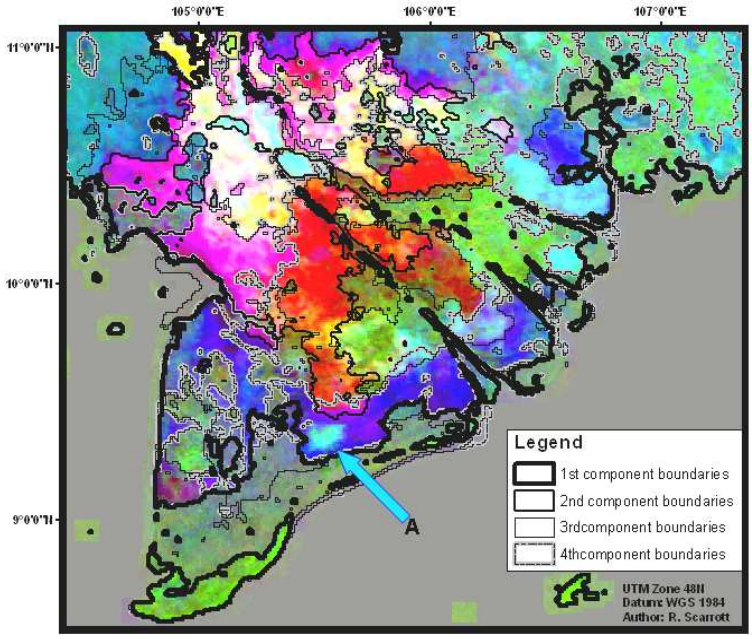

Figure 43: Component boundaries and principal component composites. RGB (2nd, 3rd, 4th principal component) image overlaid by the four mid-value boundaries as identified from the principal components.

4.2.2. Edge Detection

Shown figure 44 are the boundaries extracted by the 3x3 and the 5x5 ED methods. Both methods were successful in producing bounded regions (as can be seen in figure 44). However, the two methods extracted visibly different boundaries. Figure 45 shows the common pixels extracted by both methods (green). It also shows those pixels, which were extracted by one method, but not extracted by the other.

These also show a patterning in their distributions. Those edges extracted by the 3x3 method are more spatially spread out, and are located further away from the commonly identified edge pixels. In contrast, those solely identified by the 5x5 method, appear to be restricted to either side of commonly identified boundaries.

These differences in identified boundaries, have also resulted in a difference of regions bounded by those boundaries. As can be seen in figure 44, these regions can differ considerably in spatial extent.

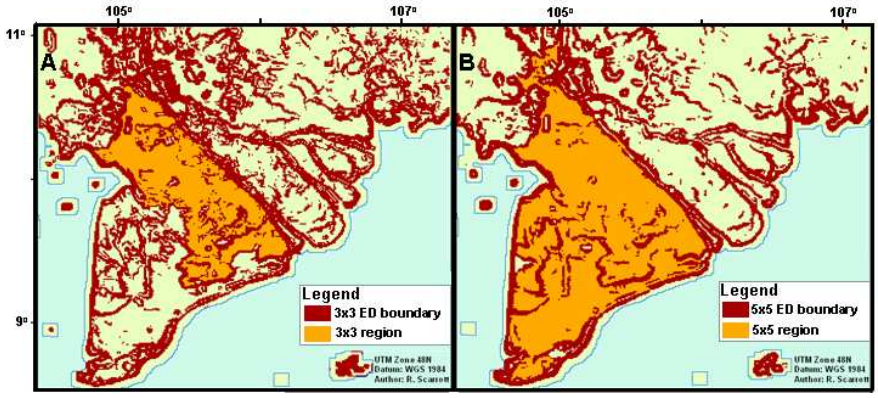

Figure 44: Boundaries and regions extracted using the pixel edge detection methods. A shows those edges extracted by 3x3 kernel edge detection, and a sample region as defined by these boundaries.
B shows edges extracted by 5x5 kernel Edge Detection, and a sample region as defined by these boundaries.

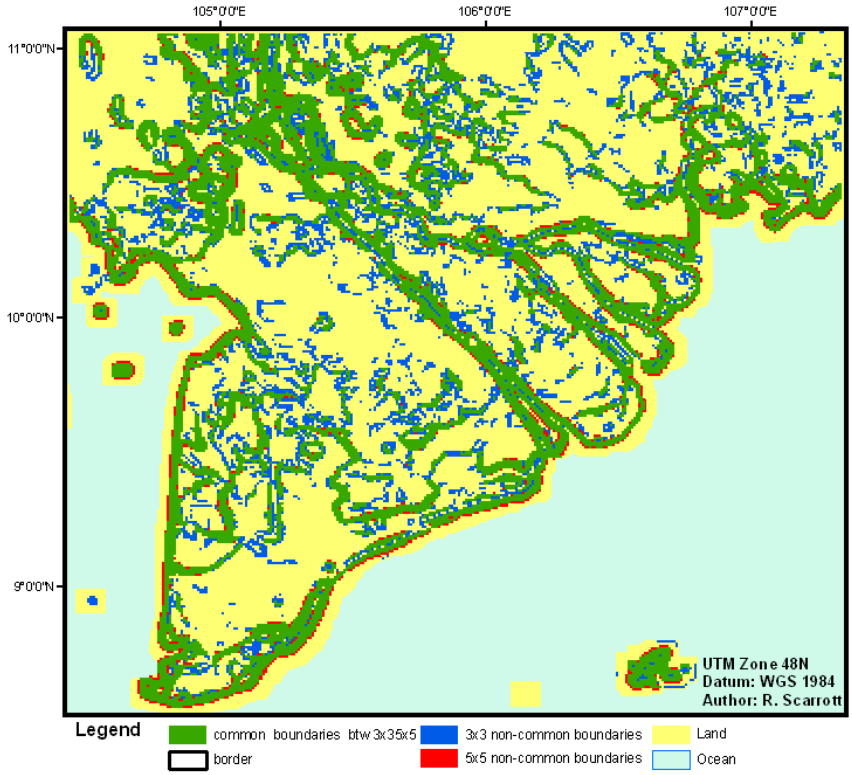

Figure 45: Contrasts in derived edges. Pixels identified as edges by both methodologies (green), and those identified as edges by only one of either of the two methodologies (red, or blue).

4.3. Product Comparison

Figure 46 shows a combination of the boundaries extracted from the 4 principal components, and the 76 classes identified by ISODATA classification. The component boundaries are overlaid in an order derived from the proportion of variability they summarise. Hence, the 1st component (summarising 79.41% of the variability) is overlaying the 2nd (7.57%), which further overlays the 3rd component (1.50%), all of which overlay the 4th (0.93%). In this way a hierarchy has been established, which is derived from their contribution to the dataset. It could be viewed as the larger regions derived from the 1st Component, are subdivided by the 2nd, which are subdivided again by the 3rd, and again by the 4th. Despite the extensive subdivision, within the areas left, it can be seen that IDODATA still derived multiple classes.

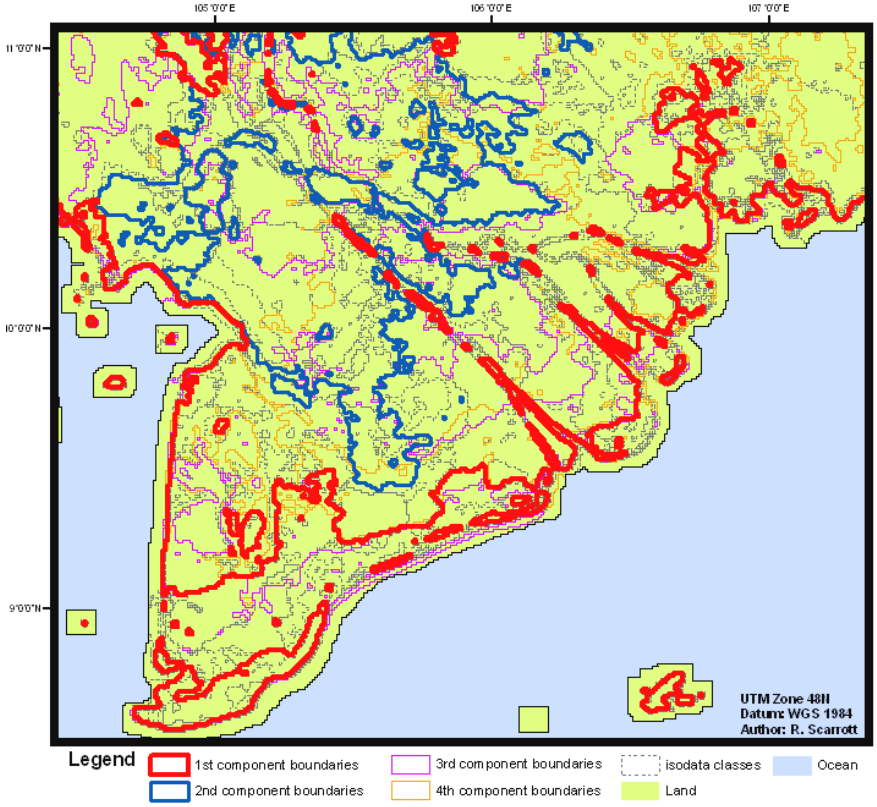

Figure 46: Principal component boundaries identified overlaying the 76 ISODATA classes.

These principal component boundaries also show visibly identifiable similarities to those identified by ED. Both those boundaries identified by the 3x3 ED method (figures 47 and 48), and the 5x5 ED method (see Appendix G) show remarkable boundary overlap with portions of those boundaries identified from the PCA. These edges identified by ED, often overlay the areas of rapid transition from which the principal component boundaries were derived. A, B, and C, in figures 47 and 48, show principal component boundaries overlaying boundaries extracted using the 3x3 kernel ED method. Comparable images of the 5x5 kernel ED boundaries can be found in appendix G.

When the 76 classes identified by ISODATA clustering, were compared to the principal component images, further notable features were revealed (figure 49). As can be seen, overlaying the 76 classes on the 2nd Component (as an example) revealed some interesting features highlighted at A, B, and C. These highlighted areas are visually distinct from their surrounding areas according to PCA, in a

pattern that is spatially coherent with that outlined by ISODATA classification. Whilst not all classes stand out as being so distinctive, some features of the various components do appear to be expressed by ISODATA classification. Other examples can be found in appendix H.

In looking at false colour composites of the different components, the same characterisation of classes as occurred with individual components is apparent. For example, in figure 50, overlaying a RGB:1st, 2nd, 3rd Component composite with the 76 ISODATA classes reveals similar class characterisation to that shown by the 2nd component (figure 49). Of interest, the feature at B in figure 50, though showing strongly in the composite image, is not featured as distinct by ISODATA classification. Figure 51 shows another composite, with the 2nd, 3rd and 4th components combined in an RGB image. Note that whilst the principal components composite feature at A, visibly matches the overlying ISODATA class, at B, a visibly distinct feature is not distinguished by ISODATA clustering. Furthermore, though the 4th component only summarises 0.93% of the variability, it is enough to draw out ISODATA classed features such as those at C, which have been missed by the 1st three components (figure 51).

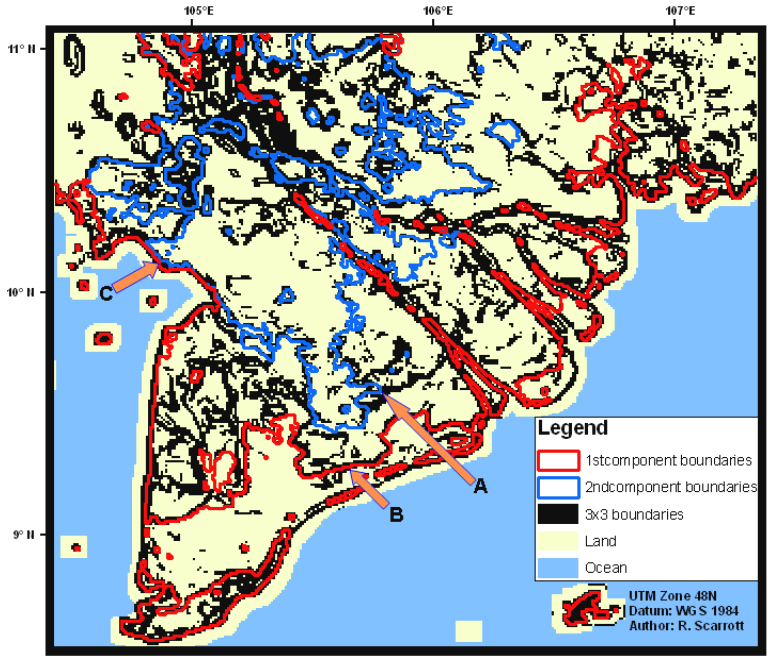

Figure 47: Comparing boundaries from 3x3 edge detection, and those from the 1st and 2nd Principal components. Arrows indicate notable areas where boundaries coincide.

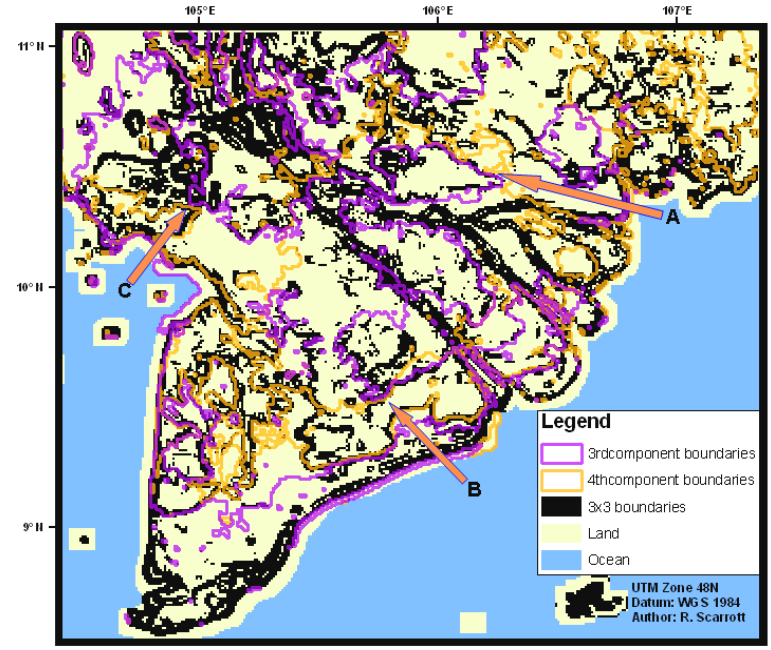

Figure 48: Comparing boundaries from 3x3 edge detection, and those from the 3rd and 4th Principal Components. Arrows indicate notable areas where boundaries coincide.

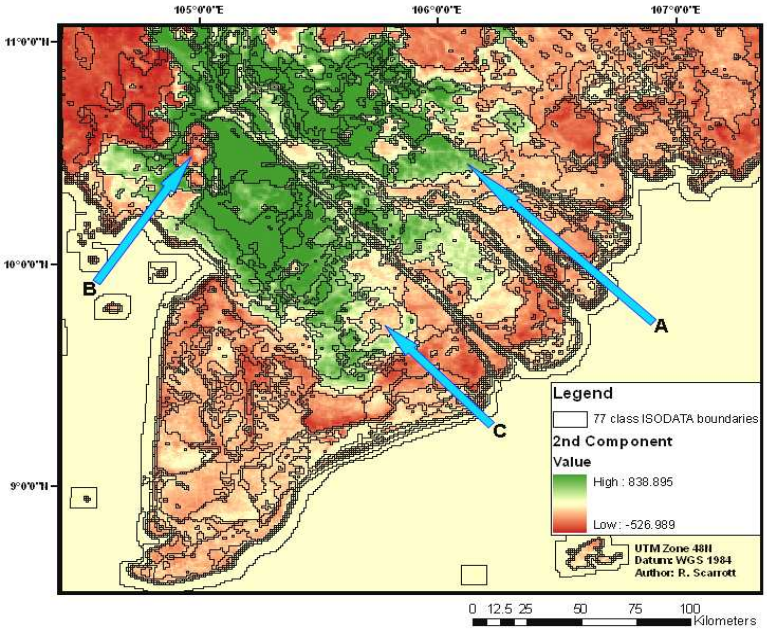

Figure 49: Principal component characterising ISODATA classes. 76 classes identified from ISODATA classification, overlaying the 2nd Principal Component image. Arrows point to noteworthy classes and how they are being characterised by the Principal Components

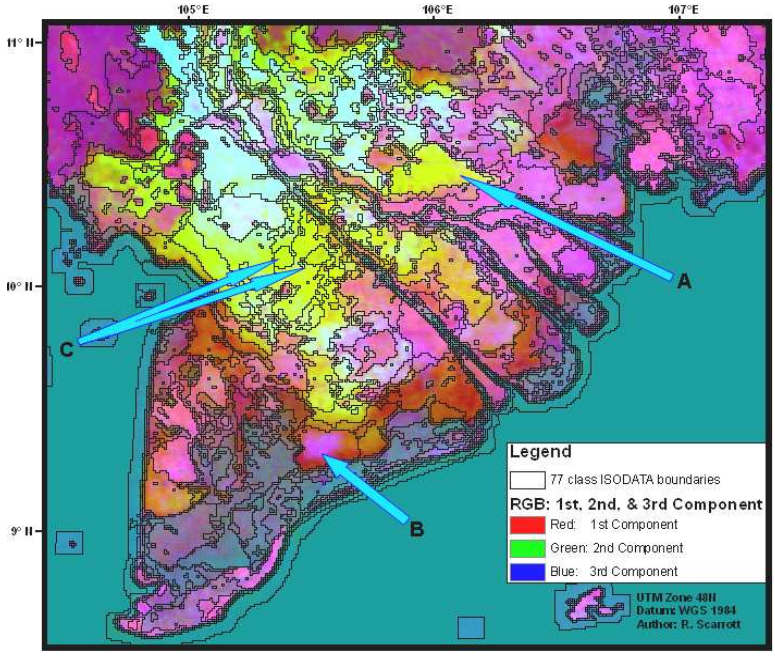

Figure 50: Component composite 1 characterising ISODATA classes. RGB:1st, 2nd, 3rd Component composite, overlaid by the 76 ISODATA classes. Arrows highlight noteworthy classes.

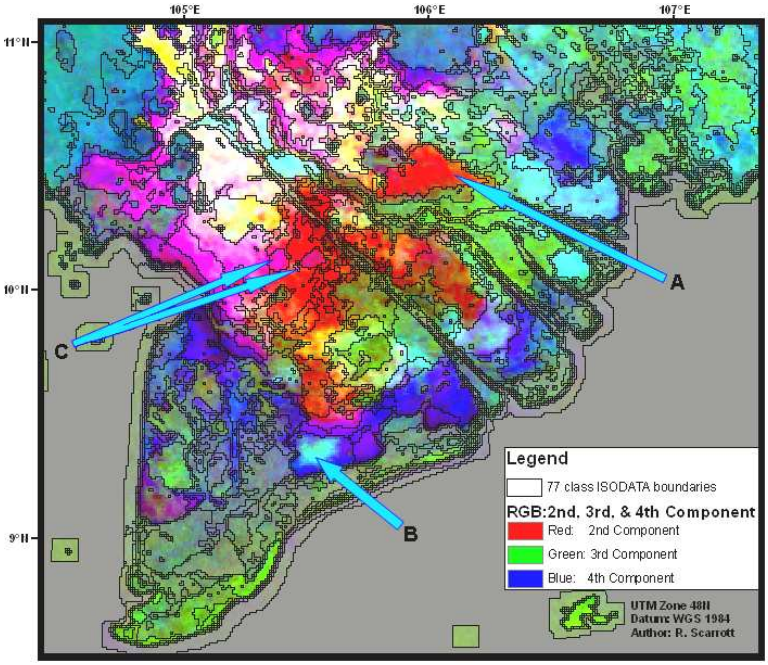

Figure 51: Component composites 2 characterising ISODATA classes .RGB: 2nd, 3rd, 4th Component composite, overlaid by the 76 ISODATA classes. Arrows highlight noteworthy classes.

The boundaries extracted using ED also provided some noteworthy points. Shown in figures 52 and 53, are samples of the larger regions delineated by the 3x3 ED method, and the 5x5 ED method respectively. These are subdivided by the 76 ISODATA classes. Note that the 3x3 and 5x5 kernel edge detected regions essentially group ISODATA classes together within the edge detected regions, though to different spatial extents.

Note for example, that region A in Figure 52 partially covers the same area covered by area B in figure 53. Furthermore, note that not only are larger regions produced by the 5x5 ED method, but consequently, more ISODATA classes are grouped by the 5x5 edge detected regions, due to their extent. Also worth noting, is how the regions produced by both ED methods not only encompass rice classes, but also include unsampled classes (some of which are non-rice) into the groupings (see figures 54 and 55).

The orientation of ED boundaries also shows remarkable similarity to the areas of highly fragmented classes identified by the ISODATA classification (figure 56). Shown at points A are example areas of where the edge detected boundaries from either the 3x3 method, or the 5x5 method, coincide with the borders of ISODATA classes. Furthermore, such ED boundaries, coincide considerably with areas where multiple class transitions occur over a short spatial extent.

Of particular interest is how some of the boundaries, derived using the edge detection methodologies, do not coincide with the ISODATA class borders, or even areas of extensive ISODATA class fragmentation. Shown in figure 56, sample areas can be seen at points marked B.

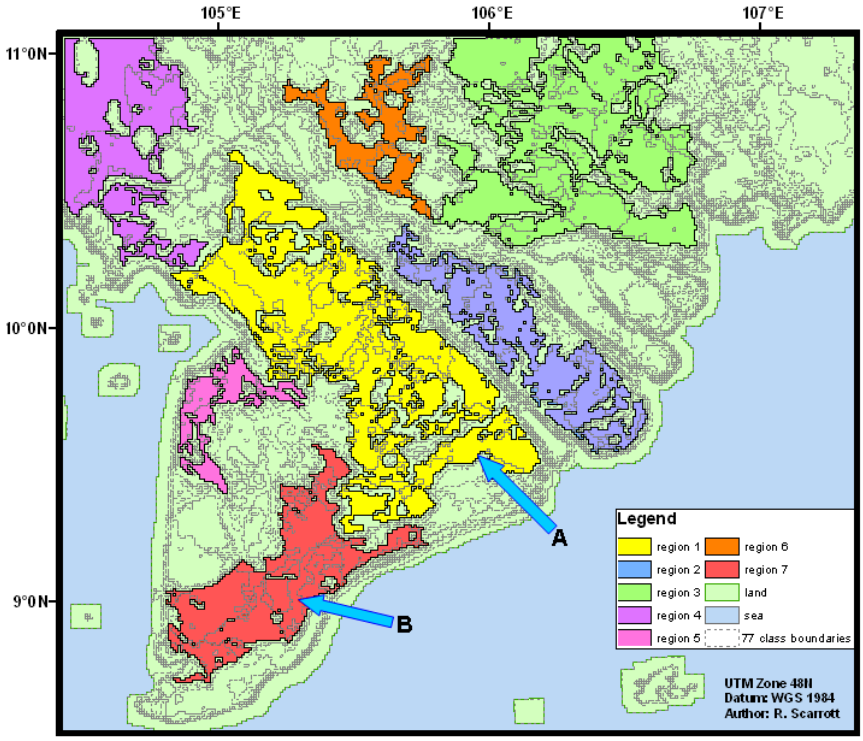

Figure 52: Regions as defined by the 3x3 edge detected boundaries, and the ISODATA classes subdividing them.

Edge detection also extracted some boundaries, some of which were comparable to areas of high NDVI class fragmentation (e.g. figure 56). Meanwhile other boundary segments were comparable to those extracted by PCA. This is evident for example in Figure 57, which shows the 3x3 edge detected boundaries, overlaying an RGB 2nd, 3rd, 4th component composite. Note that the edges, which did not match the ISODATA classes at points B in figure 56, do outline features in the principal component composite at points A and B in figure 57. Furthermore, these features were not highlighted by the boundaries extracted from the principal components themselves (A in figure 43).

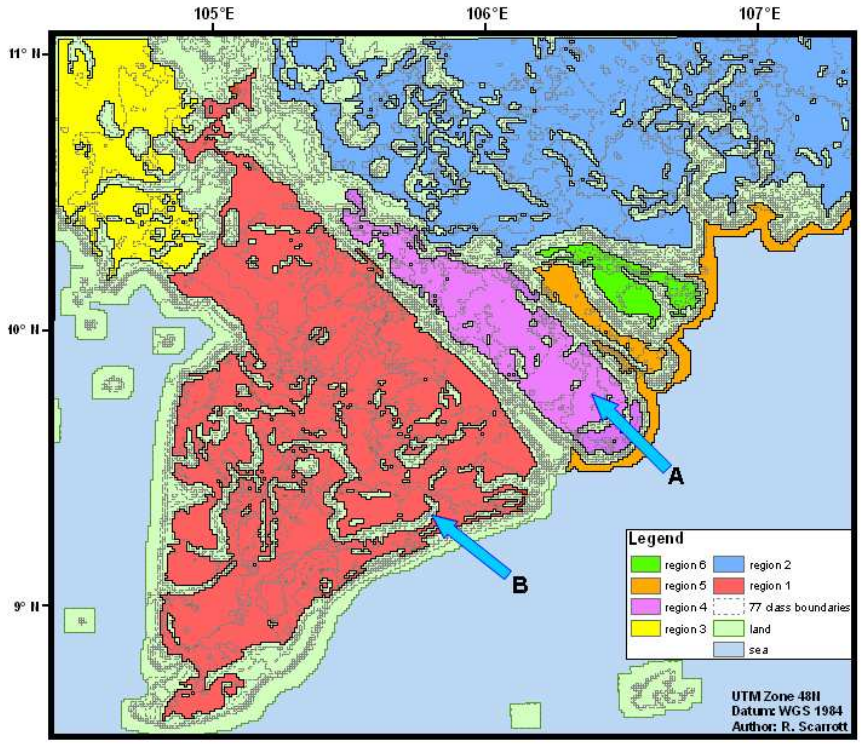

Figure 53: Regions as defined by the 5x5 edge detected boundaries, and the ISODATA classes subdividing them.

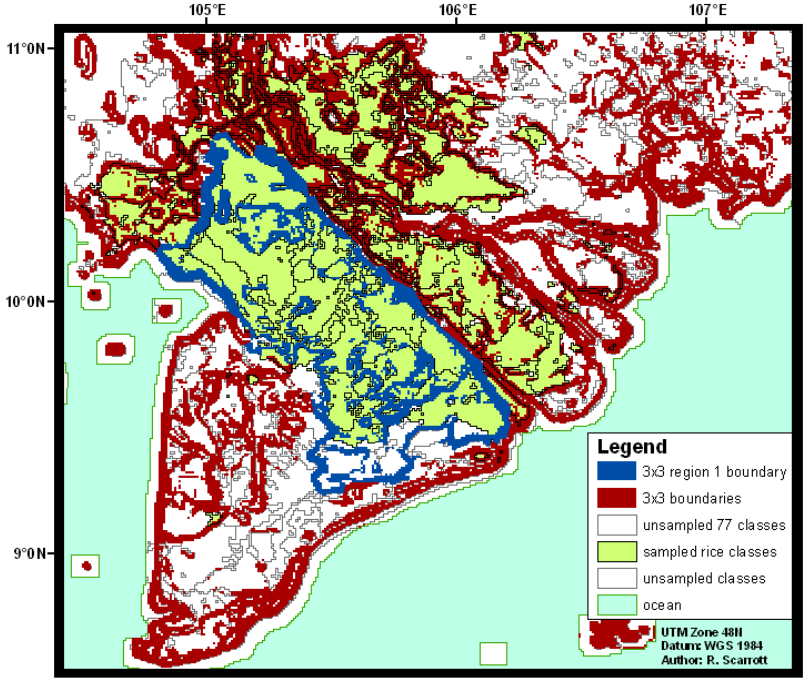

Figure 54: 3x3 edge detected boundaries grouping rice and non-rice ISODATA classes.

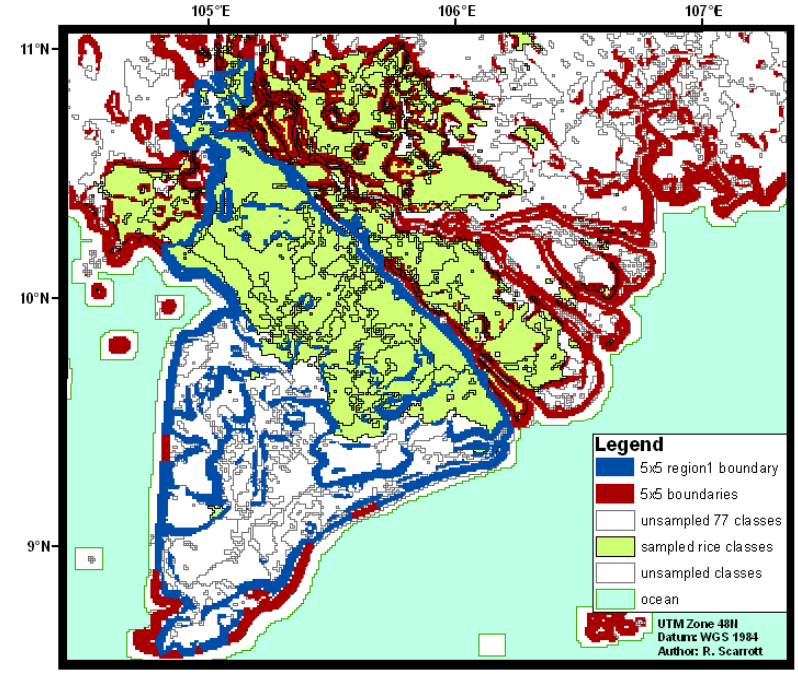

Figure 55: 5x5 edge detected boundaries grouping rice and non-rice ISODATA classes.

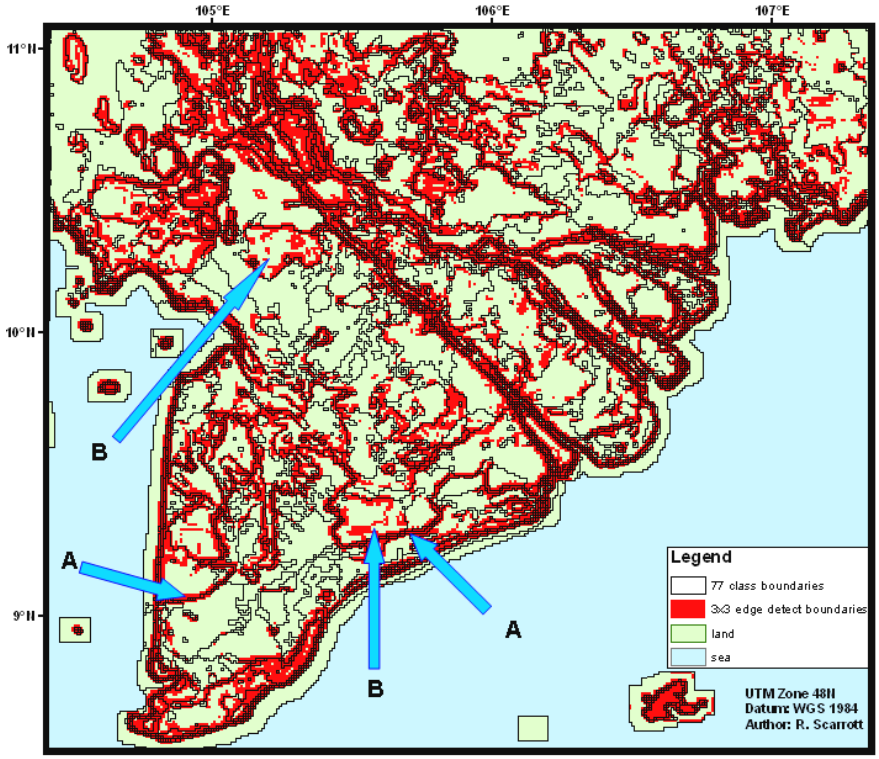

Figure 56: 3x3 Edge detected boundaries overlaid by 76 ISODATA classes. Areas of noteworthy overlap are highlighted at points A, whilst noteworthy areas where edge boundaries do not coincide with ISODATA class borders are highlighted at points B.

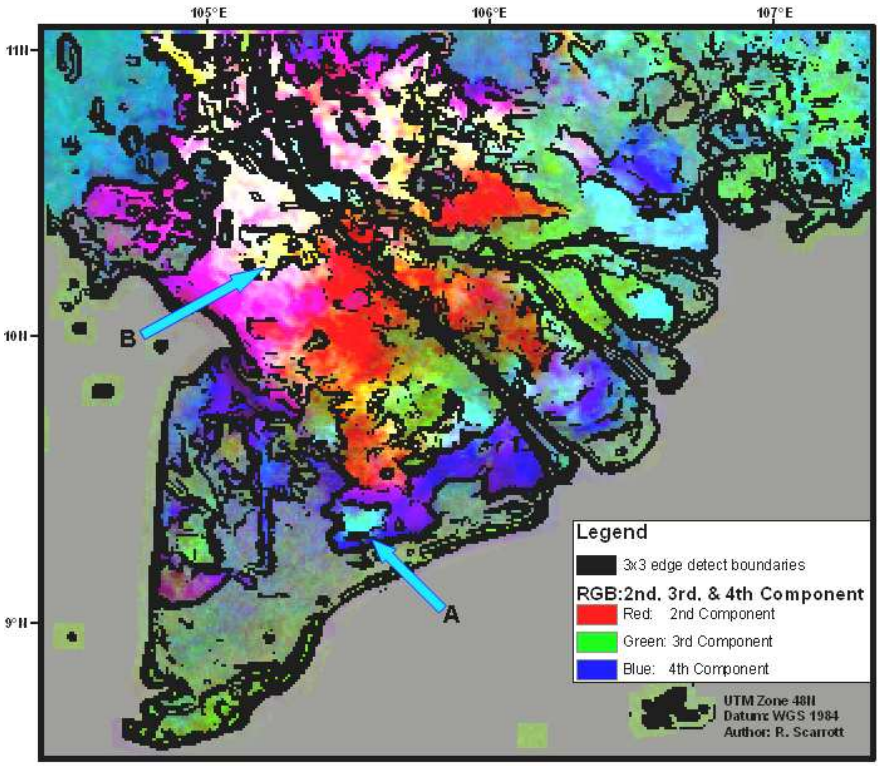

Figure 57: Component composites overlaid by edge detected boundaries. Features in an RGB 2nd 3rd, 4th Component composite, which are outlined by boundaries extracted by 3x3 edge detection. Arrows point to noteworthy features.

5. Discussion

5.1. Heterogeneity in the Mekong Delta

The world can be viewed as a "heterogeneity of heterogeneities" according to Sparrow (1999), and apparently, so too can the Mekong Delta. As could be seen, even within a "single" crop species, varieties varied across the delta, driven by the farmers need to gain the maximum yield from the local environment. Furthermore, rice crop calendars exhibited temporal shifting along environmental conditions, most notably reflecting changes in flood regime.

These findings of shifting crop calendars serve to support those findings of Sakimoto *et al.*, (2006). They studied rice crop calendars in the Mekong delta, though they were more concerned with how they changed over the years, attributing these changes to seasonal and localised changes in water resources. However, they also characterised the cropping calendar shifts across the delta. They noted that the fluctuating water resource conditions, affected those crop calendars predominantly in the Northwest of the Delta, where the flooding (figure 20) prevented rice growth. Conversely, in the South East of the Delta, flooding was a requirement, mitigating against saline intrusion (show in figure 18) and commencing the rice crop calendars.

Combining the findings of Sakimoto *et al.*, (2006), and the information in the landuse map and legend produced in this research, lends strong evidence to the concept of the Mekong Delta in reality being a complex mosaic of environmental conditions.

Furthermore, lower levels of edge had to be removed during the initial stages of edge detection. This allowed temporal cleaning to proceed. Whilst the method essentially defined these lower levels of edge as "non-edges" they do represent a minor flux across the landscape in NDVI values. Few homogeneous NDVI areas actually existed (whilst those that did could be attributable to cloud cover- figure 58). This serves to further develop the idea that the Mekong Delta is truly heterogeneous, echoing Chesson and Case's (1989) statement that "the world is heterogeneous and non-equilibrial.

In overlaying the 76 ISODATA classes over the edge detected boundaries, a further interesting coincidence was revealed. Areas with edges, identified by the edge detection method, appeared to be spatially coincident with areas of high NDVI class fragmentation (figure 56). Gosz (1992) noted that community transitions take the

form of complex mosaics. NDVI class fragmentation over boundaries detected by edge detection could be interpreted as such community transitions.

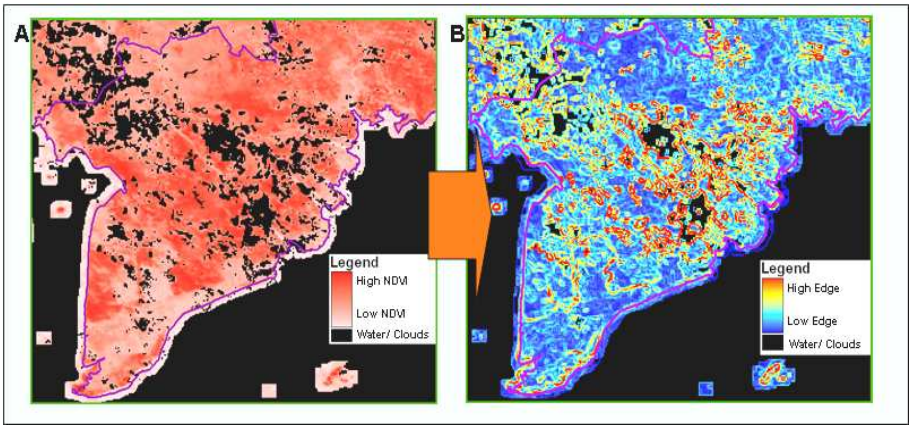

Figure 58: Edges enhanced around cloud pixels during Edge Detection. A shows the NDVI composite image of the 21st July, 2005. Cloud pixels have been given a value of zero by the cloud removal process. Edges (B) are then determined from this zero value.

Alternatively, the fragmented classes are thought as elements of the larger classes surrounding them. These larger classes are bounded by the edge detection boundaries. If, as the research assumed (and landscape heterogeneity evidence supported), the Mekong Delta is a large, heterogeneous, transitional area, then the areas of high class fragmentation represent areas of rapid change in vegetation communities and their underlying gradients. Furthermore, these fragmentations occur over edges originally envisioned to represent ecotones. The bounded regions (with spatially large, though multiple NDVI classes) could therefore logically be interpreted as ecoclines (see figure 59). This conceptualisation of the landscape and how it is being expressed through its' vegetation, serves to support that the landscape could indeed be conceived to be a complex mosaic of ecotones and ecoclines. Both of these transitional areas would be of interest to ecologists and gradient analysts, as they represent gradient flux on different scales.

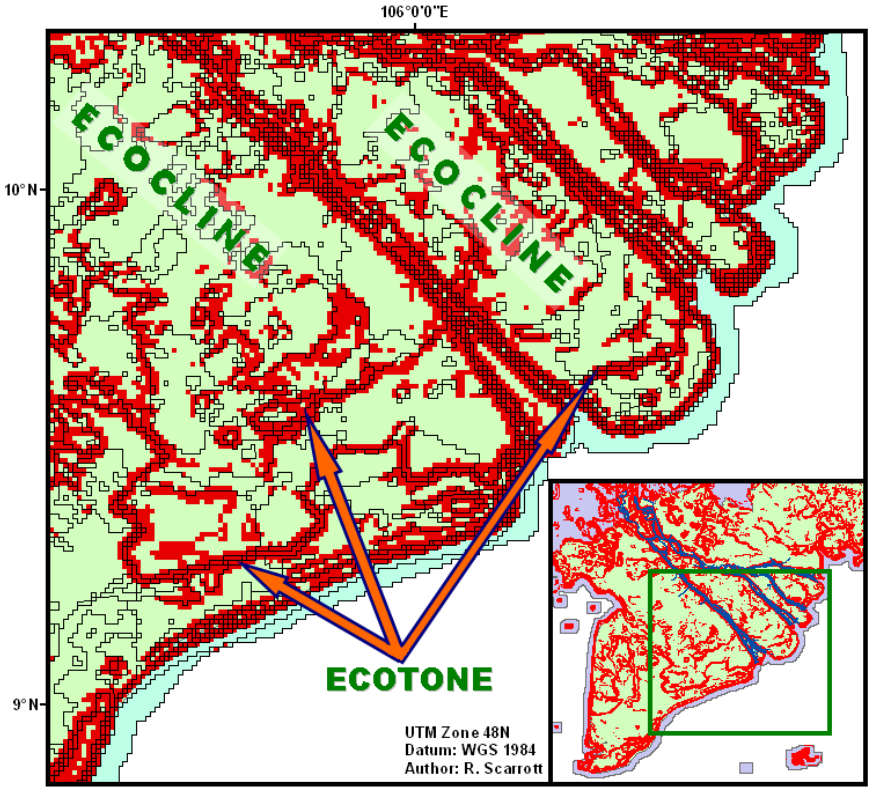

Figure 59: Edge detected boundaries and ISODATA classes indicating ecotones and ecoclines.

5.2. Methodology appraisal

The ISODATA classification served to exploit hyper-temporal differences in NDVI into NDVI classes. These NDVI classes (and ultimately the map units characterised by various crop calendars) did have distinct differences between them. Despite this difference, the classes could successfully be grouped by boundaries, extracted solely from satellite hyper-temporal imagery.

Furthermore, both methodologies attempted (Principal Components Analysis, and Edge Detection) extracted grouping boundaries of some form or another. In these groupings, non-rice and unsampled rice classes were included. This indicates that the class groupings went beyond simply grouping rice, but also indicating that rice

NDVI classes had aspects in common with their surrounding NDVI classes, despite some of these not being rice areas. This supports the assumption that fundamentally different classes would be linked to each other along factors such as gradients. The borders of these classes are therefore relatively meaningless when interpreted as a border. As such they should be interpreted as arbitrary lines denoting a certain (unknown) level of transition between two contrasting areas.

The methodologies themselves each held promise. The principal components derived from the hyper-temporal dataset visibly displayed sharp transition boundaries (where the value is approximately equal to 0). This visible feature was exploited to yield the boundaries, which tracked the zero value of the component. However, the middle value of the 1st component was all that could be used. It lacks values below the zero value, despite visibly displaying boundaries which are logically meaningful. In future, perhaps some other, more statistically appreciable extraction could be developed. It could involve histogram analysis, so boundary choice is entirely data driven, and not depend, even to a small degree, on human interpretation.

Interestingly, the components inherently established a hierarchy of boundaries. Boundaries derived from the 1st component, were derived from a summary of 79.41% of the variability in the 3 year hyper-temporal dataset. The second component boundaries were drawn from 7.57%, the 3rd component, 1.5%, and so on. However, in total, the first four components here only summarised 89.41% of the variability. Whilst there are as yet, no clear guidelines on how many components should be used (Eastman & Fulk, 1993), perhaps it would be more appropriate to set a threshold. This threshold level would be a proportion of the variability that should be summarised (for example 95% of the variability). All components summarising up to that threshold would then have to be used.

The method using Principal Components Analysis was also considered flawed as it fails to take advantage to the asymmetry of time inherent in sequential hyper-temporal datasets. Edge detection was therefore seen as logical avenue of exploration. Each image was edge detected in succession, whilst a temporally cleaning step acted on a before and after concept of edge permanence.

This temporal cleaning could also be helpful in removing suspect edges caused by cloud values. As shown in figure 58, this could be considered an issue in the ED method. Any suspect cloud pixels in the NDVI images were given a value of zero. Therefore, edges were calculated from these values (figure 58). Temporal cleaning

removes those edges not present in three successive images. Therefore the process may help to remove a quantity of temporary edges caused by cloud removal from the dataset, though the exact amount of contamination should be investigated further.

Overall, the method did provide boundaries, which successfully grouped ISODATA classes. Though the definitions of edge "persistence" and how weak an edge must be before it is considered "weak" need to be clarified and researched. As is, the choice of median values probably screened out some edges that should not have been removed. Only the strongest and most persistent edges were kept, which could have been above the true level of when an edge could be considered "strong".

Unfortunately, currently available literature holds no answers to this problem. Despite the extensive use of edge detection, information on what makes an edge a true "edge" is notably absent. However the principal appears to hold. This means that the choice of edges should come from the data itself, and not from outside knowledge. This is why a feature of the histogram was twice used to screen out the lower levels of edge. It serves to highlight that a more rigorous statistical determination of what can be removed is required. This principal is applicable to both stages of lower edge removal, and should be researched if further progress is to be made.

Within the Edge Detection method, two kernels were used. A 3x3 pixel kernel, and an adapted 5x5 pixel kernel. In general, the 5x5 kernel produced spatially wider boundaries. Figure 45 shows how the pixels identified as edges by the 5x5 method, lie to either side of the pixels commonly identified as edges by both methods. Furthermore, a 10 pixel noise threshold was used with the 5x5 method, in contrast to the 6 pixel noise threshold used by the 3x3 method. In hindsight, perhaps this level of 10 pixels was too high, and should had been left at 6 pixels, maintaining consistency in the methodologies.

Another issue was that the distance function used to combine the four directions of the 5x5 pixel edge detection, was simply an extension of that used by the 3x3 kernel method. However, the function still achieved the aim of exaggerating large fluctuations, and minimising minor fluctuations, and was appropriate for use.

When the boundaries were compared, it was apparent that all methods identified boundaries that had some sections that coincided across methodologies, and others that differed spatially. Notably, even the different boundaries, identified by Principal components Analysis, coincided frequently with those identified by edge detection,

despite not being universal matches. The lack of universality could be interpreted that the Principal Components Analysis and Edge Detection methods are in fact extracting boundaries based on different definitions. For example, the edge detection method was devised specifically to take the asymmetry of time into account.

It was also clear that the boundaries identified from principal components, missed visibly obvious features within the components themselves (e.g. A in figure 43). Furthermore, ISODATA classification also missed these features. This could indicate that ISODATA classification does not detect all variability present. However, this could have been a consequence of the use of a subset image stack for the PCA method, and should be reviewed before any concrete conclusions are made. Notably however, the edge detection methodology successfully bounded the features, determining that they had viable permanent, and strong boundaries (A and B in figure 57).

This serves to highlight that no one single methodology worked. As such the research failed to define a single methodology to determine the boundaries of "gradient effects zones" within the time frame. However, it did suggest a plausible route for further research. Each method extracted boundaries. These different boundaries had similarities, and differences. This dissimilarity should therefore be exploited. Perhaps, the utility of Principal Components Analysis data reduction capability, and Edge Detections ability to exploit the sequential nature of hyper-temporal datasets, could be combined in a hybrid method.

For example, it can be logically argued that the nature of the boundaries extracted from the principal components, was hierarchical (.Furthermore, different components coincide with different sections (and common sections) of the edge detected boundaries. Perhaps the principal components boundaries could be used to weight the importance of the edge detected boundaries according to how much they contribute to the dataset. Otherwise, perhaps component boundaries, summarising 95% (for example) of the hyper-temporal datasets variability, could be used to extract viable temporally cleaned edges (negating the need for a second histogram analysis). These are simply some possible future avenues of research, though they do serve to highlight the further work required and the plausibility of a hybrid method.

6. Limitations, concludions and recommendations

6.1. Limitations

- The NDVI signature of vegetation within the 1km SPOT pixel, was assumed to represent a indicator of vegetation responses to environmental gradients in that pixel
- 1km pixels were seen to be of sufficient resolution to adequately capture landscape level gradients
- a composite product of 10 days was seen to be of adequately high temporal resolution to represent the values occurring over the ten daily images.
- the temporal fluctuations in NDVI value of an NDVI class, were assumed to be of sufficient magnitude to allow for ISODATA classification.
- it was assumed that the landscape of the Mekong contained sufficient heterogeneity in NDVI to be divisible into classes.
- the use of the peak in both average, and minimum separability was assumed to represent a level of optimum class number for ISODATA classification.
- it was assumed that NDVI classes were equivalent to map units
- it was assumed that these map units could be characterised concerning their crop calendars.
- rice crop varieties were assumed to be adapted to optimise productivity under variations in specific environmental conditions.
- it was assumed that the 10 year stack of hyper-temporal images used for the ISODATA classification, was adequately summarised in the 3 year stack used to develop the various methodologies, whilst still being comparable.
- concerning boundary extraction from the principal components, the mid-value of the 1st component (1022) was assumed to be comparative to the zero value of the subsequent components.
- the zero value of components 2, 3, and 4, was viewed as a transition point in the data, and representative of a boundary.
- the median value in the ED methods' 1st histogram analysis, was assumed to represent an adequate level below which edges could be considered as "weak" and were removed as noise.
- Concerning the ED methods' 2nd histogram analysis, the mode of the logarithmic value of average edges was deemed to be an adequate value, below which edges were removed as noise.
- one month was the period of time an edge had to remain, in order to be considered representative of a permanent boundary during the temporal cleaning portion of the ED methodology.

- the NDVI images were deemed to have undergone adequate processing for cloud interference

6.2. Conclusions

1 - Assuming the ISODATA classification results are NDVI classes that are fundamentally different, can these differences be seen, expressed in rice crop calendar data collected in the field?

The rice crop profiles characterised in the landuse map and legend, demonstrate shifts in crop calendars between map units. Whilst in some classes, harvesting has only begun, other classes have already completed sowing the next crop. In another instance, whilst crops are only been sown, rice crops in another class are already half way through their growth cycle. Therefore differences can be seen in crop calendars characterising NDVI classes derived by ISODATA classification.

2 – Could shifts in rice crop calendars be attributable to landscape heterogeneity in environmental conditions across the Mekong Delta?

The research showed that shifts in rice crop calendars for each class were been accompanied by shifts in the class' flood regime. Furthermore, the multitude of rice varieties grown indicated a need for farmers to adapt to environmental conditions across the delta. This argument was also supported by work done by Sakamoto *et al.* (2006), who found that rice crop calendars were being affected by seasonal and localised conditions such as flooding and salinity. Therefore, arguably, the shifts in rice crop calendars could be attributable in part to landscape heterogeneity in environmental conditions across the delta.

3 - Are there methods capable of recognizing and delineating boundaries, or "natural breaks" in a gradients' effects upon the landscape, using hyper-temporal satellite data alone?

Both attempted methods successfully grouped NDVI classes obtained by ISODATA classification of hyper-temporal data. Both methods explored derived their boundaries entirely from the hyper-temporal dataset, with no other information data being used to guide the boundary extraction process. The methods need to be refined however, despite extracting logical boundaries, more sensitive and robust histogram

analysis should be researched for the Edge Detection methodology, whilst a more appropriate boundary extraction for the first component should be sought.

4 - Of any promising method(s), how do they compare at recognising boundaries or natural breaks, thus delineating the borders of regions within which crop calendar heterogeneity occur, as caused by the same landscape level gradient.

Both methods show an ability to extract boundaries. These different boundaries often coincide, though in many cases differed spatially. These boundaries are all feasibly attributable to gradients, despite their spatial differences. Boundaries extracted by PCA are seen as inherently hierarchical in nature. Meanwhile those extracted by ED are seen as 4 dimensional, taking into account the asymmetry of time. Visible features in principal components were only outlined by boundaries extracted by ED methodology, and not by those extracted by the PCA methodology. This indicates the need for a hybrid methodology, which would combine the boundary extracting capabilities of both (and maybe more) methodologies.

6.3. Recommendations

1. The PCA methodology requires further refinement. Despite logical boundaries being extracted, the first component requires a more rigorous determination of the value indicative of a transition boundary. Furthermore, a threshold should be determined on how many components are required to adequately summarise the variability in hyper-temporal datasets.

2. The ED methodology requires further refinement. Concerning the first and second histogram analysis, lower thresholds of edge values need to be determined. Therefore, A logical way of extracting this threshold from histograms needs to be developed.

3. Following the development of refined PCA, and ED methodologies, a hybrid method should be investigated to take into account the hierarchical and data reductive properties of PCA, and the ED method's exploitation of the asymmetry of time. This should not preclude the development of other, alternative methodologies which may serve to augment the information gained from hyper-temporal datasets.

6.4. Summary

The research successfully followed the logic of gradients to outline various methodologies, capable of grouping hyper-temporal data classes. This could eventually lead to a tool being produced to aid gradient analysts to stratify their sampling regimes along less subjective stratifications as are currently used. The methods investigated need to be refined, despite exhibiting a considerable degree of promise. Evidence was also presented, showing the need for a hybrid method, composed of the advantageous aspects of Principal Components Analysis, and those of Edge detection.

7. References

Ali, A. (2009) *Comparison of the landscape, ecological and hyper-temporal NDVI mapping techniques to develop an integrated approach*. ITC Msc. Thesis, ITC, Enschede.

Austin, M.P. (1985) Continuum concept, ordination methods, and niche theory. *Annual Reviews of Ecological Systems*, 16, 39-61.

Begon, M., Harper, J.L., Townsend, C.R. (1990) *Ecology: Individuals, populations and communities*. Blackwell Scientific Publications,

Campbell, J.B. (1996) *Introduction to Remote Sensing*, 2nd edition. Taylor and Francis, London.

Chavez, P,G Jr., Kwarteng, A.Y. (1989) Extracting spectral contrast in Landsat Thematic Mapper image data using selective Principal Components. *Photogrammametric and Engineering in Remote Sensing*, **55**(3), 339-348.

Chesson, P.L., Case, T.J. (1986) Overview: non-equilibrium community theories; chance variability, history and coexistence. In: Diamond, J. and Case, T.J. (eds.) *Community Ecology*, Harper and Row, New York.

Cracknell, A.P., Hayes L. (2007) *Introduction to Remote Sensing, 2nd edition*. CRC Press, London. pp 67-68.

De Bie, C.A.J.M. (2000). *Comparative performance analysis of agro - ecosystems*, Doctoral thesis, Wageningen University and Research Centre. ITC dissertation no. 75, Enschede, 232 pp.

De Bie, C.A.J.M., Khan, M.R., Toxopeus, A.G., Venus, V. and Skidmore, A.K. (2008) Hypertemporal image analysis for crop mapping and change detection. In: *Proceedings of the XXI congress : Silk road for information from imagery : the International Society for Photogrammetry and Remote Sensing*, 3-11 July, Beijing, China. Comm. VII, WG VII/5. Beijing : ISPRS, 2008. pp. 803-812.

Eastman, J.R. (1992) Time series map analysis using Standardised Principal Components. *ASPRS/ACSM/RT 92 Technical Papers, Volume 1: Global Change and Education*. 3-8 August, Washington D.C., pp 195-204.

Eastman, J.R., Fulk, M. (1993) Long sequence time series evaluation using standardised Principal Components. *Photogrammametric Engineering and Remote Sensing*, **59**(8), 1307-1312.

Fung, T., Le Drew, E. (1987) Application of Principal Components Analysis to Change Detection. *Photogrammametric Engineering and Remote Sensing*, **53**(12), 1649-1658.

Giller, P. (1984) *Community Structure and the Niche*. Chapman & Hall, London.

Gleason, H.A. (1917) The structure and development of the plant association. *Bulletin of the Torrey Botanical Club*, **43**, 436-481

Gleason, H.A. (1926) The individualistic nature of plant community development. *Bulletin of the Torrey Botanical Club*, **53**, 1-20

Gleason, H.A. (1939) The individualistic concept of the plant association. *American Midland Naturalist*, **21**, 92-110.

Gosz, J.R. (1992) Gradient analysis of ecological change in time and space: implications for forest management. *Ecological Applications*, **2**(3), 248-261.

Hori, H. (1996) The Mekong: Development and its environmental effects. Kokon-Shoin Publishing, Tokyo (in Japanese).

Hugget, R.J. (1995) *Geoecology: An evolutionary approach*. Routledge Ltd., London.

Hutchinson, G.E. (1958) Concluding Remarks. *Cold Spring Symposium on Quantitative Biology*, 22, 415-427.

IRRI (International Rice Research Institute) (1993) *IRRI Rice Almanac, 1993-1995*. International Rice Research Institute, Los Banos, Philippines.

Jingyong, Z., Wenjie, D., Congbin, F., Lingyun, W. (2003) The influence of vegetation cover on summer precipitation in China, a statistical analysis of NDVI and climate data. *Advances in Atmospheric Science*, **20**, 1002-1006.

Keddy, P.A. (1991) Working with heterogeneity: an operator's guide to environmental gradients. In: Kolasa, J., Pickett, S.T.A. (eds.) *Ecological Heterogeneity*. Springer-Verlag, New York, pp 181-200.

Kent, M., Gill, W.J., Weaver, R.E., Armitage, R.P. (1997) Landscape and plant community boundaries in biogeography. *Progress in Physical Geography*, **21**(3), 315-353.

Le Toan, T., Ribbes, F., Wang, L-F, Floury, N., Sing, K-H, Kong, J.A., Fujita, M., Kurosu, T (1997) Rice crop mapping and monitoring using ERS-1 data based on experiment and modelling results. *IEEE Transactions on Geoscience and Remote Sensing*, 35(1) 41-56.

Leica Geosystems (2005) *Erdas Field Guide*. Leica Geosystems Geospatial Imaging, LLC, USA.. Obtainable at http://duff.ess.washington.edu/data/erdas_pdfs/FieldGuide.pdf
[accessed on 5th February, 2009]

Maisongrande, P., Duchemin, B., Dedieu, G. (2004) VEGETATION/SPOT: an operational mission for the Earth monitoring: presentation of new standard products. *International Journal of Remote Sensing*, **25**(1), 9-14.

Nguyen, V.N., Do, M.H., Nguyen, N.A., Le, V.K. (2004) Rice production in the Mekong Delta (Vietnam): trends of development and diversification. *Mekong Rice Conference, 2004: Rice, the Environment and Livelihoods for the Poor*. 15th-17th October, 2004, Ho Chi Minh City, Vietnam.

Nguyen, H.N. (2007) Flooding in Mekong River Delta, Vietnam. In: *Fighting climate change: Human solidarity in a divided world*. Human Development Report 2007/2008, Human Development Report Office, UNDP.

Peet, R.K. (1978) Latitudinal variation in southern Rocky Mountain forests. *Journal of Biogeography*, **5**, 275-289.

Pettorelli, N., Vik, J.O., Mysterud, A., Gaillard, J-M., Tucker, C.J., Stenseth, N.C.(2005) Using the satellite derived NDVI to assess ecological responses to environmental change. *Trends in Ecology and Evolution*, **20**(9), 503-510.

Piwowar, J.M., LeDrew, E.F. (1995) Hypertemporal analysis of remotely sensed sea ice data for climate change studies. *Progress in Physical Geography*, **19**(2) 216-242.

Richards, J.A., Jia, X. (1999) *Digital Image Processing*. Springer-Verlag, New York. Pp 133-143.

Roerick, G.J., Meneti, M., Soepboer, W., Su, Z. (2003) Assessment if climate impact on vegetation dynamics by using remote sensing. *Physical Chemistry of the Earth*, **28**, 103-109.

Saab, D.A., Haythornthwaite, T.W. (1990) Application of spacio-temporal database models to street network files. *Proceedings :GIS for the 1990s*; Ottawa, Canada: Canadian Institute of Surveying and Mapping. pp 1072-1085.

Sakamoto, T., Nguyen, N.V., Ohno, H., Ishitsuka, N., Yokozawa, M. (2006) Spatio-temporal distribution of rice phenology and cropping systems in the Mekong Delta with special reference to the seasonal flow of the Mekong and Bassac rivers. *Remote Sensing of the Environment*, **100**, 1-16.

Singh, A., Harrison, A. (1985) Standardised Principal Components. *International Journal of Remote Sensing*, **6**(6), 883-896.

Sklenár, P., Bendix, J., Balslev, H. (2008) Cloud frequency correlates to plant species composition in the high Andes of Ecuador. *Basic and Applied Ecology*, **9**, 504-513.

Sparrow, A.D. (1999) A heterogeneity of heterogeneities. *TREE*, **14**(11), 422-423.

Staenz, K., Goodenough, D.G. (1990) Airborne imaging spectrometer data analysis applied to an agricultural dataset. Global and Environmental monitoring techniques and impacts. *Proceedings: ISPRS Commission VII Mid-term Symposium*: September 1990, Victoria, Canada. International Society for Photogrammetry and Remote Sensing, pp 552-559.

Stutheit, J. (1991) Temporal GIS investigates global change. *GIS World*, **4**(9) 68-72.

Swain, P.H. (1973) *Pattern Recognition: A basis for remote sensing data analysis* (LARS Information Note 111572). The Laboratory for Applications of Remote Sensing, Purdue University, West Lafayette, Indiana.

Ter Braak, C.J.F. and Prentice, I.C. (1988) A theory of gradient analysis. *Advances in Ecological Research*, **18**, 271-317.

Thenkabail, P.S., Biradar, C.M., Turral, H., Noojipady, P., Li, Y.J., Vithanage, J., Dheeravath, V., Velpuri, M., Schull, M., Cai, X. L., Dutta, R. (1999) *An Irrigated Area Map of the World (1999) derived from Remote Sensing*. IMWI Research Report 105. International Water Management Institute, Columbo, Sri Lanka.

Thenkabail, P.S., Gangadhararao, P., Biggs, T.W., Krishna, M., Turral, H.(2007) Spectral Matching Techniques to determine historical landuse/land-cover (LULC) and irrigated areas using time-series 0.1 degree AVHRR pathfinder datasets. *Photogrammametric Engineering and Remote Sensing*, **73**(9), 1029-1040.

Tucker, C.J. (1979) Red and photographic infrared linear combinations for monitoring vegetation. *Remote Sensing of the Environment*, **8**, 127-150.

Van der Maarel, E. (1990) Ecotones and ecoclines are different (*Journal of Vegetation Science*, **1**, 135-138.

Wang, J., Rich, P.M., Price, K.P. (2003) Temporal responses of NDVI to precipitation and temperature in the central Great Plains, USA. *International Journal of Remote Sensing*, **24**, 2345-2364.

White, D.A., Hood, C.S. (2004) Vegetation patterns and environmental gradients in tropical dry forests of the northern Yucatan Peninsula. *Journal of Vegetation Science*, **15**, 151-160.

Whittaker, R.H. (1953) A consideration of climax theory: the climax as a population and pattern. *Ecological Monographs*, **23**, 41-78.

Whittaker, R.H. (1967) Gradient analysis of vegetation. *Biological Reviews*, **4**, 207-264.

Whittaker, R.H. (1973) Direct gradient analysis. In: Whittaker, R.H. (ed.) *Ordination and Classification of Communities*. Dr. W. Junk, The Hague, Netherlands.

Xiao, X., Boles, S., Frolking, S., Salas, W., Moore III, B., Li, C. (2002) Observation of flooding and rice transplanting of paddy rice fields at the site to landscape scales in China using VEGETATION sensor data. *International Journal of Remote Sensing*, **23**(15), 3009-3022.

Zhang, X., Friedl, M.A., Schaaf, C.B., Strahler, A.H., Hodges, J.C.F., Gao, F., Reed,B.C., Huete, A. (2003) Monitoring vegetation phenology using MODIS. *Remote Sensing of the Environment*,**84**, 471-475.

Zhang, X., Friedl, M.A., Schaaf, C.B., Strahler, A.H. (2004) Climate controls on vegetation phonological patterns in northern mid- and high latitude inferred from MODIS data. *Global Change Biology*, **10**, 1133-1145.

cache.daylife.com, (2009) Image of a sand dune successional system. Derived from: http://cache.daylife.com/imageserve/029u2x18KReDm/610x.jpg
[accessed 31st January, 2009]

www.cantho.cool.ne.jp (2009a) Salinity intrusion map of the Mekong Delta from: http://cantho.cool.ne.jp/mekong/water/surface.gif
[accessed 5th February, 2009]

www.cantho.cool.ne.jp (2009b) Soil Map of the Mekong Delta from: http://cantho.cool.ne.jp/mekong/geo/geo.gif
[accessed 5th February, 2009]

www.cantho.cool.ne.jp (2009c) Flood Map of the Mekong lower reaches from: http://cantho.cool.ne.jp/mekong/water/upflood.gif
[accessed 5th February, 2009]

www.envisat.int (2009) Image of the Mekong Delta, Southern Vietnam. From: http://earth.esa.int/satelliteimages/1611/Vietnam_MekongDelta_MER_FR_Orbit25809_20070206_or.jpg
[accessed 3rd February, 2009]

www.kscience.co.uk (2009a) Image of the colonising front of a sand dune successional system. From: http://www.kscience.co.uk/as/module5/succession/others.htm"
[accessed 31st January, 2009]

www.kscience.co.uk (2009b) Image of the grassland to shrub succession in the dune successional ecosystem. From:
http://www.kscience.co.uk/as/module5/succession/dune.htm"
[accessed 31st January, 2009]

www.ltid.inpe.br (2009) Website tutorial for utilising ENVI to study hyperspectral signatures. From:www.ltid.inpe.br/tutorial/tut7.htm
[accessed 4th February, 2009]

www.wikipedia.org (2009a) Image of the upper ecosystem of a tepui in Canaima National Park. From: http://upload.wikimedia.org/wikipedia/commons/c/c1/Roraima-Tepui_Plateau.jpg **[accessed 31st January, 2009]**

www.wikipedia.org (2009b)
Image of the escarpment or cliff that forms the ecotone between the upper ecosystem and the basal forest of the tepui. From: http://upload.wikimedia.org/wikipedia/commons/c/c7/Roraima-Tepui_Wand.jpg
[accessed 31st January, 2009]

www.wikipedia.org (2009c) Image of the cliff viewed from the basal forest. From: http://upload.wikimedia.org/wikipedia/commons/0/07/Salto_Angel_from_Raton.JPG **[accessed 31st January, 2009]**

8. Appendices

8.1. Appendix A

Landuse Map 2002 of the Mekong Delta.

8.2. Appendix B

Inputs and outputs of the various Edge Detection methodology's stages.

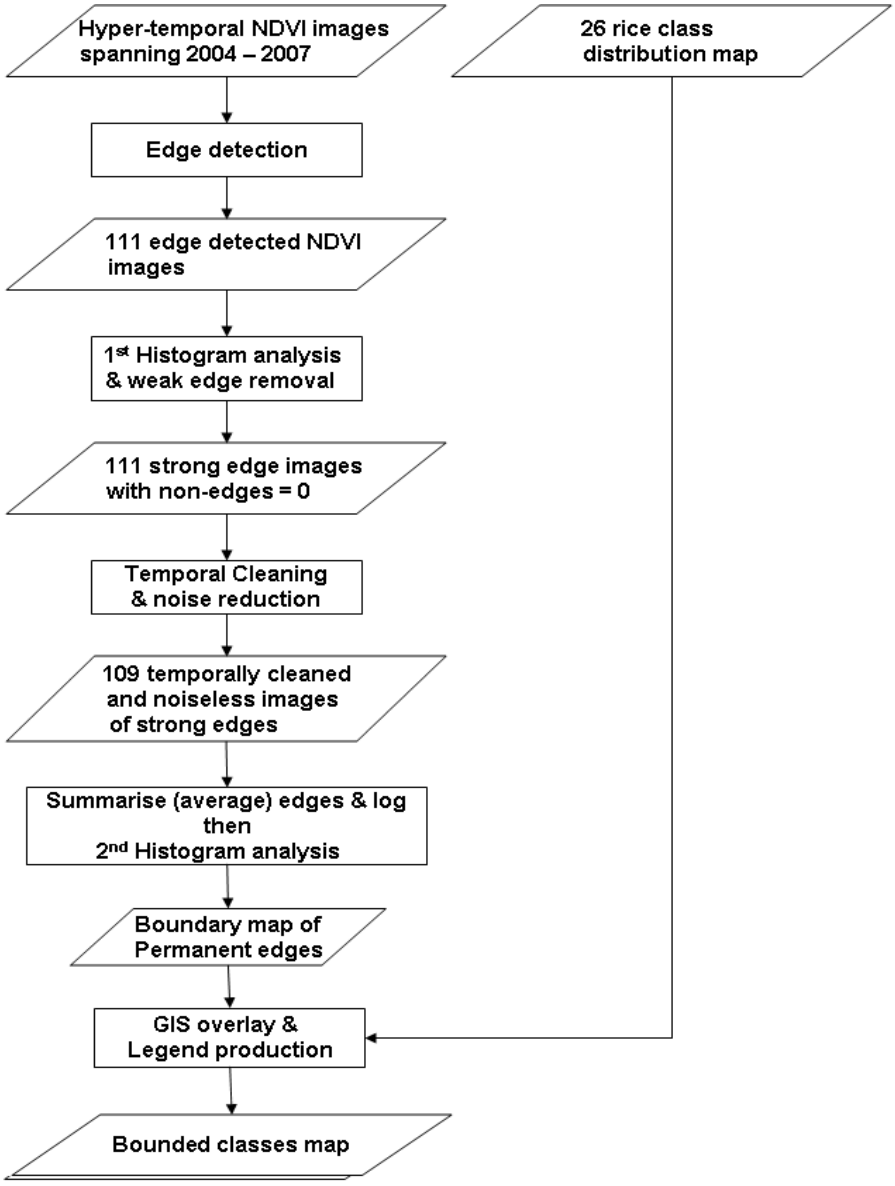

8.3. Appendix C

Model details of edge detection algorithms

(i) 3x3 kernel edge detection algorithm (Prewitt)

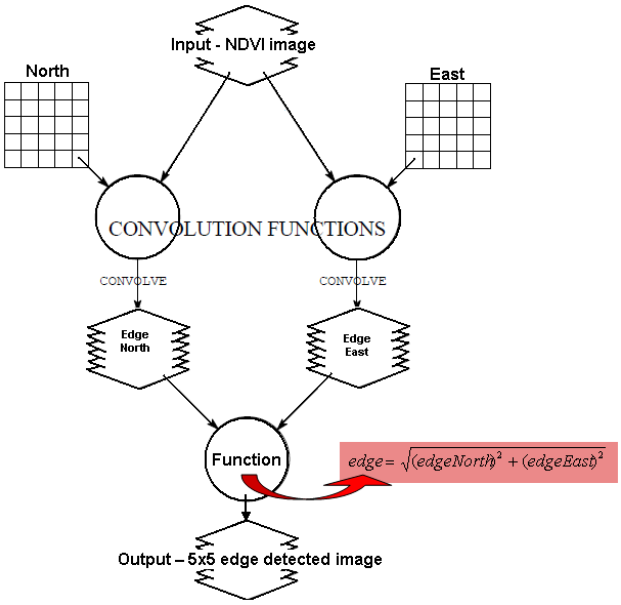

(ii) 5x5 kernel edge detection algorithm (prewitt adaptation)

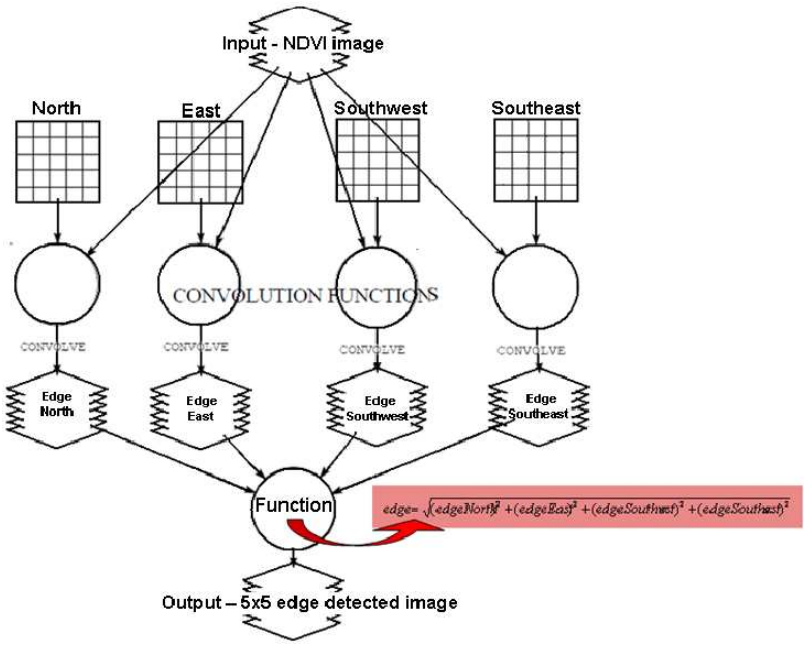

8.4. Appendix D

Unidentified software difficulties encountered when processing images edge detected with the sobel edge detection model

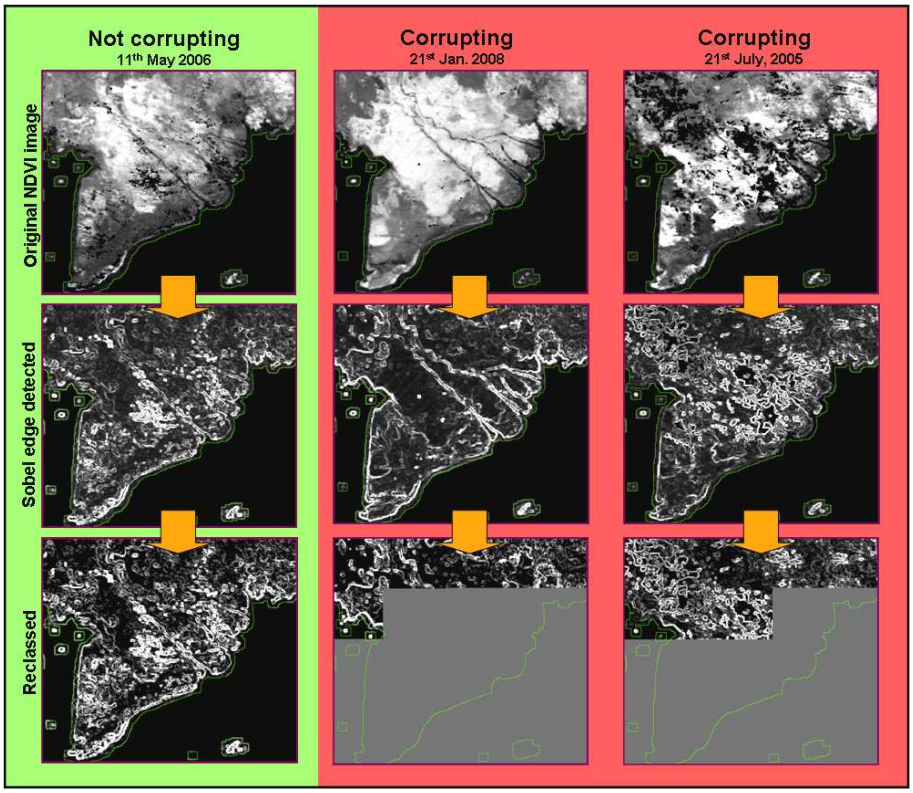

8.5. Appendix E

Eigenvalues for all components derived from a Principal Components Analysis of 111 NDVI images in a 3 year hyper-temporal image stack

Component	Eigenvalue	Proportion of variability summarised	Percentage	Cumulative percentage
1st	538120.11	0.79409	79.41	79.41
2nd	51324.63	0.07574	7.57	86.98
3rd	10182.17	0.01503	1.50	88.49
4th	6326.81	0.00934	0.93	89.42
5th	5180.38	0.00764	0.76	90.18
6th	4449.20	0.00657	0.66	90.84
7th	3733.71	0.00551	0.55	91.39
8th	2873.59	0.00424	0.42	91.82
9th	2606.54	0.00385	0.38	92.20
10th	2160.18	0.00319	0.32	92.52
11th	1987.83	0.00293	0.29	92.81
12th	1736.17	0.00256	0.26	93.07
13th	1583.22	0.00234	0.23	93.30
14th	1479.63	0.00218	0.22	93.52
15th	1465.63	0.00216	0.22	93.74
16th	1411.53	0.00208	0.21	93.95
17th	1323.65	0.00195	0.20	94.14
18th	1318.03	0.00194	0.19	94.33
19th	1234.01	0.00182	0.18	94.52
20th	1235.67	0.00182	0.18	94.70
21st	1170.26	0.00173	0.17	94.87
22nd	1072.99	0.00158	0.16	95.03
23rd	1043.38	0.00154	0.15	95.18
24th	992.92	0.00147	0.15	95.33
25th	955.83	0.00141	0.14	95.47
26th	887.80	0.00131	0.13	95.60
27th	862.20	0.00127	0.13	95.73
28th	863.24	0.00127	0.13	95.86
29th	834.47	0.00123	0.12	95.98
30th	753.21	0.00111	0.11	96.09
31st	776.77	0.00115	0.11	96.21
32nd	713.66	0.00105	0.11	96.31
33rd	711.05	0.00105	0.10	96.42
34th	705.88	0.00104	0.10	96.52
35th	676.64	0.00100	0.10	96.62
36th	635.92	0.00094	0.09	96.71
37th	619.28	0.00091	0.09	96.81
38th	608.27	0.00090	0.09	96.90
39th	570.31	0.00084	0.08	96.98
40th	562.49	0.00083	0.08	97.06
41st	558.50	0.00082	0.08	97.15
42nd	552.13	0.00081	0.08	97.23
43rd	525.84	0.00078	0.08	97.30
44th	519.96	0.00077	0.08	97.38
45th	514.17	0.00076	0.08	97.46
46th	507.54	0.00075	0.07	97.53
47th	502.56	0.00074	0.07	97.61
48th	471.73	0.00070	0.07	97.68
49th	462.10	0.00068	0.07	97.74
50th	476.23	0.00070	0.07	97.81
51st	464.86	0.00069	0.07	97.88
52nd	454.02	0.00067	0.07	97.95
53rd	441.39	0.00065	0.07	98.01
54th	449.59	0.00066	0.07	98.08
55th	432.09	0.00064	0.06	98.14
56th	428.23	0.00063	0.06	98.21
57th	433.09	0.00064	0.06	98.27
58th	415.89	0.00061	0.06	98.33
59th	413.27	0.00061	0.06	98.39
60th	411.75	0.00061	0.06	98.46
61st	396.78	0.00059	0.06	98.51
62nd	387.48	0.00057	0.06	98.57
63rd	375.73	0.00055	0.06	98.63
64th	371.15	0.00055	0.05	98.68
65th	369.22	0.00054	0.05	98.74
66th	358.93	0.00053	0.05	98.79
67th	355.70	0.00052	0.05	98.84
68th	344.64	0.00051	0.05	98.89
69th	330.61	0.00049	0.05	98.94
70th	318.41	0.00047	0.05	98.99
71st	299.33	0.00044	0.04	99.03
72nd	305.10	0.00045	0.05	99.08
73rd	291.67	0.00043	0.04	99.12
74th	291.99	0.00043	0.04	99.16
75th	283.23	0.00042	0.04	99.20
76th	275.11	0.00041	0.04	99.25
77th	270.42	0.00040	0.04	99.29
78th	260.77	0.00038	0.04	99.32
79th	248.63	0.00037	0.04	99.36
80th	244.14	0.00036	0.04	99.40
81st	221.68	0.00033	0.03	99.43
82nd	227.58	0.00034	0.03	99.46
83rd	207.01	0.00031	0.03	99.49
84th	201.57	0.00030	0.03	99.52
85th	196.86	0.00029	0.03	99.55
86th	192.22	0.00028	0.03	99.58
87th	184.95	0.00027	0.03	99.61
88th	172.41	0.00025	0.03	99.63
89th	177.45	0.00026	0.03	99.66
90th	159.93	0.00024	0.02	99.68
91st	150.52	0.00022	0.02	99.71
92nd	139.14	0.00021	0.02	99.73
93rd	139.04	0.00021	0.02	99.75
94th	139.94	0.00021	0.02	99.77
95th	128.11	0.00019	0.02	99.79
96th	126.96	0.00019	0.02	99.80
97th	114.78	0.00017	0.02	99.82
98th	117.55	0.00017	0.02	99.84
99th	112.23	0.00017	0.02	99.86
100th	105.39	0.00016	0.02	99.87
101st	105.48	0.00016	0.02	99.89
102nd	97.98	0.00014	0.01	99.90
103rd	94.09	0.00014	0.01	99.91
104th	80.63	0.00012	0.01	99.93
105th	83.75	0.00012	0.01	99.94
106th	75.68	0.00011	0.01	99.95
107th	73.48	0.00011	0.01	99.96
108th	70.36	0.00010	0.01	99.97
109th	68.94	0.00010	0.01	99.98
110th	62.18	0.00009	0.01	99.99
111th	61.51	0.00009	0.01	100.00

Green shading indicates the 1st four components which were used in this research. Red shading indicates those components which should be added so the process summarised over 95% of the hyper-temporal variability.

8.6. Appendix F

Boundaries extracted from all four principal components.

(i) 1st component (mid-value = 1022.54)

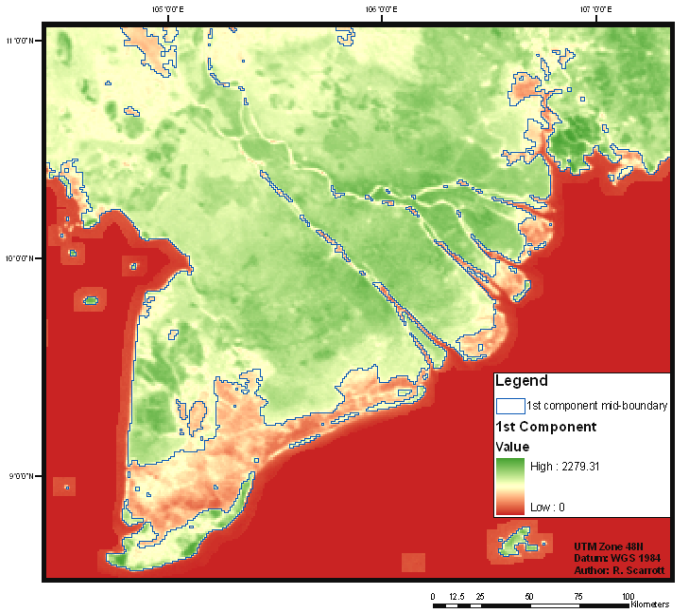

(ii) 2nd component (mid-value = 0)

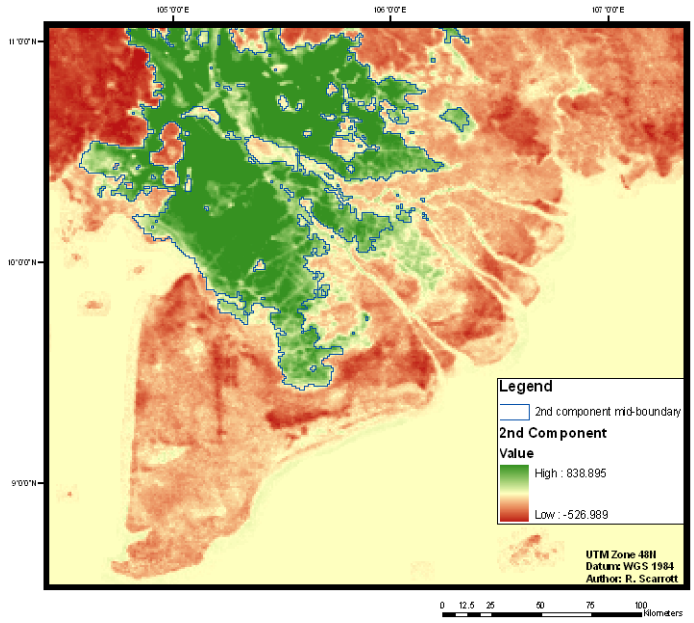

(iii) 3rd component (mid-value = 0)

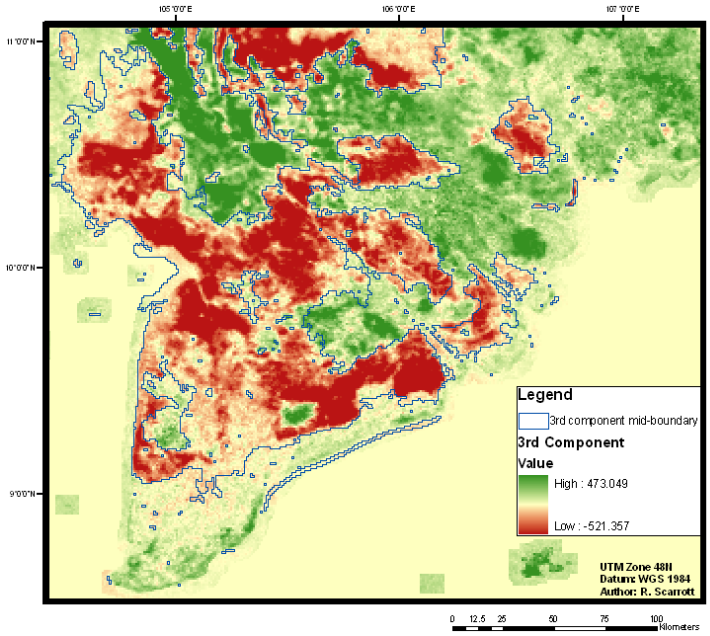

(iv) 4th component (mid-value = 0)

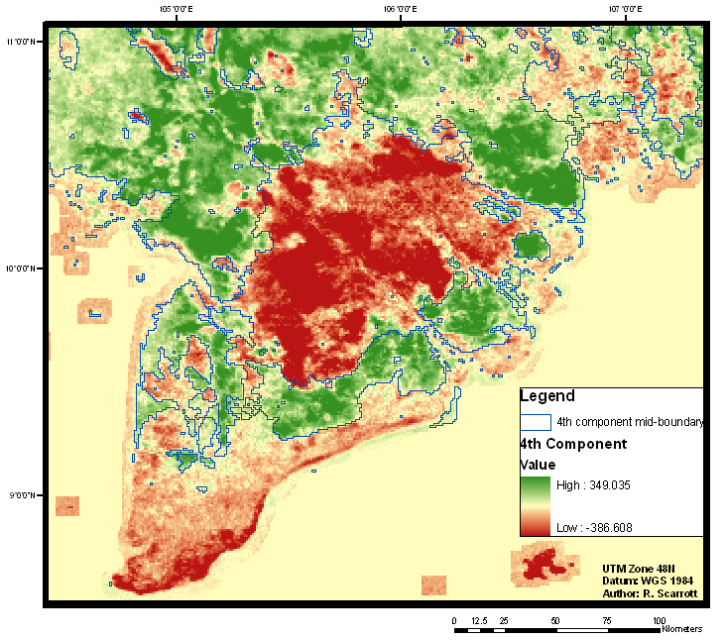

8.7. Appendix G

Principal component boundaries overlaying those extracted using 5x5 kernel Edge Detection.

(i) 1st and 2nd component boundaries over 5x5 kernel boundaries. Arrows indicate example sections of coinciding boundaries.

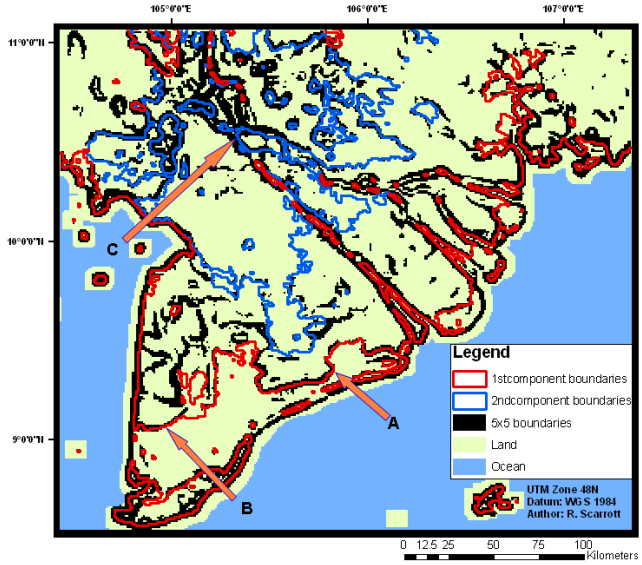

(ii) 1st and 2nd component boundaries over 5x5 kernel boundaries. Arrows indicate example sections of coinciding boundaries.

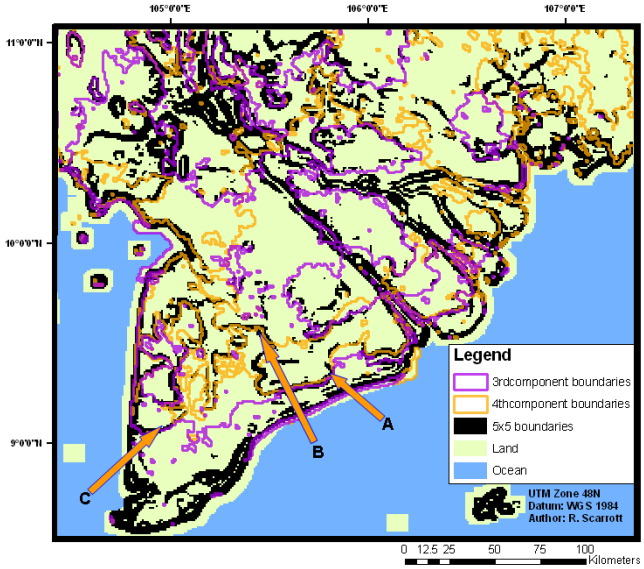

8.8. Appendix H

76 ISODATA classes overlaying principal components.

(i) 76 ISODATA classes overlaying the 1st Component

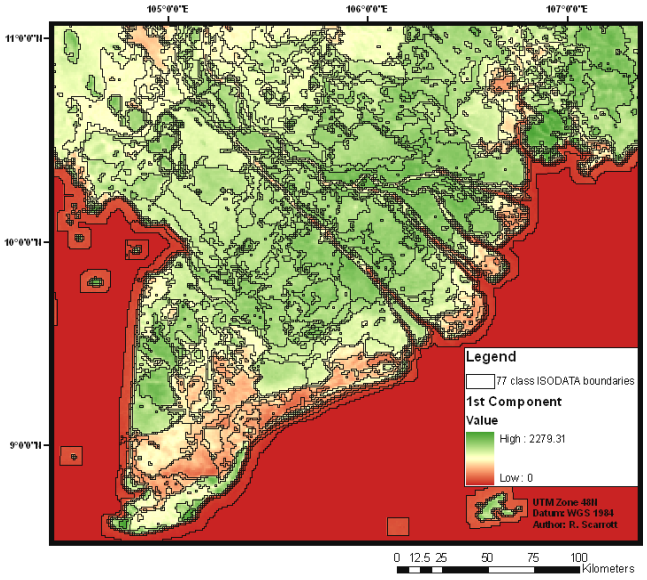

(ii) 76 ISODATA classes overlaying the 2nd Component

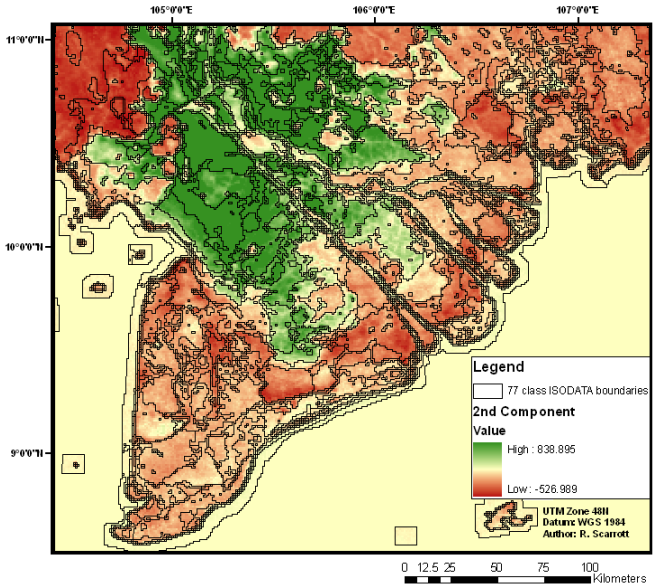

(iii) 76 ISODATA classes overlaying the 2nd Component

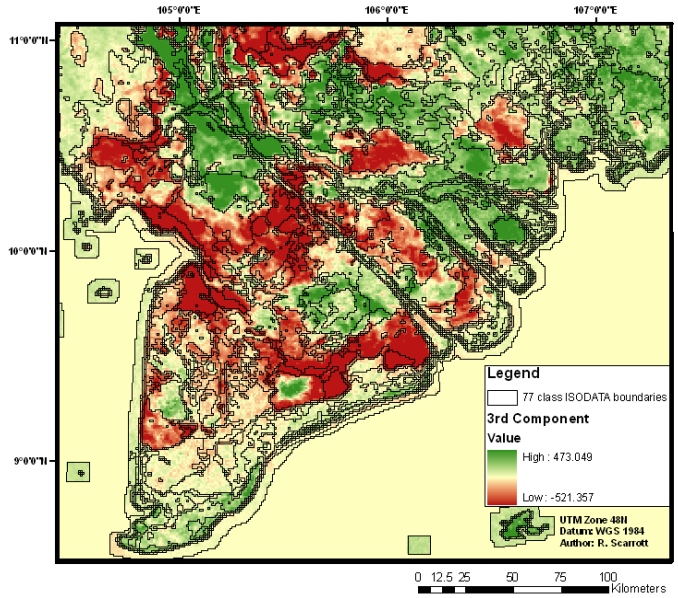

(iv) 76 ISODATA classes overlaying the 3rd Component